Remote Sensing of the Ecosystem Impact of Invasive Alien Plant Species

Von der KIT-Fakultät für
Bauingenieur-, Geo- und Umweltwissenschaften
des Karlsruher Instituts für Technologie (KIT)
genehmigte

Dissertation
zur Erlangung des akademischen Grades eines
Doktors der Naturwissenschaften
von

Michael Wolfgang Ewald
aus Marburg

Tag der mündlichen Prüfung:
7. November 2019

Referent: Prof. Dr. Sebastian Schmidtlein
Korreferentin: Prof. Dr. Birgit Kleinschmit

Karlsruhe, 2019

Abstract

Invasive alien plant species can adversely affect ecosystems by altering native plant communities and ecosystem functioning. Such ecosystem impacts have been studied extensively using small-scale experiments or field surveys. However, there is a lack of studies investigating the severity of invasion impacts across larger scale, for example at the habitat or landscape level. Remote sensing techniques have high potential to provide insight on large-scale impacts by delivering spatially explicit information on species distribution and ecosystem properties. So far, remote sensing has frequently been used to map occurrences of invasive plant species, but only rarely to assess their impacts. This thesis aims to evaluate the benefit of remote sensing for assessing ecosystem impacts of invasive plant species. Based on three research papers this thesis is evaluating different aspects of this potential. These aspects include the retrieval of vegetation properties from invaded ecosystems, the detection of invasion impacts at different spatial scales, and a spatially explicit assessment of ecosystem impact of invasive plant species.

Paper 1 focused on mapping canopy nitrogen (N) and phosphorus (P) in a temperate forest invaded by the American black cherry (*Prunus serotina* Ehrh.) using a combination of imaging spectroscopy and airborne Laserscanning (LiDAR) data. This study revealed that high structural canopy heterogeneity hampers remote sensing of canopy chemistry, but also co-variation between canopy chemistry and structure. Thus, LiDAR-derived structural information can improve predictions of canopy chemistry from imaging spectroscopy in structurally heterogeneous ecosystems. Paper 2 compared differences in remotely sensed ecosystem properties between invaded and non-invaded parts of the same temperate forest. These properties included canopy N and P, the N:P ratio, timber volume and leaf area index (LAI). The study revealed differences in canopy chemical and forest structural properties indicating causes and effects of *P. serotina* occurrence. Differences were also detectable at the level of forest stands, albeit to a minor degree. Paper 3 focused on mapping fractional covers of the heath star moss (*Campylopus introflexus* (Hedw.) Brid.) in a dune ecosystem. Predicted covers were used as an indicator of impact magnitude in different habitat types. Paper 3 further assessed the relationship between *C. introflexus* cover and plant alpha diversity based on field data. These results were combined to highlight potential high impact areas.

This thesis identified and applied two basic approaches to assess ecosystem impacts of invasive plant species using advanced Earth observation techniques. One approach is using maps of ecosystem properties derived from remote sensing to compare characteristics of

invaded and non-invaded areas. As demonstrated, this approach allows to study ecosystem impacts of invasive plant species across large areas, for example at the habitat or landscape level, and contribute to a better understanding of invasion impacts. The second approach is based on mapping abundances of invasive species and using these abundances as an indicator of ecosystem impact. An ideal abundance measure, from a remote sensing perspective is the fractional cover of a species in a reference area. Cover maps can then be used to identify high impact areas. Moreover, this approach compares the impact severity of different species or one species in different habitats, therefore delivering valuable information for management decisions.

Since the retrieval of many ecosystem properties is still challenging, future research should aim at understanding the linkages between vegetation attributes and reflectance. This is a prerequisite for reliable prediction of these properties from remote sensing. Future studies should focus on the retrieval of quantitative information when mapping invasive species distributions. More research is also necessary to ensure a successful identification of species in different ecological contexts. Finally, this thesis should encourage invasion ecologists to use remote sensing products when assessing large scale ecosystem impacts of invasive alien plant species.

Zusammenfassung

Invasive Pflanzenarten können Ökosysteme durch Beeinflussung von einheimischen Pflanzen-gesellschaften und Ökosystemprozessen verändern. Solche Ökosystemauswirkungen wurden mit Hilfe von Experimenten oder Feldaufnahmen umfassend untersucht. Großflächige Auswirkungen, zum Beispiel auf Habitat- oder Landschaftsebene wurden bisher jedoch kaum untersucht. Mit Hilfe von Fernerkundung können räumlich explizite Informationen über die Verteilung von Arten und Ökosystemeigenschaften erfasst werden und somit die Lücke in der Erforschung der großflächigen Auswirkungen invasiver Arten geschlossen werden. Bisher wurde Fernerkundung vor allem zur Kartierung von Vorkommen invasiver Pflanzenarten eingesetzt, jedoch nur selten zur Abschätzung ihrer Auswirkungen. Diese Arbeit zielt darauf ab, das Potential der Fernerkundung für die Bewertung von Ökosystemauswirkungen invasiver Pflanzenarten zu analysieren. Zu diesem Zweck wurden drei Forschungsarbeiten angefertigt, die verschiedene Aspekte dieses Potenzials beleuchten: (1) Die Ermittlung von Vegetationseigenschaften in von Invasionen betroffenen Ökosystemen, (2) die Analyse von Auswirkungen invasiver Arten auf unterschiedlichen räumlichen Skalen und (3) eine räumlich explizite Darstellung von Ökosystemauswirkungen invasiver Pflanzenarten.

Die erste Studie beschäftigt sich mit der Kartierung von Blattstickstoff (N) und - phosphor-gehalten (P) in einem Laubmischwald mit Vorkommen der frühblühenden Traubenkirsche (*Prunus serotina* Ehrh.). Für die Kartierung wurden hyperspektrale und Laserscanning (LiDAR) Daten kombiniert. Die Studie ergab, dass die Bestimmung von N und P aus hyperspektralen Fernerkundungdaten in Baumkronen mit hoher struktureller Heterogenität erschwert wird. Allerdings konnte auch ein Zusammenhang zwischen chemischer Zusammensetzung und der Struktur des Kronendaches festgestellt werden. So konnten die von LiDAR-Daten abgeleiteten Strukturinformationen genutzt werden, um die Vorhersagen von N und P zu verbessern. In der zweiten Studie wurden aus Fernerkundungsdaten erstellte Karten von Ökosystemeigenschaften genutzt, um Gebiete mit und ohne *P. serotina* zu vergleichen. Die Karten umfassten N und P, sowie das N:P-Verhältnis von Blättern, das Holzvolumen und den Blattflächenindex (LAI). Es wurden sowohl Unterschiede in den Werten von Blattinhaltsstoffen als auch in der Waldstruktur für Standorte mit und ohne *P. serotina* festgestellt. Diese Unterschiede waren auch auf Bestandsebene erkennbar, wenn auch in geringem Maße. In der dritten Studie wurden hyperspektrale Luftbilder verwendet um die prozentuale Deckung des Kaktusmooses (*Campylopus introflexus* (Hedw.) Brid.) in einem Dünenökosystem großflächig zu kartieren. Darüber hinaus wurde der Zusammenhang zwischen dem Deckungsgrad von *C. introflexus* und der Artenvielfalt von Pflanzen untersucht.

In Kombination wurden diese Ergebnisse verwendet, um potenzielle Bereiche mit hohen Auswirkungen zu kennzeichnen.

Basierend auf diesen drei Studien wurden in dieser Arbeit zwei grundlegende methodische Ansätze zur Analyse von Ökosystemauswirkungen invasiver Pflanzenarten per Fernerkundung identifiziert und angewandt. Der erste Ansatz besteht darin, mit Hilfe von Fernerkundung erstellte Karten von Ökosystemeigenschaften zu verwenden, um diese Eigenschaften in Abhängigkeit des Vorkommens invasiver Arten auszuwerten. Wie gezeigt werden konnte, ist dies auch für große Flächen, beispielsweise auf der Habitat- oder Landschaftsebene, möglich. Somit kann Fernerkundung zu einem besseren Verständnis der Auswirkungen von invasiven Arten beitragen. Der zweite Ansatz basiert auf der Kartierung von Abundanzen invasiver Pflanzenarten. Diese können als Indikator für die Stärke der Auswirkungen genutzt werden. Die resultierenden Karten können verwendet werden, um Bereiche mit hohen Auswirkungen zu identifizieren. Darüber hinaus ermöglicht dieser zweite Ansatz den Vergleich der Auswirkungen zwischen verschiedenen Arten oder Lebensraumtypen und kann somit wertvolle Informationen für Managemententscheidungen liefern.

Da die Ableitung vieler Ökosystemeigenschaften aus Fernerkundungsdaten nach wie vor eine Herausforderung darstellt, sollte die zukünftige Forschung darauf abzielen, die Zusammenhänge zwischen den Eigenschaften und der Reflektanz der Vegetation besser zu verstehen. Dies ist eine wesentliche Voraussetzung für eine zuverlässige Vorhersage über verschiedene Lebensräume hinweg. Zukünftige Fernerkundungsstudien, mit dem Ziel invasive Arten zu kartieren, sollten sich auf die Vorhersage von Deckungsgraden konzentrieren. Darüber hinaus sind generalisierte Verfahren wünschenswert, die eine erfolgreiche Identifizierung von Arten unter verschiedenen ökologischen Gegebenheiten gewährleisten. Nicht zuletzt sollte diese Arbeit Invasionsökologen ermutigen, existierende Fernerkundungsprodukte häufiger zu verwenden, um großflächige Auswirkungen von invasiven Pflanzenarten auf Ökosysteme zu analysieren.

Contents

1 Introduction

1.1 Invasion Ecology

1.1.1 Definitions

The research field of invasion ecology deals with questions related to organisms occurring outside their natural distribution range, as determined by their natural dispersal mechanism (Richardson and Pyšek, 2008). While introduced species were reported by ecologists in the 19th century already, the field of invasion ecology evolved slowly during the 20th century, with the book "The ecology of invasions by animals and plant" by Charles Elton (1958) as milestone (Richardson and Pyšek, 2008). However, it took until the 1980s that introduced species were widely recognized as problematic and the modern field of invasion ecology was shaped (Simberloff, 2011).

The frequently used synonyms "introduced" or "alien species" refer to species whose presence can be attributed to human activity (Pyšek et al., 2004). They can be grouped into casual, naturalized, and invasive species (Richardson et al., 2000). Casual species are alien species that occur only occasionally outside their native range, are not able to sustain self-reproducing populations and therefore rely on repeated introductions. Naturalized species represent established alien species that are able sustain self-reproducing populations over long time periods. Naturalized alien species that have high potential to distribute over large areas and often occur in very large numbers are regarded as invasive species (Pyšek et al., 2004). In this thesis I will use the term invasive species following Richardson et al. (2011) as

> "alien species that sustain self-replacing populations over several life cycles, produce reproductive offspring, often in very large numbers at considerable distances from the parent and/or site of introduction, and have the potential to spread over long distances."

This definition is solely based ecological and biogeographical criteria and does not imply any impact. In contrast, definitions used in legislation often imply an adverse impact on ecosystems or human health. For example, the European Union (EU, 2014) defines invasive species as

> "alien species whose introduction or spread has been found to threaten or adversely impact upon biodiversity and related ecosystem services."

Similarly the United States legislation (USDA, 1999) defines invasive species as

> "alien species whose introduction does or is likely to cause economic or environmental harm or harm to human health."

Species regarded as invasive are determined at the level of individual countries based on local risk assessments (e. g. Baker et al., 2008; Branquart, 2009; Nehring et al., 2013).

1.1.2 Invasive plants

Vascular plants make up the largest group of known alien species. In Europe, there are almost 6000 terrestrial alien plant species listed (Vilà et al., 2010). About half of them have an extra-European origin, making up more than 20 % of the present flora (Pyšek and Hulme, 2010). More than 4000 species are listed as naturalized in at least one European country (van Kleunen et al., 2015). At the level of individual countries the highest proportion of invasive plant species is only occurring casually (Richardson and Pyšek, 2012) and usually only a small proportion will become invasive (Mack et al., 2000). In Germany, for example, about 3 % of the alien flora is regarded as invasive or potentially invasive (Nehring et al., 2013). Large numbers of invasive species are generally observed in highly developed countries (Seebens et al., 2015). Relative to their area, Australia and the pacific islands are most affected by invasive plant species (van Kleunen et al., 2015). Temperate Asia and Europe are regarded as biggest donors of invasive plant species (van Kleunen et al., 2015). Important to note is that most invasive species are introduced intentionally (Turbelin et al., 2017).

The presence of invasive plants and the level of invasion depends on two major factors: resource availability defining the susceptibility of ecosystem for invasions, and propagule pressure of potential invaders (Pyšek and Richardson, 2010). Resource availability is closely linked to disturbances that facilitate plant invasions (Catford et al., 2012). Both factors strongly affect the local and global distribution patterns of alien species. Highly developed countries, where large numbers of alien species are recorded are characterized by both; a high frequency of human disturbances and high propagule pressure through the exchange of trade goods (Seebens et al., 2015).

In general, the highest number of alien plant species can be expected in areas with high human activity. Several studies found high probabilities for alien species occurrence near major cities, in areas with high population density or land use intensity, and along main traffic routes (Vicente et al., 2010; Gallardo et al., 2015, 2017; Ronk et al., 2017; Fuentes et al., 2015). There is also evidence that invasive plants are promoted by environmental change like elevated temperature and nutrient enrichment (Liu et al., 2017; Seabloom et al., 2015).

The number of worldwide newly introduced plant species remained high during the 20th century (Seebens et al., 2017), illustrating the high relevance for research on causes and effects of plant invasions.

1.1.3 Ecosystem impact

In this thesis I refer to ecosystem impact following Ricciardi et al. (2013) as

> "a measurable change to the properties of an ecosystem by a non-native species."

Such impact can vary in magnitude and direction, and can be regarded as positive or negative. The definition includes both ecological and socio-economic changes, as both may be caused by the presence of an invasive species. Invasive plants can have a wide range of possible ecosystem impacts affecting native species communities, abiotic ecosystem properties, ecological interactions, and natural disturbance regimes. These impacts vary among species and are further strongly dependent on the affected habitat and its biotic and abiotic conditions (Ehrenfeld, 2010; Vilà et al., 2011).

Due to the high relevance of biodiversity conservation, potential impacts of invasive plant species on native plant communities received most attention of scientific research by far (Strayer, 2012; Stricker et al., 2015). In many cases, the presence of invasive plants is associated with reduced species numbers of vascular plants compared to non-invaded reference sites (Vilà et al., 2011; Pyšek et al., 2012; Gaertner et al., 2009). There is also evidence that the presence of invaders is associated with reduced phylogenetic and functional diversity of native plant communities (Loiola et al., 2018). Effects on diversity can be attributed to the high competitiveness of many invasive plant species, due to higher resource use efficiency and better growth performance, compared to co-occurring native species (Vitousek, 1990; van Kleunen et al., 2010; Vilà et al., 2011). The presence of invasive plants therefore often has an negative effect on the productivity of resident species (Pyšek et al., 2012). In extreme cases this invasion process can lead to the persistent dominance of a single plant species.

Impacts of invasive plants on abiotic ecosystem properties refer to alterations of chemical or physical conditions. Chemical conditions can be affected by alterations of nutrient or carbon cycling. Nutrient cycles are most directly affected by the introduction of legume species that contribute to nitrogen enrichment through the symbiosis with nitrogen fixing microbes (Castro-Díez et al., 2014). Non-legume invaders can influence nutrient distributions by relocating nutrients from soil to plant biomass (Pyšek et al., 2012), or by enriching nutrients in the topsoil (Dassonville et al., 2008). Plant invasions are often found to influence carbon cycling by accelerating process rates, mainly due to increased primary production (Liao et al., 2008). Moreover, the presence of invasive plant species is related to high decomposition rates, which can be regarded as a joint effect of increased litter biomass and leaf nutrient contents (Liao et al., 2008; Castro-Díez et al., 2014). Changes of physical ecosystem conditions most commonly refer to increased vegetation height or density, affecting the light penetration through the canopy (Ehrenfeld, 2010). Moreover, introduced plants species can influence water cycling by altering rainfall interception or evapotranspiration (Takahashi et al., 2011; Cavaleri et al., 2014).

Biological interactions can be influenced by invasive plants in various ways, including both negative and positive feedbacks. For example, the presence of invasive plant species can increase the availability of flowers, while decreasing the visitation and pollination rate of native plant species (Gibson et al., 2013; Albrecht et al., 2016). On the other hand, the higher availability of exotic flowers attracted pollinators and increased their total numbers (Albrecht et al., 2016). Pollinator diversity can be affected positively or negatively by the presence of invasive plant species (Moroń et al., 2009; Davis et al., 2018). Similarly, species numbers of herbivore insects can be influenced in both directions (Sunny et al., 2015). Besides interaction with pollinators and herbivores, plant invasions can furthermore affect the mutualism between native plant species and mycorrhizal fungi (Hale et al., 2016; Birnbaum et al., 2018).

How an invasive species is affects its environment strongly depends on local biotic and abiotic conditions (Ehrenfeld, 2010; Kumschick et al., 2015). The magnitude and even the direction of impact may differ between ecosystems (Vilà et al., 2006; Scharfy et al., 2009; Koutika et al., 2007). The impact magnitude depends on the interplay between traits of the introduced plant and the specific properties of the invaded habitat. Ecosystem impact is more likely to be observed when trait differences exist between introduced species and the invaded plant community (Lee et al., 2017; Castro-Díez et al., 2014). Growth form and height are examples of traits that strongly determine the ecosystem impact of an introduced species with grasses and trees being associated with higher impact strengths (Pyšek et al., 2012). Islands isolated from the main continents tend to be most susceptible to the impact of invasive species (Pyšek et al., 2012; Castro-Díez et al., 2014; Celesti-Grapow et al., 2016). This high sensitivity is probably due to the incompletely filled niche space on islands, leading to the availability of unused resources, that is promoting the growth of introduced species (Denslow, 2003). Moreover, islands often contain rare endemic species, so that extinctions are more likely than on continents (Celesti-Grapow et al., 2016; Bellard et al., 2016).

The overall impact of a species is primarily determined by its local abundance and spatial distribution (Parker et al., 1999). Species forming dense and widespread populations are more likely to cause changes than species with a low and restricted abundance. Most crucial impacts can be expected, when an invader becomes the dominant species of a plant community. Understanding the relationship between the abundance of an invader and its impact is a main issue in the evaluation of biological invasions (Yokomizo et al., 2009; Thiele et al., 2009). However, such relationships have been studied only for few species (e. g. Elgersma and Ehrenfeld, 2010; Staska et al., 2014; Fried and Panetta, 2016). Most studies indicate non-linear relationships between ecosystem impact and the abundance of an invader with moderate impact at low abundances (Panetta and Gooden, 2017).

1.1.4 Management

Since it is costly to eradicate an established invasive species (Rejmanek and J. Pitcairn, 2002), management of plant invasions focuses on the prevention of new introductions and eradication at early stage of invasion (Pyšek and Richardson, 2010; Courchamp et al., 2017). Risk assessments are needed to identify potentially new invaders, for example by evaluating the floras of neighboring countries. Such assessments are usually conducted at the country level and constitute the legal basis for management actions (e. g. Baker et al., 2008; Branquart, 2009; Nehring et al., 2013). Some transnational assessments were carried out in the past. For example, the European Union maintains a list of introduced species of Union concern, currently including 23 terrestrial plant species (European Commission, 2017). These species are subject to restrictions, particularly concerning keeping and trade, in order to prevent further spread in the European Union. Furthermore, member states are requested to establish early detection and rapid eradication of these particular species (EU, 2014).

The management of established species is usually focused on invaders with the most severe impacts. Since resources are limited, management actions require a strong prioritization (Alberternst and Nawrath, 2018), focusing on the most harmful species and on valuable, susceptible habitats (McGeoch et al., 2016; Blackburn et al., 2014; Kumschick et al., 2012). In Germany management primarily focuses on introduced species occurring in protected areas with a high abundance. Still, management actions with a low cost-benefit ratio should be implemented with higher priority (Alberternst and Nawrath, 2018). According to an estimation of the European environmental agency, the costs of invasive species is amounting to € 12 billion per year (Sundseth, 2014). To manage invasive species, information on the distribution and abundance of introduced species, and information on the ecosystem impact of present and potential invaders is essential (Latombe et al., 2016).

1.2 Remote sensing

1.2.1 Basics

Remote sensing refers to collecting information about an object without touching it. Here, I refer to remote sensing to describe the study of the Earth's surface characteristics from above. Remote sensing is usually based on intensity measurements of electromagnetic radiation, giving the density of radiation energy in $\frac{W}{m^2}$. This intensity is usually specified relative to intensity of simultaneously measured solar irradiance, describing the reflectance percentage of the Earth's surface. These measurements cover one or more sections of the electromagnetic spectrum. For example, an color photograph displays the reflectance in the red, green, and blue part of the visible wavelength region (VIS, 400 nm — 700 nm) (Jones and Vaughan, 2010). Apart from VIS, remote sensing can cover several regions of

the electromagnetic spectrum, including the infrared region separated into near-infrared (NIR, $700\,\text{nm}$ — $1000\,\text{nm}$), shortwave-infrared (SWIR, $1\,\mu\text{m}$ nm $3\,\mu\text{m}$) and thermal-infrared (TIR, $3\,\mu\text{m}$ — $1000\,\mu\text{m}$), and the microwave region ($\approx 1\,\text{mm}$ — $1\,\text{m}$) (Turner et al., 2003). Remote sensing can be used to differentiate objects or materials based on their characteristic optical properties. These optical properties are characterized by its interaction with incoming electromagnetic radiation, that can be either absorption, reflectance, scattering or transmission (Jones and Vaughan, 2010).

Remote sensing instruments can be grouped into passive and active instruments. Passive remote sensing instruments capture the reflectance of solar radiation. Most commonly, the output is an image consisting of layers that represent information from various parts of the electromagnetic spectrum. Such part of the spectrum is referred to as a spectral band, and can vary in band width, depending on the covered wavelength range. Every layer is represented by pixels of a specific size which defines the spatial resolution of the image. The spatial resolution of images can strongly vary depending on the instrument and its distance from the object. Apart from the spatial resolution of data, imaging instruments can also differ in spectral resolution. A high spectral resolution is associated with a larger number of bands and narrower band widths.

In contrast to passive instruments, active instruments record the returned energy of radiation that was beforehand actively emitted. Examples are Radar or LiDAR instruments, both taking point-wise measurements from a moving platform. Recordings of active instruments usually cover one wavelength only. Apart from the used instrument, data properties are dependent on the platform they were recorded from. Remote sensing data is acquired either from ground-based platforms, airborne platforms like aircrafts and unmanned aerial vehicles (UAV), or satellites. Airborne platforms usually cover small spatial extents in high spatial resolution compared to satellite platforms (Turner et al., 2003; Jones and Vaughan, 2010). For this thesis two different remote sensing techniques were used: Imaging spectroscopy and Airborne Laserscanning. Both techniques will be described in more detail in sections 1.2.2 and 1.2.3.

1.2.2 Imaging spectroscopy

Imaging spectroscopy (also referred to as hyperspectral remote sensing) is a remote sensing technique recording high numbers (usually > 100) of spectral bands with very narrow band widths. Although still covering discrete wavelength sections, the spectral resolution is sufficiently high to approximate the recordings in each band as a continuous reflectance spectrum (Fig. 1.1). Due to its high spectral resolution imaging spectroscopy is very useful to distinguish objects or materials, that differ in spectral signature. So far, imaging spectroscopy data has been most commonly recorded from airborne platforms. Frequently used sensors usually cover the spectral wavelength regions from the VIS to the SWIR (Jones

and Vaughan, 2010; Wang et al., 2010; Ortenberg, 2011). There are also examples of imaging spectrometers operated from satellite platforms (e. g., Hyperion imaging spectrometer on board of the earth observing-1 (EO-1) 2000 — 2017). However, the use of satellite imaging spectroscopy data is still limited by technical issues, and much potential is expected from recently started or future planned hyperspectral satellite missions (e. g., EnMAP, PRISMA, HISUI) (Ortenberg, 2011; Transon et al., 2018).
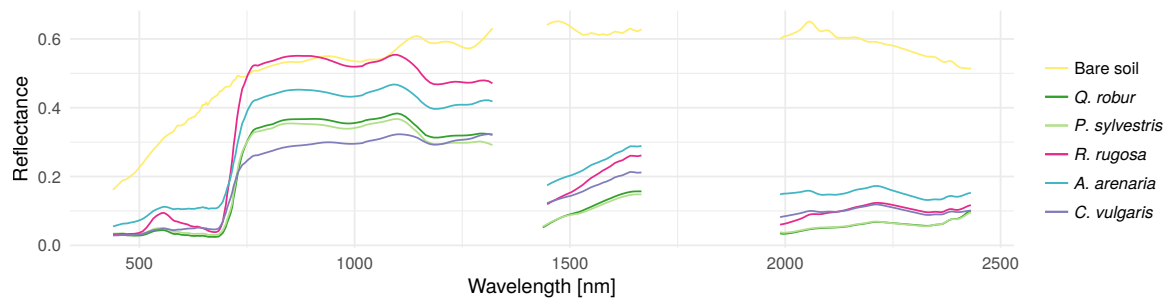
Figure 1.1 Soil spectrum and canopy spectra of selected plant species (*Quercus robur*, *Pinus sylvestris*, *Rosa rugosa*, *Ammophila arenaria*, *Calluna vulgaris*).

1.2.3 Airborne Laserscanning

Laserscanning (Light detection and ranging, LiDAR) is an active remote sensing technique, that is frequently used to measure distances. Distance measurements are based on the elapsed time between the emission of a laser pulse and the return of its reflection. With knowledge of the position and orientation of the LiDAR instrument it is possible to determine the accurate position of the object that reflected the beam. Depending on the device used, LiDAR can detect multiple returns from one emitted pulse. Repeated measurements from a moving platform can thus be used to create a three dimensional point cloud that represent the return points (Fig. 1.2). Used platforms usually include aircrafts or helicopters. For terrestrial application, airborne LiDAR instruments used usually cover discrete wavelengths between 900 nm and 1064 nm (Wehr and Lohr, 1999; Lefsky et al., 2002).

1.2.4 Remote sensing of vegetation

Compared to non-living surfaces, remote sensing of vegetation is complicated by its high spatio-temporal variability. In general, the spectral reflectance of vegetation is characterized by strong absorbance in the VIS and relatively high reflection in the NIR (Fig. 1.1). In the transition zone from VIS to NIR, vegetation spectra are characterized by a stong increase of reflectance, which is referred to as red edge. Depending on the vegetation type, reflectance can differ considerably (Fig. 1.1). Differences between vegetation types can be usually detected in the wavelength region ranging from 300 nm to 15 μm (Jones and Vaughan, 2010). These differences are determined by the interactions of incoming radiation and components
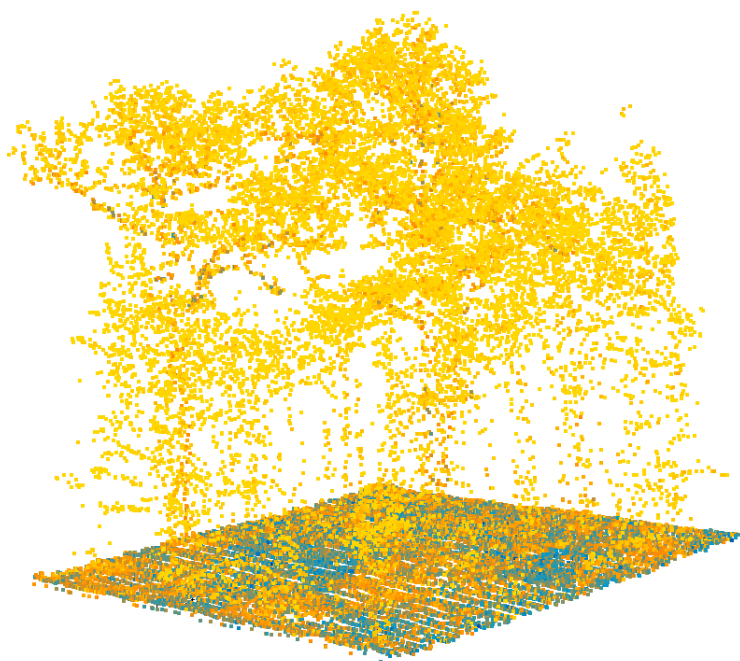
Figure 1.2 Visualization of a LiDAR point cloud, displaying the invasive tree species *Prunus serotina* in the mid-canopy of an oak forest.

of the canopy. The reflectance of canopies is strongly influenced by leaf properties and the spatial arrangement of the leaves (Ollinger, 2011).

Leaf-level spectral reflectance is influenced by chemical properties and anatomical structure (Ollinger, 2011). Chemical properties that influence reflectance patterns include leaf pigments, water content, and other leaf compounds such as fibers and proteins (Kokaly et al., 2009). Pigments such as chlorophyll, carotenoides and anthocynins are characterized by strong absorbance in the VIS (Ustin et al., 2009). Leaf water content has a substantial influence on reflectance patters in the SWIR region also due to high absorbance (Kokaly et al., 2009; Ollinger, 2011). In contrast, the influence of proteins and fibers such as cellulose or lignin on the reflectance of leaves is less strongly developed (Kokaly et al., 2009). Their influence is based on absorbance of radiation by molecular bonds such as the C-H bond in cellulose and the C-N bond in proteins (Curran, 1989). In addition, the radiative properties of leaves strongly depend on their anatomical structure. Here, reflectance patterns are influenced by the arrangement of cells within the mesophyll, but also by the leaf form. For example, flat and thin leaves are characterized by a higher reflection in the NIR region, compared to thicker cylindrical leaves. Most commonly, the specific leaf area (SLA), defined by the ratio of leaf area to leaf mass, or its reciprocal leaf mass per area (LMA) is used as descriptor for leaf structure (Ollinger, 2011).

At the level of entire plants or plant communities, spectral reflectance is furthermore substantially influenced by the canopy structure (Asner, 1998; Knyazikhin et al., 2013;

Kattenborn et al., 2018). This includes canopy depth, density, and leaf arrangement (Ollinger, 2011). Canopy depth and density, also characterized by the leaf area index (LAI), affect reflectance patterns ranging from the VIS to SWIR (Jacquemoud et al., 2009) Variations in leaf arrangements are mainly visible in the NIR. Here, the effect of canopy structure can be explained by the scattering of incoming radiation by leaves before it is either reflected or absorbed by other surfaces such as branches, stems or the ground (Ollinger, 2011; Knyazikhin et al., 2013).

Based on differences in spectral properties it is possible to differentiate single vegetation types (Ustin and Gamon, 2010) or plant species (e. g. Fassnacht et al., 2014; Lopatin et al., 2017). Examples include discrete classifications of dominant vegetation types at the global scale (Bonan et al., 2002), to the delineation of single habitats at a local scale (Mack et al., 2016; Stenzel et al., 2017). Species classifications have most prominently been used to map tree species (Fassnacht et al., 2016), but were also used to identify smaller plant individuals (Singh and Glenn, 2009; Skowronek et al., 2017a). Moreover, remote sensing also proved useful to map plant functional types (Schmidtlein et al., 2012; Schmidt et al., 2017a). These maps can for example be used to asses vegetation change related to alterations of environmental conditions or in land use (Ustin and Gamon, 2010). Remote sensing can also be used to assess a gradual change in vegetation types, and to evaluate habitat degradation (Fassnacht et al., 2015; Schmidt et al., 2017b).

Moreover, imaging remote sensing can be used to derive a multitude of other vegetation attributes. Examples mainly refer to characteristics directly influencing the canopy reflectance, such as leaf pigment (e. g. Curran et al., 1997; Schlerf et al., 2010) or water contents (e. g. Huber et al., 2008; Dahlin et al., 2013), SLA (e. g. Asner et al., 2015; Singh et al., 2015) and LAI (e. g. Fernandes et al., 2004; Lu et al., 2018). In addition, vegetation properties with only minor influence on canopy reflectance have been successfully mapped using optical remote sensing, such as canopy nitrogen (e. g. Curran et al., 1997; Serrano et al., 2002; Huber et al., 2008; Schlerf et al., 2010; Dahlin et al., 2013), phosphorus (e. g. Porder et al., 2005; Asner et al., 2015; Pullanagari et al., 2016), and cellulose or lignin content (e. g. Curran et al., 1997; Singh et al., 2015; Asner et al., 2015).

Information from LiDAR point clouds can be used to derive structure-related vegetation characteristics across large areas. Particularly, vegetation height can be derived with high accuracy (van Leeuwen and Nieuwenhuis, 2010). In contrast to passive remote sensing techniques, LiDAR can penetrate through plant canopies. LiDAR can therefore be used to measure the vegetation density in different canopy strata (Morsdorf et al., 2010; Ewald et al., 2014), and to measure LAI (Sasaki et al., 2008; Korhonen et al., 2011). Due to the high correlation of tree growth height and biomass, LiDAR is frequently used to map standing wood biomass or volume of forests (Lefsky et al., 2005; Næsset and Gobakken, 2008).

Usually the acquisition of detailed information on leaf traits requires images of high spectral and spatial resolution. However, some vegetation attributes, such as LAI can also

be mapped at courser resolutions using multi-spectral data. To identify species based on spectral reflectance, typically hyperspectral data is used (Bradley, 2014). Depending on the species, data with a lower spectral resolution may be sufficient. The optimal pixel size to map species depends on the size of the species and can vary between several centimeters and meters. LiDAR data to map vegetation characteristics usually include several discrete measurements per square meter.

The success for mapping these vegetation characteristics relies on the co-variation with traits that influence reflectance patterns (Ustin and Gamon, 2010; Ollinger, 2011). Such co-variation was, for example, observed between canopy structure and nitrogen content (Knyazikhin et al., 2013). These indirect links between vegetation characteristics and spectral reflectance are, however, not well understood. One aim of current research is dedicated to understanding indirect links and eventually identify the ones that are more universally applicable. Of particular interest are approaches to map biochemical leaf traits, because they are fundamental for our understanding of ecological processes related to carbon or nutrient cycling (Melillo et al., 1982; Ollinger et al., 2002; Reich, 2012).

Reflectance is commonly linked to vegetation properties using empirical models. As hyperspectral data contain lots of information with a high level of collinearity they require the use of machine learning to establish relationships between single bands and vegetation properties derived from field surveys. A major advantage of empirical approaches is that they can also find indirect links between vegetation characteristics and reflectance. One major drawback is that empirical approaches are contributing only little to understanding of ecological mechanisms underlying these links. Furthermore, linkages established using empirical models can not easily be transferred to different study areas or points in time (Verrelst et al., 2015; Skowronek et al., 2018). Alternatively, radiative transfer models (RTMs) can be used. RTMs are physical-based models that predict the spectral reflectance of vegetation using a set of properties based on tested cause-effect relationships. Through model inversion, radiative transfer models can also be used to predict vegetation characteristics from measured canopy spectra (Jacquemoud et al., 2009; Verrelst et al., 2015).

1.2.5 Remote sensing of plant invasions

Previous remote sensing studies on plant invasions so far have mainly focused on the detection and the mapping of invasive species distribution (Vaz et al., 2018). This has been shown to work properly for growth forms such as cryptogams (Skowronek et al., 2017a), grasses and herbs (Singh and Glenn, 2009; Skowronek et al., 2018) or shrubs and trees (Somers and Asner, 2013; Kattenborn et al., 2019). Moreover, remote sensing has been used as information basis to model potential distributions by highlighting areas susceptible to future invasions (Andrew and Ustin, 2009; Rocchini et al., 2015; Hattab et al., 2017).

In contrast, remote sensing studies that focus on ecosystem impact or change attributed to the presence of invasive plants are still rare. Asner and Vitousek (2005), for example,
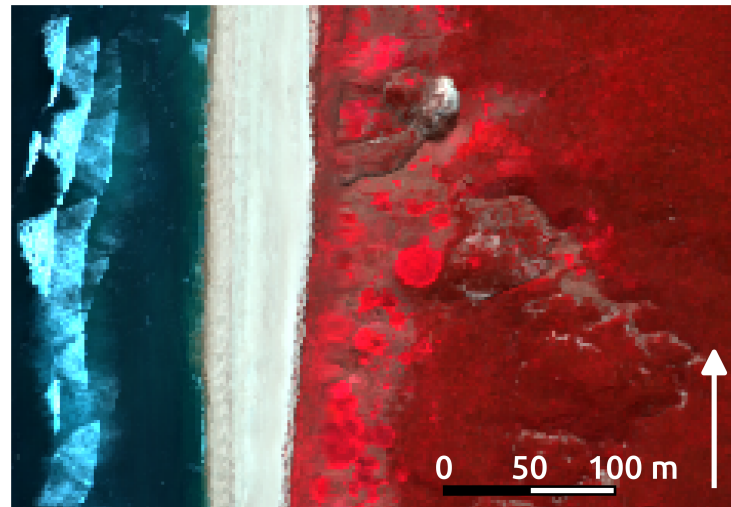
Figure 1.3 Color infrared representation the coastal dunes of the island Sylt, Germany. Patches in light red display presences of the invasive shrub *Rosa rugosa*.

used airborne imaging spectroscopy to map the influence of *Myrica faya* on canopy N and water content in a mountain rain forest ecosystem. Dzikiti et al. (2016) used satellite remote sensing to estimate the area-based effect of the invasive tree *Eucalyptus camaldulensis* on evapotranspiration in a river catchment. Vicente et al. (2013) used a spatially explicit approach to connect the richness of alien invasive alien plant species to remotely sensed primary productivity and the provision of other ecosystem services. Barbosa et al. (2017) related changes in gross primary production, derived from high resolution imaging spectroscopy, to the canopy cover of the invasive tree species *Psidium cattleianum* in a tropical forest. Similarly, Große-Stoltenberg et al. (2018) used imaging spectroscopy data in combination with a spectral index to link gross primary production to the cover of *Acacia longifolia* in a dune ecosystem.

1.3 Research needs

The ecosystem impact of invasive plant species has been the subject of many research papers, comprising hundreds of case studies (Stricker et al., 2015), several review papers (e. g. Parker et al., 1999; Weidenhamer and Callaway, 2010; Stricker et al., 2015), and a multitude of meta-analyses (e. g. Vilà et al., 2011; Powell et al., 2011; Pyšek et al., 2012). Still, there is a high demand for ongoing research, because the potential influence of each species has to be evaluated separately, and fundamental ecological information is lacking even for species that are considered as the worst invaders (McLaughlan et al., 2014). Moreover, a research gap remains on many aspects of impact research. While impacts on plant communities are generally well studied, impacts on ecosystem processes such as nutrient, carbon, and water cycling or on related ecosystem properties received less attention (Ehrenfeld, 2010; Strayer,

2012; Stricker et al., 2015). At this point remote sensing can deliver valuable insights, offering a non-destructive way to predict vegetation properties at the community level, and thus provide valuable information to evaluate carbon- or nutrient cycling (Andrew et al., 2014; de Araujo Barbosa et al., 2015). However, so far only few studies used remote sensing techniques to distinguish between invaded and non-invaded parts of affected habitats. To my knowledge no other study uses the high potential to evaluate plant invasion impacts across different spatial scales.

Most research on plant invasions is based on experiments or field studies with a limited spatial extent. Stricker et al. (2015) found that in 50 % of the studies on invasion impacts the sampling units covered $1\,m^2$ or less. Less than one third of the studies used sampling units larger than $4\,m^2$. In most cases it is unclear whether observed small scale changes of ecosystem conditions can also be detected when larger extents are considered, at which the target plants occur less frequently (Parker et al., 1999; Pauchard and Shea, 2006). Information acquired over large spatial extents is particularly relevant for the evaluation of nutrient and carbon cycles. Imaging remote sensing can deliver spatially explicit information on ecosystem properties across large areas and thus has potential to study invasion impact at multiple spatial scales.

Moreover, remote sensing techniques are well suited to map the spatial distributions of individual plant species, which is important information to evaluate large scale impacts. Indeed, most studies so far focused on mapping presence or absence of individual species. Remote sensing offers the additional opportunity to map species abundances (e. g. Peterson, 2005; Andrew and Ustin, 2008; Guo et al., 2018). Most of these studies focused on large conspicuous species, and methods need to be tested also for small species. Such maps can be used to identify high-impact areas, particularly when they are combined with abundance-impact relationships, depicting the impact magnitude of a particular species in dependence of its abundance. Although this possibly represents the easiest approach to evaluate landscape level impact of invasive species, to my knowledge this has not been done before.

Remote sensing is regarded to have high potential to assess ecosystem changes related to invasion processes (Vaz et al., 2018). However, only few studies address this topic, so that research in this field is still in an early stage of development. One major task at this point is to demonstrate and evaluate potential approaches, in order to develop applications that increase the understanding of invasion-related processes and furthermore provide valuable information as basis for management decisions.

1.4 Thesis outline and research questions

The overarching aim of this thesis is to evaluate the benefit of remote sensing to assess ecosystem impact caused by invasive plant species. For this purpose, this thesis presents and examines different applications of remote sensing that hold promise to improve our understanding of invasion impacts, or are beneficial for the management of invasive species. The applications that I used are presented in three research papers as included in this thesis. Paper 1 focuses on mapping the canopy nitrogen and phosphorus content of a forest affected by the presence of an invasive tree species. This paper specifically addresses the potential of remote sensing to map leaf chemical properties of canopies in invaded ecosystems characterized by a high structural complexity. In paper 2, the same maps are combined with remotely sensed maps of structural forest properties, to compare invaded and non-invaded forest stands at different spatial scales. This paper addresses the potential of remote sensing to detect invasion-related changes of ecosystem properties across large areas. Finally, paper 3 aims to map the abundance of an invasive plant species as an indicator of ecosystem impact using imaging spectroscopy data. It addresses the potential of remote sensing to provide a spatially-explicit evaluation of the impact of invasive species. Based on these research papers this thesis aims to answer the following research questions:

1. Can remote sensing be used to map nitrogen and phosphorus contents of canopies characterized by high structural complexity to analyze plant invasion impact? (Paper 1)

2. How do remotely sensed structural and chemical canopy properties differ between invaded and non-invaded sites? (Paper 2)

3. How accurately can we map fractional covers of invasive plant species using imaging spectroscopy data? (Paper 3)

The studies for paper 1 and 2 were located in a temperate deciduous forest using the tree black cherry (*Prunus serotina* Ehrh.) as study species. Paper 3 focuses on occurrences of the heath star moss (*Campylopus introflexus* (Hedw.) Brid.) in a dune ecosystem. Both species are listed among the most invasive alien species in Europe (Pyšek et al., 2009; Essl and Lambdon, 2009). The remote sensing data comprised very high-resolution airborne imaging spectroscopy data with a pixel size of 3m̊ × 3m̊ and airborne LiDAR data with an average point density of 23 points/m^2.

1.5 List of papers

The research papers included in this thesis are listed below. Papers 1 and 2 are published in international peer-reviewed scientific journals. Paper 3 is currently submitted.

1. Ewald, M., Aerts, R., Lenoir, J., Fassnacht, F. E., Nicolas, M., Skowronek, S., Piat, J., Honnay, O., Garzón-López, C. X., Feilhauer, H., Van de Kerchove, R., Somers, B.,

Hattab, T., Rocchini, D., Schmidtlein, S. (2018): LIDAR derived forest structure data improves predictions of canopy N and P concentrations from imaging spectroscopy. Remote Sensing of Environment 211, 13–25. 10.1016/j.rse.2018.03.038

2. Ewald, M., Skowronek, S., Aerts, R., Dolos, K., Lenoir, J., Nicolas, M., Warrie, J., Hattab, T., Feilhauer, H., Honnay, O., Garzón-López, C. X., Decocq, G., Van de Kerchove, R., Somers, B., Rocchini, D., Schmidtlein, S. (2018): Analyzing remotely sensed structural and chemical canopy traits of a forest invaded by *Prunus serotina* over multiple spatial scales. Biological Invasions 20 (8), 2257–2271. 10.1007/s10530-018-1700-9

3. Ewald, M., Skowronek, S., Aerts, R., Lenoir, J., Feilhauer, H., Van de Kerchove, R., Honnay, O., Somers, B., Garzón-López, C., Rocchini, D., Schmidtlein, S. (submitted) Evaluating the ecosystem impact of an invasive moss using high resolution imaging spectroscopy.

1.6 Summary of the authors contribution

The research papers were prepared in collaboration with several co-authors within the scope of the project DIARS (Detection of invasive plant species and assessment of their impact on ecosystem properties through remote sensing) funded by the ERA-Net BiodivERsA network. All manuscripts were originally drafted by me and subsequently revised by the co-authors. Apart of writing I was involved in the study design and conducted the field work with the help of several co-authors (and others). Remote sensing data was provided by the Flemish Institute of Technological Research (VITO) and the French Office of Forestry (ONF). I performed the data processing and analysis, stimulated by the ideas of the co-authors. Finally, the results were discussed and interpreted in collaboration with the co-authors.

2 Research papers

2.1 LiDAR derived forest structure data improves predictions of canopy N and P concentrations from imaging spectroscopy

Michael Ewald, Raf Aerts, Jonathan Lenoir, Fabian Ewald Fassnacht, Manuel Nicolas, Sandra Skowronek, Jérôme Piat, Olivier Honnay, Carol Ximena Garzón-López, Hannes Feilhauer, Ruben Van De Kerchove, Ben Somers, Tarek Hattab, Duccio Rocchini, Sebastian Schmidtlein

Abstract

Imaging spectroscopy is a powerful tool for mapping chemical leaf traits at the canopy level. However, covariance with structural canopy properties is hampering the ability to predict leaf biochemical traits in structurally heterogeneous forests. Here, we used imaging spectroscopy data to map canopy level leaf nitrogen (N_{mass}) and phosphorus concentrations (P_{mass}) of a temperate mixed forest. By integrating predictor variables derived from airborne laser scanning (LiDAR), capturing the biophysical complexity of the canopy, we aimed at improving predictions of N_{mass} and P_{mass}. We used partial least squared regression (PLSR) models to link community weighted means of both leaf constituents with 245 hyperspectral bands (450 - 2450 nm) and 38 LiDAR-derived variables. LiDAR-derived variables improved the model's explained variances for N_{mass} (R^2_{cv} 0.31 vs. 0.41, % $RMSE_{cv}$ 3.3 vs. 3.0) and P_{mass} (R^2_{cv} 0.45 vs. 0.63, % $RMSE_{cv}$ 15.3 vs. 12.5). The predictive performances of N_{mass} models using hyperspectral bands only, decreased with increasing structural heterogeneity included in the calibration dataset. To test the independent contribution of canopy structure we additionally fit the models using only LiDAR-derived variables as predictors. Resulting R^2_{cv} values ranged from 0.26 for N_{mass} to 0.54 for P_{mass} indicating considerable covariation between these biochemical traits and forest structural properties. N_{mass} was negatively related to the spatial heterogeneity of canopy density, whereas P_{mass} was negatively related to canopy height and to the total cover of tree canopies. In the specific setting of this study, the importance of structural variables can be attributed to the presence of two tree species, featuring structural and biochemical properties different from co-occurring species. Still, existing functional linkages between structure and biochemistry at the leaf and canopy level suggest that canopy structure, used as proxy, can in general support the mapping of leaf biochemistry over broad spatial extents.

2.1.1 Introduction

Plant traits are important indicators of ecosystem functioning and are widely used in ecological research to detect responses to environmental change (Chapin, 2003; Garnier et al., 2007; Kimberley et al., 2014) or to quantify ecosystem services (Lamarque et al., 2014; Lavorel et al., 2011). Biochemical traits like leaf nitrogen and phosphorus content respond to changing environmental conditions, such as soil nutrients or climate (Di Palo and Fornara, 2015; Sardans et al., 2015) and are key factors related to important ecological processes including net primary production and litter deiosition (Melillo et al., 1982; Ollinger et al., 2002; Reich, 2012). Temporal trends, like increasing N:P ratios caused by nitrogen deposition can serve as indicators for ecosystem health and sustainability (Jonard et al., 2015; Talkner et al., 2015). Using leaf traits to answer questions related to ecosystem functioning often requires scaling from the leaf to the plant community or ecosystem level (Masek et al., 2015; Suding et al., 2008). Due to the fact that certain leaf biochemical traits are closely linked to the reflectance signature of leaves (Kokaly et al., 2009) the use of imaging spectroscopy has proved to be an efficient method for scaling and the prediction of these traits across large spatial scales (Homolová et al., 2013). By far, most studies relating foliage biochemistry to airborne imaging spectroscopy data focused on leaf nitrogen (e.g. Dahlin et al., 2013; Huber et al., 2008; Martin and Aber, 1997; Wang et al., 2016). But also other biochemical leaf ingredients like chlorophyll, cellulose and lignin (Curran et al., 1997; Schlerf et al., 2010; Serrano et al., 2002) and even micronutrients like iron and copper (Asner et al., 2015; Pullanagari et al., 2016) have been successfully related to imaging spectroscopy data. Compared to leaf nitrogen, mapping of leaf phosphorus concentrations received less attention (but see Asner et al., 2015; Porder et al., 2005; Pullanagari et al., 2016).

The link between leaf biochemistry and reflectance established in optical remote sensing applications strongly depends on the observational level. At the leaf level, nitrogen concentrations, for example, are directly expressed in the spectral signal. For dried and ground samples, characteristic absorption features can be found in the shortwave infrared (SWIR) region of the electromagnetic spectrum. The absorption of radiation in the SWIR can be attributed to nitrogen bonds in organic compounds primarily of leaf proteins (Kokaly et al., 2009). In fresh leaves the nitrogen concentration is additionally strongly related to absorption in the visible part of the spectrum (VIS) (Asner and Martin, 2008), which can be attributed to the correlation between chlorophyll and leaf nitrogen (Homolová et al., 2013; Ollinger, 2011). At the canopy level, spectral reflectance is strongly influenced by canopy structure (Asner, 1998; Gerard and North, 1997; Rautiainen et al., 2004). Thus, the estimation of leaf traits from canopy reflectance is more complex due to the confounding effects of structural properties like crown morphology, leaf area index (LAI), leaf clumping or stand height (Ali et al., 2016; Simic et al., 2011; Xiao et al., 2014). Consequently, variability in canopy structure can strongly influence the accuracy of nitrogen estimations from remote sensing (Asner and Martin, 2008). On the other hand, canopy structure has been found

to explain part of the relation between reflectance and canopy nitrogen. This relation is revealed by a strong importance of reflectance in the near infrared (NIR) for mapping canopy nitrogen reported by previous studies (Martin et al., 2008; Ollinger et al., 2008). Reflection in the NIR region is dominated by multiple scattering between leaves of the canopy, and thus very sensitive to variation in canopy structure (Knyazikhin et al., 2013; Ollinger, 2011). Covariation between canopy structure and nitrogen was found across different types of forest ecosystems and hence points at the existence of a functional link between canopy structure and biochemical composition. However, the foundation of this functional link has not been fully understood.

In this study, we aim at scaling leaf level measurements of mass based leaf nitrogen (N_{mass}) and phosphorus content (P_{mass}) to the canopy scale for a temperate mixed forest. To capture the forest's diversity in terms of tree species, age distribution and canopy structure we propose to explicitly integrate information on forest structure derived from airborne laser scanning (Light Detection And Ranging, LiDAR) into the empirical models. Airborne LiDAR data can depict the 3D structure of the vegetation and has been successfully used to map forest attributes like the leaf area index and standing biomass (Fassnacht et al., 2014; Korhonen et al., 2011; Zolkos et al., 2013). The benefit of LiDAR-derived information on forest structure for mapping of canopy biochemistry has not been assessed yet. We argue that the integration of structural properties allows for a better acquisition of leaf chemical traits in heterogeneous forests canopies. We furthermore expect that LiDAR data can help to understand expected covariation between canopy structural properties and biochemical leaf traits. Specifically, we aim at: (1.) improving predictions of N_{mass} and P_{mass} using imaging spectroscopy through the integration of LiDAR-derived information on forest structure and (2.) finding out which structural canopy properties correlate with N_{mass} and P_{mass} in canopies of mixed forests.

2.1.2 Materials and Methods

2.1.2.1 Study area

The study area is the forest of Compiègne (northern France, 49.370° N, 2.886° E), covering an area of $144.2\,km^2$. This lowland forest is located in the humid temperate climate zone with a mean annual temperature of 10.3°Cand mean annual precipitation of 677 mm. The soils cover a range from acidic nutrient-poor sandy soils to basic and hydromorphic soils (Closset-Kopp et al., 2010). The forest mainly consists of even-aged managed stands of beech (*Fagus sylvatica*), oaks (*Quercus robur*, *Quercus petraea*) and pine (*Pinus sylvestris*) growing in mono-culture as well as in mixed stands, frequently intermingled with European hornbeam (*Carpinus betulus*) and ash (*Fraxinius excelsior*) (Chabrerie et al., 2008). Stands are covering a range from early pioneer stages to more than 200-year-old mature forests. As a result of thinning activities and windthrow the forest is characterized by frequent canopy

gaps which are often filled by the American black cherry (*Prunus serotina*), an alien invasive tree species in central Europe. *Prunus serotina* is in some parts also highly abundant in the upper canopy of earlier pioneer stages.

2.1.2.2 Field data

Field data were acquired from 50 north-facing field plots (25 m $\times$ 25 m) established in July 2014. Of those plots, 44 plots were randomly selected from an initial set of 64 field plots established in 2004 during a previous field study by Chabrerie et al. (2008). Six additional plots were selected to include stands in earlier stages of forest succession, aiming to cover the entire range of structural canopy complexity. The plots covered all main forest stand types including mixed tree species stands in different age classes (supplementary material, Tab. 2.3). In each plot we recorded the diameter at breast height for all trees and shrubs higher than 2 m.

In July 2015, we sampled leaves from the most abundant tree species making up at least 80% of the basal area in one plot. This resulted in up to five sampled species per plot. For each species in each plot, we took three independent samples, if possible from different individuals. Taller trees were sampled by shooting branches using shotguns (Marlin Model 55 Goose, Marlin Firearms Co, Madison, USA and Winchester Select Sporting II 12M, Winchester, Morgan, USA) with Buckshot 27 ammunition (27 $\times$ 6.2 mm pellets), aiming at single branches (Aerts et al., 2017). Samples from smaller trees were taken using a pole clipper. In both cases leaves from the upper part of the crown were preferably chosen. Trees growing in canopy gaps were sampled in the center of these gaps, in order to collect the most sunlit leaves from these individuals. For broadleaved trees, each sample consisted of 10 to 15 undamaged leaves, depending on leaf size. The samples of the only coniferous tree species *P. sylvestris* consisted of at least 20 needles from both the current and the last growing season. In total, we collected 328 leaf samples from nine different tree species. Leaves were put in sealed plastic bags and stored in cooling boxes. At the end of each field day samples were weighed, and then dried at 80°C for 48 hours.

Back from the field, leaves were milled prior to the analysis. N_{mass} was measured applying the Dumas method using a vario MACRO element analyzer (Elementar Analysensysteme, Hanau, Germany). P_{mass} was measured using an inductively coupled plasma-optical emission spectrometer (ICP-OES) (Varian 725ES, Varian Inc., Palo Alto, CA, USA). For each field plot, we calculated community weighted mean values for N_{mass} and P_{mass}, taking the basal area of each species in the corresponding plot as the weight. The relative basal area is a good approximation for relative canopy cover of the tree species co-occurring in a forest stand (Cade, 1997; Gill et al., 2000). The relative canopy cover corresponds to the contribution of each species to the reflectance signal of a mixed forest canopy. Although field samples were collected one year after the acquisition of remote sensing data, we consider our field data set as a solid basis for the prediction of N_{mass} and P_{mass}. Previous studies indicate

that in temperate tree species there are no remarkable differences in leaf chemical contents between two consecutive years (Reich et al., 1991; Smith et al., 2003). Furthermore, N$_{mass}$ in deciduous broadleaved species typically shows only little variation during the mid-growing season (McKown et al., 2013; Niinemets, 2016; Reich et al., 1991) and remains stable under drought conditions (Grassi et al., 2005; Wilson et al., 2000). The latter point is noteworthy, because the early summer of 2015 was dryer compared to the year 2014.

2.1.2.3 Remote sensing data

We used airborne imaging spectroscopy data (284 bands, 380 nm – 2500 nm) acquired by the Airborne Prism Experiment (APEX) spectrometer with a spatial resolution of 3 m × 3 m, and airborne discrete return LiDAR data with an average point density of 23 points per m^2, both covering the entire study area. APEX data were acquired on July 24, 2014 (9:56 – 11:25 UTC + 2h) at a flight height of 5400 m by the Flemish Institute of Technology (VITO, Mol, Belgium). The data, consisting of 12 flight lines, were delivered geometrically and atmospherically corrected using the standard processing chain applied to APEX recorded images (Sterckx et al., 2016; Vreys et al., 2016). Bands from both ends of the spectra and bands disturbed by water absorption were deleted prior to the analysis. In total, we included 245 spectral bands between 426 nm and 2425 nm for subsequent analyses. We applied a Normalized Differenced Vegetation Index (NDVI) mask in order to exclude values from pixels with bare soil and ground vegetation (Asner et al., 2015). For this purpose, we calculated NDVI values for each pixel and excluded pixels with a NDVI below 0.75. For all remaining pixels we applied a brightness normalization to reduce the influence of canopy shades on the spectral signal (Feilhauer et al., 2010).

LiDAR points were recorded in February 2014 at leaf-off conditions by Aerodata (Lille, France) using a Riegl LMS-680i with a maximum scan angle of 30°and a lateral overlap of neighboring flight lines of 65%. Average flight height during LiDAR data acquisition was 530 m resulting in a beam diameter of about 0.265 m. The LiDAR data were delivered including a classification of ground and vegetation returns and a digital terrain model (DTM). Height values of LiDAR points were normalized, by subtracting values of the underlying DTM. Vegetation returns were then aggregated into a grid with a cell size of 3 m × 3 m, taking the grid matrix of the imaging spectroscopy data as reference. For each pixel we calculated 19 different LiDAR-derived variables based on point statistics resulting in 19 raster layers. Calculated LiDAR-derived variables included basic summary statistics (e.g. maximum height) based on the height values of LiDAR points in each grid cell and inverse penetration ratios representing the fractional vegetation cover within given height thresholds (Tab. 2.1) (Ewald et al., 2014). Penetration ratios were calculated using the following formula:

$$vc_{h12} = (n_{h2} - n_{h1})/n_{h2} \tag{2.1}$$

where vc_{h12} is representing the vegetation cover within the height thresholds h1 and h2 (h1 < h2) within one grid cell. n_{h1} and n_{h2} represent the sum of all LiDAR points below the given height thresholds h1 and h2, respectively.

Table 2.1 Variables calculated from LiDAR point clouds in 3 m × 3 m resolution. For the use in partial least squares regression models, variables were aggregated into a grid with a cell size of 24 m × 24 m, by calculating mean and standard deviation.

LiDAR Metric	Abbreviation	Description
Minimum	min_h_mean; min_h_sd	Basic statistics
Maximum	max_h_mean; max_h_sd	based on the
Mean	mean_h_mean; mean_h_sd	height values of
Standard deviation	sd_h_mean; sd_h_sd	vegetation LiDAR
Variance	var_h_mean; var_h_sd	points
Coefficient of variation	cov_h_mean; cov_h_sd	
10th percentile	perc10_h_mean; perc10_h_sd	
25th percentile	perc25_h_mean; perc25_h_sd	
50th percentile	perc50_h_mean; perc50_h_sd	
75th percentile	perc75_h_mean; perc75_h_sd	
90th percentile	perc90_h_mean; perc90_h_sd	
Fractional cover 0.5m – 2m	fcover_05_2_mean; fcover_05_2_sd	Inverse penetration
Fractional cover 0.5m – 60m	fcover_05_60_mean; fcover_05_60_sd	ratios representing
Fractional cover 2m – 6m	fcover_2_6_mean; fcover_2_6_sd	an estimate for
Fractional cover 2m – 60m	fcover_2_60_mean; fcover_2_60_sd	fractional cover of
Fractional cover 6m – 10m	fcover_6_10_mean; fcover_6_10_sd	the vegetation
Fractional cover 6m – 60m	fcover_6_60_mean; fcover_6_60_sd	within given height
Fractional cover 10m – 20m	fcover_10_20_mean; fcover_10_20_sd	thresholds
Fractional cover 20m – 60m	fcover_20_60_mean; fcover_20_60_sd	

From both imaging spectroscopy and LiDAR raster layers, we extracted values from all pixels overlapping with the 50 field plots to be used as input to the statistical models. For each plot, we calculated the weighted mean values of 245 hyperspectral bands and 19 LiDAR-variables (Tab. 2.1) from the extracted cell values, using the percent overlap of each cell with the plot area as weight. Similarly, we calculated the weighted standard deviation for LiDAR-derived variables which represent a measure of spatial heterogeneity of these variables.

For prediction we aggregated the pixels of the imaging spectroscopy and LiDAR raster layers to a grid with a pixel size of 24 m × 24 m, calculating the mean and the standard deviation (for LiDAR-derived variables only) of all aggregated cells. This finally resulted in a dataset containing 245 spectral bands and 38 LiDAR-derived variables (mean and standard deviation).

2.1.2.4 Model calibration and validation

For both response variables, N_{mass} and P_{mass}, we built predictive models using the extracted values from the raster layers at plot locations as predictors. We calculated partial least squares regression (PLSR) models with a step-wise backward model selection procedure implemented in the R package autopls (R Core Team, 2016; Schmidtlein et al., 2012). The

number of latent variables was chosen based on the lowest root mean squared error (RMSE) in leave-one-out cross-validation. Before model calibration predictors were normalized, dividing each predictor variable by its standard deviation.

To test the benefit of LiDAR-derived data for the prediction of community weighted means of N_{mass} and P_{mass} at the canopy level we fit two sets of models for each response variable, one incorporating the hyperspectral bands only and a second one using a combination of hyperspectral bands and LiDAR-derived variables as predictors. To test the independent contribution of LiDAR data on the predictions, we additionally fit a third set of models for both N_{mass} and P_{mass} including only LiDAR-derived variables as predictors. N_{mass} values were natural log transformed prior to the model calculations.

The model calculations and predictions were embedded in a resampling procedure with 200 permutations, in order to reduce the bias in model predictions, yielding to a better comparison between the three sets of models. In each permutation, a subsample of 40 out of the 50 field plots was randomly drawn without replacement and used for model calibration and validation. Each model was used to generate a prediction map with a grid size of $24\,\text{m} \times 24\,\text{m}$, resulting in 200 prediction maps for each response variable and each of the three predictor combinations used, respectively. From these maps we calculated a median prediction map and the associated coefficient of variation (CV), representing the spatial uncertainty of model predictions (Singh et al., 2015).

For the assessment of the predictive performance of the models, we calculated the mean Pearson r-squared as well as the absolute and normalized root mean squared error (RMSE) between predicted and observed values of each data subset. The same performance measures were calculated for each data subset in leave-one-out cross-validation data. For N_{mass}, r-squared values and RMSE were calculated based on the log-transformed dataset. The normalized RMSE was calculated by dividing the RMSE by the mean value in the response dataset. r-squared and RMSE values were used to compare the performances of models using only hyperspectral bands or a combination of hyperspectral bands and LiDAR-derived variables as predictors, for N_{mass} and P_{mass} respectively. Model performance is affected by the number of variables included, in the case of a PLSR the number of latent variables. To check for such an effect we grouped the corresponding models according to the number of latent variables included and compared the r-squared values for each group separately (supplementary material, Fig. 2.12).

2.1.3 Results

Field plots were located in forest stands with heights ranging from 3 to $40\,\text{m}$ and LAI values ranging from 1.7 to 5.9 (supplementary material, Tab. 2.4). Plot-wise community weighted mean values for N_{mass} and P_{mass} ranged from 13.8 to $25.4\,\text{g·kg}^{-1}$ and from 0.82 to $1.93\,\text{g·kg}^{-1}$, respectively. N_{mass} of *P. serotina* and *P. sylvestris* were significantly different from all other species (supplementary material, Fig. 2.13 and, Tab. 2.5). Contrary, we

observed no differences in measured N_{mass} between. *F. sylvatica*, *Q. robur* and *C. betulus*. P_{mass} differed significantly between all species except between *C. betulus* and *Q. robur* (supplementary material, Fig. 2.13). Models combining structural vegetation attributes, derived from airborne LiDAR, with imaging spectroscopy improved predictions of community weighted mean values for N_{mass} and P_{mass} compared to models using imaging spectroscopy data solely (Tab. 2.2, Fig. 2.2). In the combined N_{mass} models, hyperspectral bands had a significantly higher contribution ($p < 0.001$) to the variance explained, compared to LiDAR-derived variables (Fig. 1). By contrast, in P_{mass} models, LiDAR-derived variables showed a significantly higher contribution ($p < 0.001$). With respect to the selected spectral bands we observed only marginal differences between models including LiDAR-derived variables and models not including them (Figs. 2.3, 2.4, 2.5, 2.6).

Table 2.2 Results of PLSR models for N_{mass} and P_{mass} from 200 bootstraps. Predictors: used predictor variables being either, hyperspectral bands (HS) or LiDAR-derived variables; # LV: mean number of latent variables; # Var: mean number of selected predictor variables; R_{cal}^2: mean coefficient of determination in calibration; R_{cv}^2: mean coefficient of determination in validation; $RMSE_{cal}$: average root mean squared error in calibration; $RMSE_{cv}$: average root mean squared error in leave-one-out cross-validation

| Response	Predictors	#LV	#Var	R_{cal}^2	R_{cv}^2	$RMSE_{cal}$	$RMSE_{cv}$	$RMSE_{cal}$ [%]	$RMSE_{cv}$ [%]
N_{mass}*	HS	5.8	98	0.47	0.31	0.09	0.09	2.9	3.3
				± 0.10	± 0.14	± 0.01	± 0.01		
	HS & LiDAR	5.7	43	0.55	0.41	0.08	0.09	2.7	3.0
				± 0.12	± 0.16	± 0.01	± 0.01		
	LiDAR	3.5	8	0.39	0.26	0.09	0.10	3.1	3.4
				± 0.08	± 0.09	± 0.01	± 0.01		
P_{mass}	HS	6.3	42	0.59	0.45	0.15	0.18	13.1	15.3
				± 0.15	± 0.16	± 0.02	± 0.02		
	HS & LiDAR	6.9	38	0.73	0.63	0.13	0.14	10.8	12.5
				± 0.08	± 0.10	± 0.02	± 0.02		
	LiDAR	3.7	9	0.62	0.54	0.15	0.17	12.6	14.0
				± 0.08	± 0.10	± 0.01	± 0.01		

∗natural log-transformed
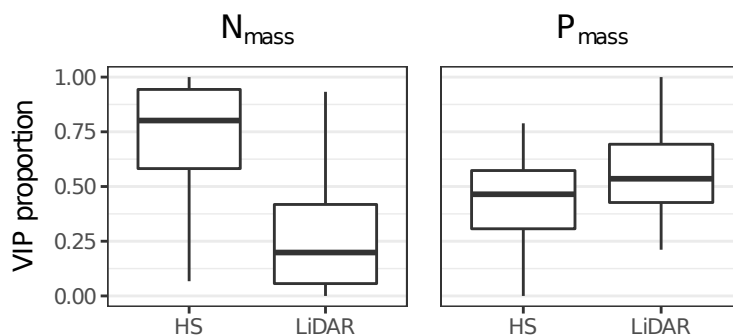
Figure 2.1 Relative contribution of hyperspectral bands (HS) and LiDAR variables to the variance explained in PLSR models for N_{mass} and P_{mass} expressed as proportion of the total VIP (Variable Importance in Projection) score.
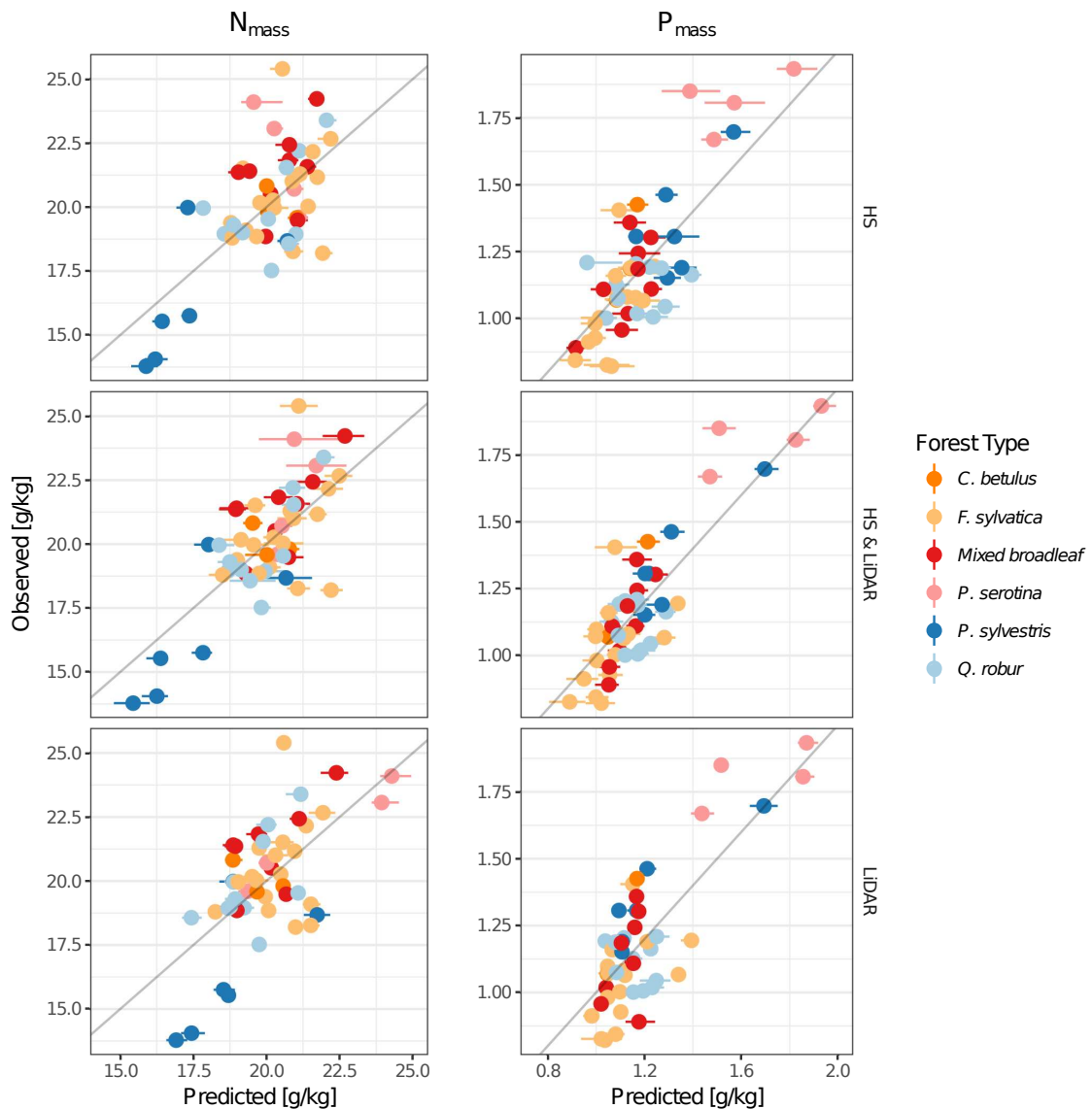
Figure 2.2 Mean predicted values resulting from 200 model predictions displayed against observed values for N_{mass} and P_{mass} of 50 field plots. Error bars represent lower and upper quantiles of the predictions. The figures show results from models using hyperspectral bands (HS, top), LiDAR-derived predictors (LiDAR, bottom) and a combination of both (HS & LiDAR, middle). The coloring highlights different forest types represented by dominant tree species.

For N_{mass} the average R^2_{cv} values resulting from leave-one-out cross-validation for each bootstrap model increased from 0.31 to 0.41 whereas the mean relative RSME decreased only moderately (see Tab. 2.2) when adding LiDAR-derived variables. Models fitted by LiDAR-derived predictors solely resulted in a mean R^2_{val} value of 0.25. The most important LiDAR-derived variables in the models predicting of N_{mass} were, according to VIP values, related to the horizontal variation of canopy cover (fcover_05_60_sd, fcover_2_6_sd, fcover_6_10_sd, fcover_6_60_sd) (Figs. 2.7, 2.8). The most important spectral bands were located in the VIS and the SWIR between 2000 and 2400 nm, irrespective of whether
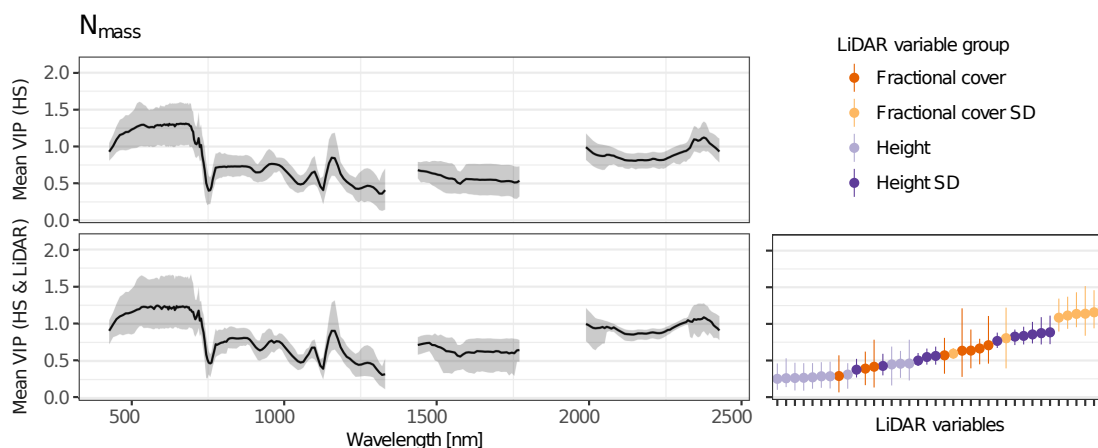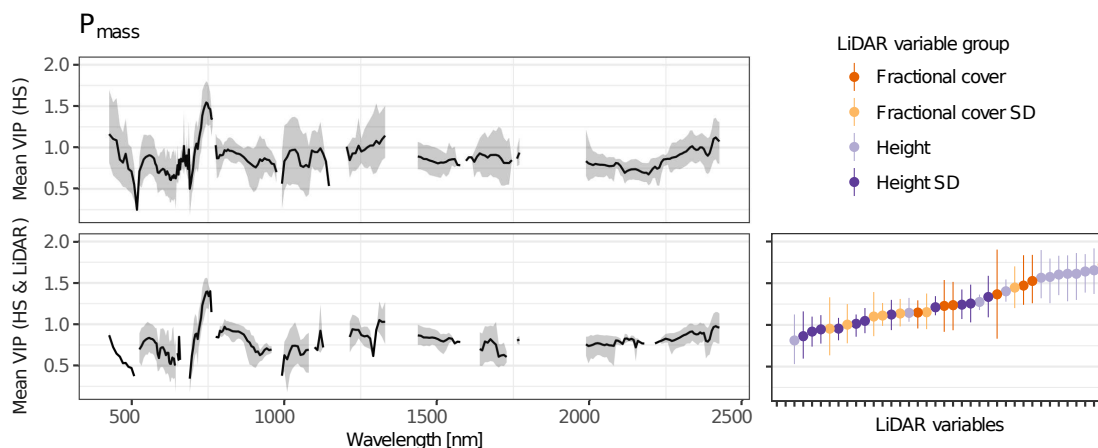
Figure 2.3 Mean VIP (Variable Importance in Projection) values of hyperspectral bands and LiDAR-derived variables resulting from 200 PLSR models for the prediction of N$_{mass}$. The top panel is showing the results from models using hyperspectral bands only, bottom panels display results from models using a combination of hyperspectral bands and LiDAR-derived predictors. Gray areas indicate the range between the 10th and the 90th percentiles. The bottom right panel is displaying mean VIP values of used LIDAR variables. For simplification LIDAR variables were grouped into four classes representing the vegetation cover (Fractional cover), the horizontal variability of vegetation cover (Fractional cover SD), LiDAR height metrics (Height), and the horizontal variability of LiDAR height metrics (Height SD).

Figure 2.4 Mean VIP (Variable Importance in Projection) values of hyperspectral bands and LiDAR-derived variables resulting from 200 PLSR models for the prediction of P$_{mass}$. The top panel is showing the results from models using hyperspectral bands only, bottom panels display results from models using a combination of hyperspectral bands and LiDAR-derived predictors. Gray areas indicate the range between the 10th and the 90th percentiles. The bottom right panel is displaying mean VIP values of used LIDAR variables. For simplification LIDAR-derived variables were grouped into four classes representing the vegetation cover (Fractional cover), the horizontal variability of vegetation cover (Fractional cover SD), LiDAR height metrics (Height), and the horizontal variability of LiDAR height metrics (Height SD).

only imaging spectroscopy or a combination of imaging spectroscopy and LiDAR data was used (Fig. 2.3).

For P$_{mass}$, average R^2_{cv} values resulting from leave-one-out cross-validation for each bootstrap model increased from 0.45 to 0.63 and the mean relative RSME decreased from
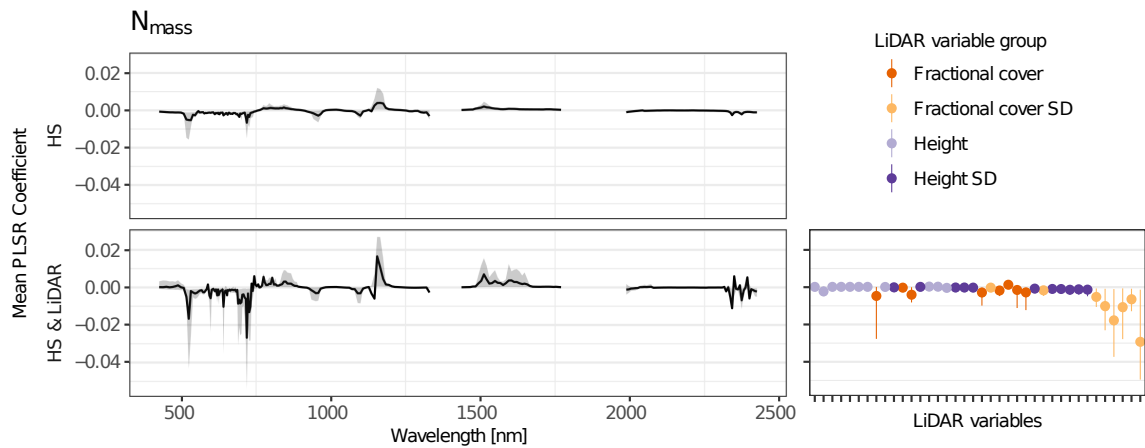
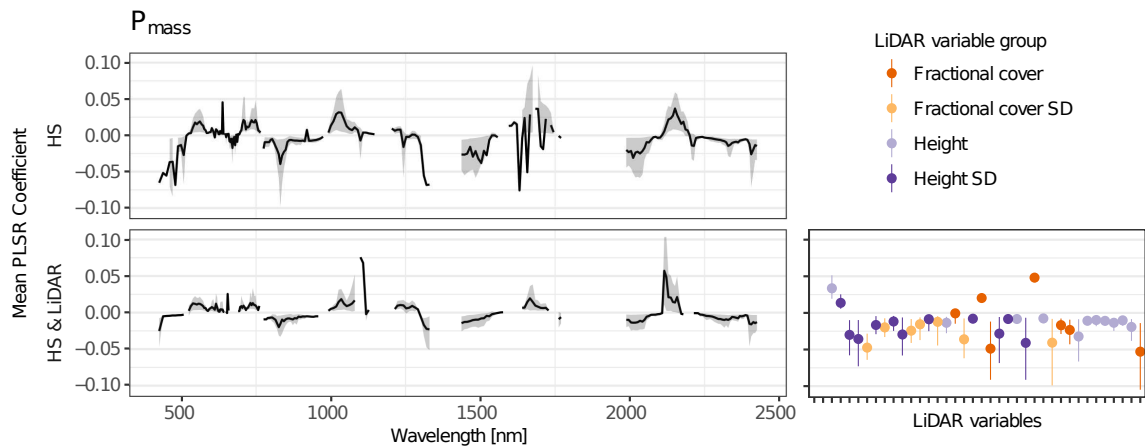**Figure 2.5** Mean PLSR Coefficients of hyperspectral bands and LiDAR-variables resulting from 200 model calculations for predicting N$_{mass}$. The top panel is showing the results from models using hyperspectral bands only, bottom panels display results from models using a combination of hyperspectral bands and LiDAR-derived variables. Gray areas indicate the range between the 10th and the 90th percentile. The bottom right panel is displaying mean PLSR coefficients of used LiDAR-derived variables. For simplification LiDAR-derived variables were grouped into four classes representing the vegetation cover (Fractional cover), the horizontal variability of vegetation cover (Fractional cover SD), LiDAR height metrics (Height), and the horizontal variability of LiDAR height metrics (Height SD). LiDAR variables are displayed in ascending order by variable importance.

Figure 2.6 Mean PLSR Coefficients of hyperspectral bands and LiDAR-derived variables resulting from 200 model calculations for predicting P$_{mass}$. The top panel is showing the results from models using hyperspectral bands only, bottom panels display the results from models using a combination of hyperspectral bands and LiDAR-derived variables. Gray areas indicate the range between the 10 th and the 90 th percentile. The bottom right panel is displaying mean PLSR Coefficients of used LiDAR-derived variables. For simplification LiDAR-derived variables were grouped into four classes representing the vegetation cover (Fractional cover), the horizontal variability of vegetation cover (Fractional cover SD), LiDAR height metrics (Height), and the horizontal variability of LiDAR height metrics (Height SD). LiDAR variables are displayed in ascending order by variable importance.

15.3 to 12.5 (see Tab. 2.2), when LiDAR-derived predictors were included. Models fitted by LiDAR-derived predictors solely resulted in a mean R^2_{cv} value of 0.54. Regression coefficients for the most important LiDAR-derived predictors, according to the relative VIP,
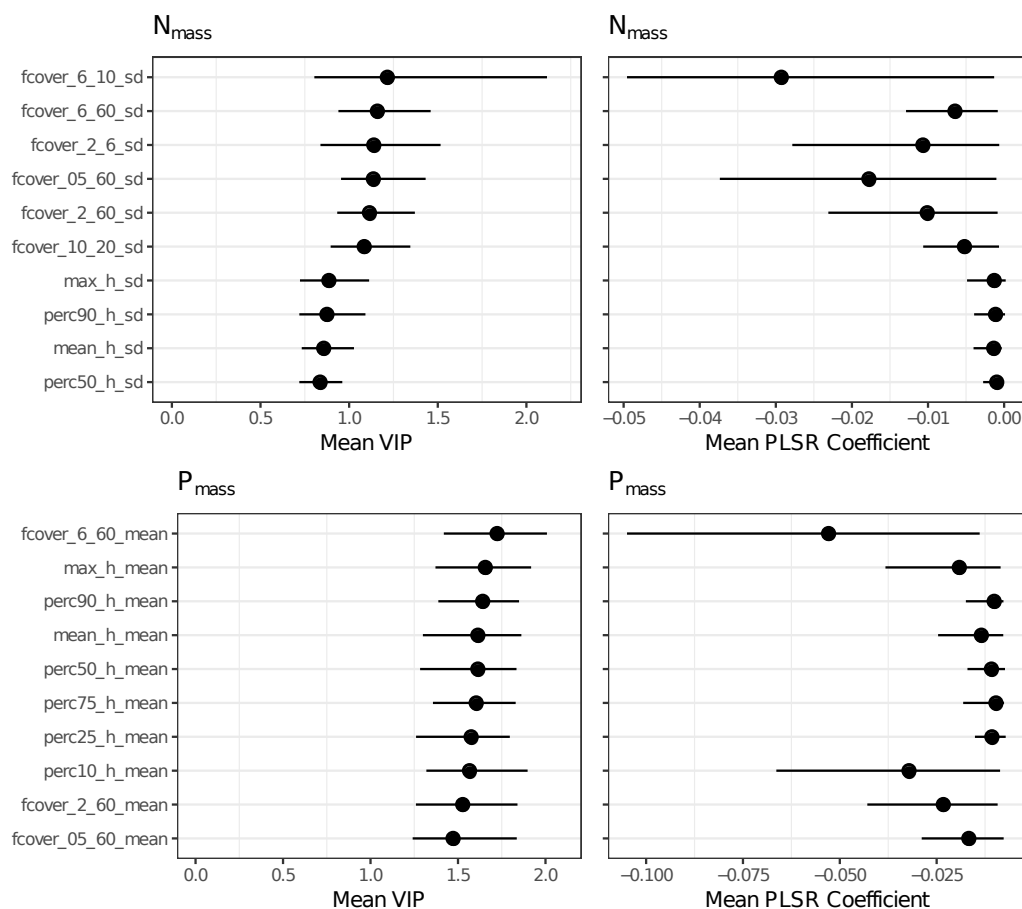
Figure 2.7 Mean VIP values (left) and mean PLSR coefficients (right) resulting from 200 PLSR models for the prediction of N_{mass} (top) and P_{mass} (bottom) for the ten most important LiDAR-derived variables in models using a combination of hyperspectral bands and LiDAR-derived as predictors. Error bars indicate the range between the 10th and 90th percentile.

indicated a negative relation between P_{mass} and the fractional cover of trees larger than 6 m (fcover_6_60_mean) (Figs. 2.7, 2.8). Moreover, important LiDAR-derived variables indicated a negative relation of P_{mass} to the stand height (max_h_mean, perc90_h_mean, mean_h_mean) (Figs. 2.7, 2.8). Additionally, fcover_2_6_mean, related to the cover of shrubs, was the most important variable in P_{mass} models using LiDAR-derived variables solely (Fig. 2.8). Important hyperspectral bands were distributed across the whole spectrum with a pronounced peak around 730 nm (Fig. 2.4). The permutation of the calibration data according to the main forest types revealed that the success of N_{mass} and P_{mass} models was strongly dependent on two forest types being included (Fig. 2.9). N_{mass} models showed poor predictive performances when *P. sylvestris* stands were not included in the calibration dataset. Similarly, the absence of *P. serotina* dominated stands resulted in poor predictive performance of P_{mass} models. This observation was consistent regardless of whether hyperspectral or LiDAR data were used as predictors. Additionally, model performances were strongly influenced by the variance in canopy height and gap fraction of
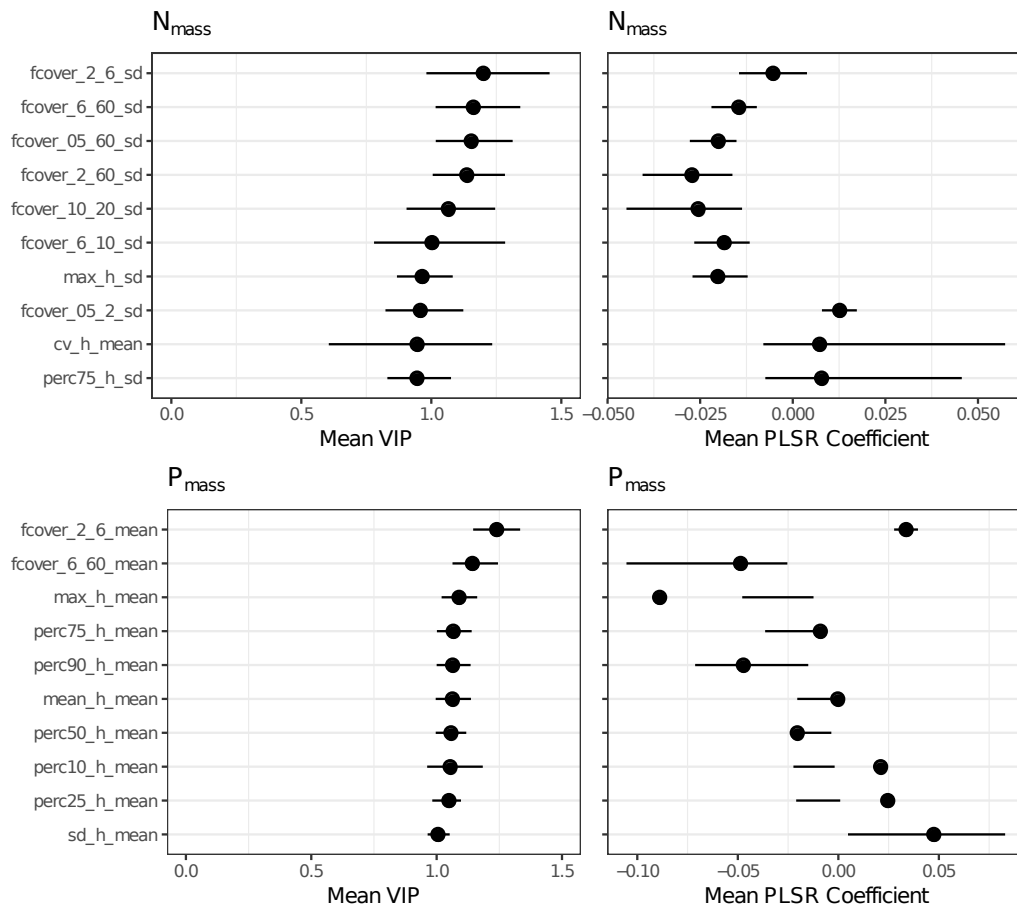
Figure 2.8 Mean VIP values (left) and mean PLSR coefficients (right) resulting from 200 PLSR models for the prediction of N_{mass} (top) and P_{mass} (bottom) for the ten most important LiDAR-derived variables in models using LiDAR-derived predictors only. Error bars indicate the range between the 10th and 90th percentiles.

field plots included in each data permutation (Fig. 2.10). P_{mass} models performed better with increasing variance in both structural properties. This contrasted with N_{mass} where the performance of imaging spectroscopy models decreased with increasing variation in canopy height and gap fraction. The performance of N_{mass} models was less affected by structural variation, when including LiDAR-derived variables (Fig. 2.10).

2.1.4 Discussion

In this study we showed that LiDAR-derived information on canopy structure improved predictions of N_{mass} and P_{mass} based imaging spectroscopy instructurally heterogeneous forest stands. This finding is in accordance with previous studies using optical remote sensing data, which report a strong contribution of NIR reflectance for the prediction of N_{mass} in forest canopies (e.g. Martin et al., 2008; Ollinger et al., 2008; Wang et al., 2016)), that can be attributed to canopy structural properties (Knyazikhin et al., 2013; Ollinger,
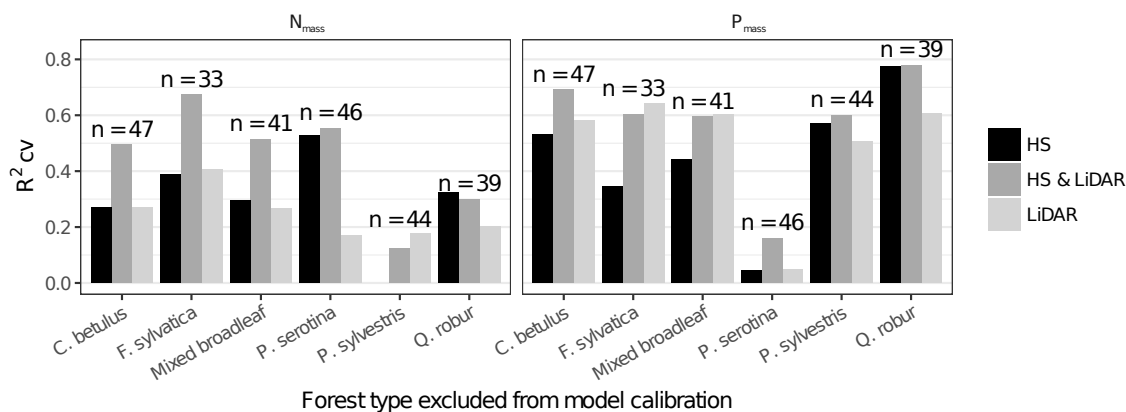
Figure 2.9 Predictive performances of N_{mass} and P_{mass} models using permuted calibration datasets according to occurring forest types. In each data permutation one forest type was excluded from the calibration dataset. Numbers above the bars represent the number of field plots included in each calibration dataset. HS: models using hyperspectral data; HS & LiDAR: models using a combination of hyperspectral and LiDAR data; LiDAR: models using LiDAR data only.
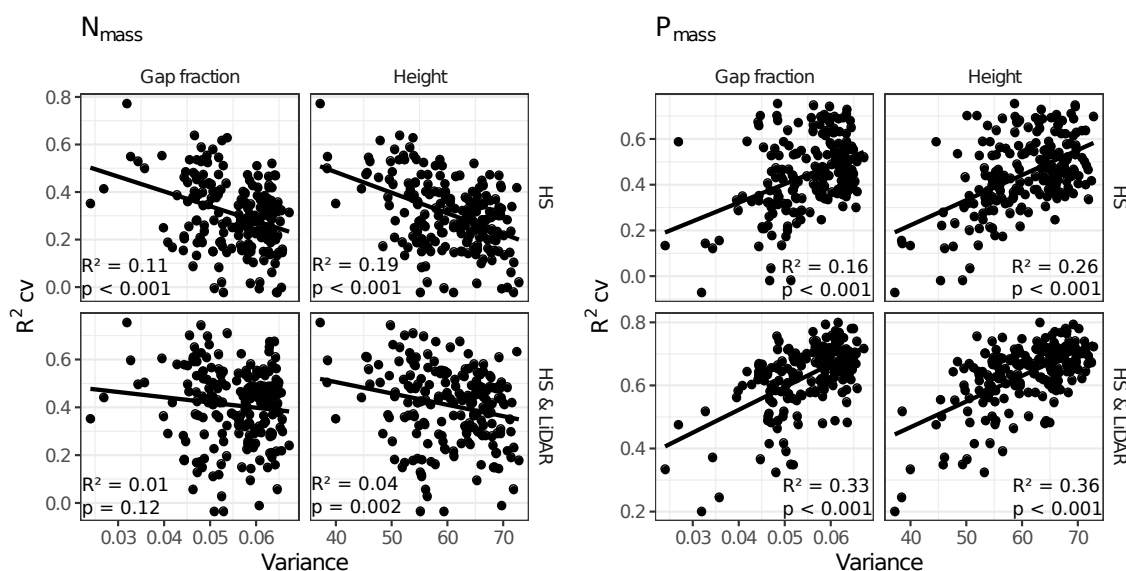

Figure 2.10 Predictive performances of N_{mass} and P_{mass} models depending on the variance of canopy gap fraction and canopy height included in the calibration dataset, Points represent the results from 200 model repetitions using permuted calibration data. Lines and values in each panel represent results from univariate linear regression between displayed variables. Top panels are showing the results from models using imaging spectroscopy data (HS) only, bottom panels the results from models using a combination of imaging spectroscopy and LiDAR data.

2011). Similarly, Badgley et al. (2017) found gross primary production on a global level to be strongly related to structure-sensitive NIR reflectance. These results point at the existence of functional links between the biochemical and structural composition of forest canopies.

An ecological explanation of such linkages follows from the economic theory (Bloom et al., 1985). The economic theory states that investments in the photosynthetic machinery of
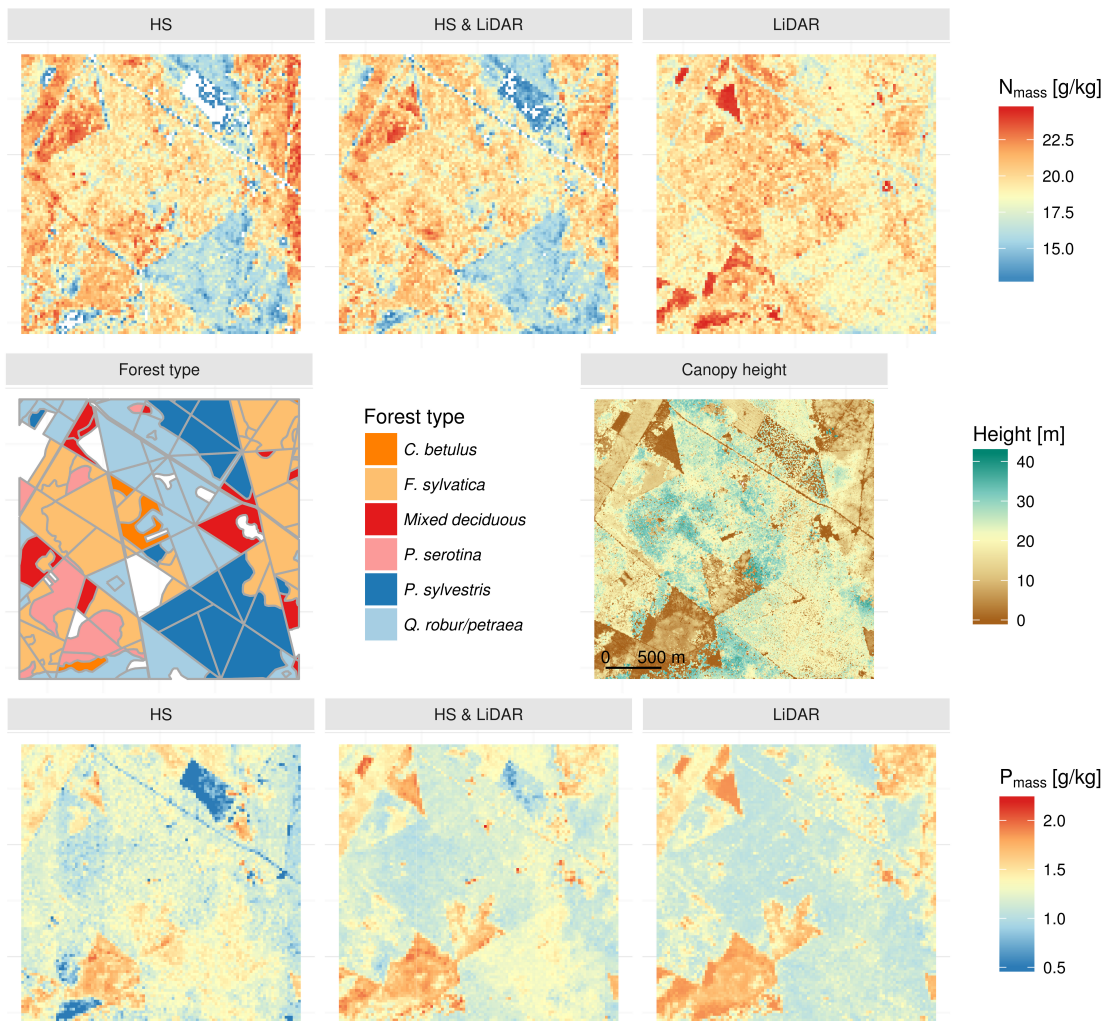
Figure 2.11 Map sections showing forest types represented by their dominant tree species, a canopy height model (both in the middle) and median predictions of canopy level N_{mass} (top) and P_{mass} (bottom) from models using hyperspectral bands (HS), LiDAR-derived predictors (LiDAR) or a combination of both (HS+LiDAR).

plants will be realized only when the benefit of these investments exceeds the anticipated costs. As a result, plant traits with small cost-to-benefit relationship are favored under resource limitation, leading to a functional convergence of structural and physiological traits. At the leaf level, for example, the negative correlation between leaf mass per area and leaf nitrogen or phosphorus concentration can be attributed to functional convergence (Díaz et al., 2016; Shipley et al., 2006; Wright et al., 2004). Ecological theory suggests that, similar to the leaf level, functional convergence can also be expected at the canopy level (Field, 1991) leading to linkages between structural and biochemical canopy properties. In temperate and boreal forest ecosystems, links between structure and biochemistry are expressed at both the leaf and the canopy level. For example, broadleaved and coniferous trees show notable structural differences at the canopy level which are expressed in different crown

geometry, branching architecture and leaf angle distribution (Ollinger, 2011). Both, leaf and canopy structural properties have shown to influence spectral reflectance in similar ways, resulting in higher reflectance of broadleaved canopies (Knyazikhin et al., 2013; Ollinger, 2011). At the same time, broadleaved trees are characterized by higher N_{mass} compared to coniferous tree species (Güsewell, 2004; Han et al., 2005; McNeil et al., 2008; Serbin et al., 2014). Furthermore, case studies show that forest canopy N_{mass} or P_{mass} can be also related to other structural properties, such as stand density, above ground biomass or crown-closure (Craven et al., 2015; Gökkaya et al., 2015; Sardans and Peñuelas, 2015; Vilà-Cabrera et al., 2015).

In the specific context of this study, the success of N_{mass} and P_{mass} predictions was strongly dependent on the presence of two forest types that exhibited biochemical and structural differences compared to the co-occuring forest types. N_{mass} predictions depended on the presence of *P. sylvestris* stands in the calibration dataset. *Pinus sylvestris* was the only coniferous species in our study and was characterized by significantly lower N_{mass} than all other species. In contrast, P_{mass} predictions were mainly driven by *P. serotina*, which was the species characterized by the highest P_{mass} concentrations in our study area. Structural differences between *P. serotina* and the other tree species in our study area mainly arise from its growth strategy and habitat preferences. *Prunus serotina* is an early successional tree species with significantly smaller growth heights compared to other tree species predominant in our study area. *Prunus serotina* is often a dominant species in young stands and often occurs in mature stands with sparse canopies or in canopy gaps. Our results suggest that species differences in structural and/or optical properties can serve as a surrogate to predict canopy chemistry using remote sensing, at least across small study extents, where differences in leaf nutrient concentrations can often be explained by differences between species (Craven et al., 2015; McNeil et al., 2008). For larger environmental gradients, differences between species are often superimposed by the high intra-specific variability of leaf biochemicals (Asner et al., 2012; Mellert and Göttlein, 2012; Vilà-Cabrera et al., 2015), which respond to strong variation in climate and soil properties (Sardans et al., 2015; Sun et al., 2015). The fact that our results were strongly dependent on the occurrence of two species is limiting the transferability of our findings to other study areas or broader spatial extents. However, functional differences (e.g. between broadleaved and coniferous species or between early and late successional species) that are manifested in structural and biochemical properties (Craven et al., 2015; Kusumoto et al., 2015; Sardans and Peñuelas, 2015; Vilà-Cabrera et al., 2015) suggest that canopy structure can serve as a surrogate for predicting biochemical properties also in different study contexts.

Mapping N_{mass}

Predicting forest canopy N_{mass} using imaging spectroscopy has a long history. Compared to previous studies, which often report good (e.g. Smith et al., 2003; Townsend et al., 2003;

Wang et al., 2016) or even excellent (e.g. Martin et al., 2008; Singh et al., 2015) predictive performances, our models performed poorly. We attribute this mainly to the high structural diversity of the forest stands used for model calibration. This high structural diversity was, for example, expressed by strong variation of LAI values even within stands of the same forest type (i.e. ranging from 1.8 to 6.1 for *F. sylvatica* stands). Canopy structure strongly affects reflectance (Gerard and North, 1997; Rautiainen et al., 2004) and a high variability in LAI has been found to hamper predictions of leaf biochemistry at the canopy level (Asner and Martin, 2008). Furthermore, we included stands of different age classes, with canopy heights ranging between 2 and 40 meters, which also increases variation in canopy reflectance, especially in the VIS (Roberts et al., 2004). Our results suggest, that including LiDAR data can help to diminish these effects of structural heterogeneity, when mapping N$_{mass}$ (see Fig. 2.10).

In part, the weak predictive performance of our N$_{mass}$ models can be attributed to the relatively low data range of N$_{mass}$ in our study area (cf. Asner et al., 2015; Huber et al., 2008; Martin et al., 2008; Singh et al., 2015; Smith et al., 2003; Wang et al., 2016). The range was especially low for all broadleaved species, with no significant differences between the two main species (*F. sylvatica*, *Q. robur*), which were predominant in 36 of 50 field plots (including mixed broadleaf). Furthermore, the weak model performance can, presumably, also be attributed to the usage of mass related nitrogen measures, because spectral reflectance is more closely linked to leaf biochemistry on an area basis (Grossman et al., 1996; Roelofsen et al., 2014).

Furthermore, the performance of the N$_{mass}$ models may also be explained by the fact that image acquisition and leaf sampling were from different years. Although previous studies suggest, that there is only low variation of N$_{mass}$ in temperate forest species between two consecutive years and during one growing season (McKown et al., 2013; Niinemets, 2016; Reich et al., 1991; Smith et al., 2003), we cannot be 100% sure that relative differences between the species in our study area were stable between the years. Fajardo and Siefert (2016) found different patterns in N$_{mass}$ between coniferous and broad leaf species in the course of one growing season. However, they also found that overall species rankings concerning N$_{mass}$ were stable throughout a growing season.

The most important spectral bands selected in our N$_{mass}$ models were situated in the visible part of the spectrum. A high contribution of the VIS region for N$_{mass}$ prediction, using imaging spectroscopy, was also observed by Asner et al. (2015) and Singh et al. (2015). In our study the importance of bands in the VIS can be attributed to differences in reflectance between coniferous and broadleaved forest stands in this spectral region. (see supplementary material Fig. S4). These differences may arise from light absorption of chlorophyll but may also be due to other leaf pigments, like carotenoids and anthocyanins, that also have absorption characteristics in the VIS (Ollinger, 2011; Ustin et al., 2009). Moreover, structural canopy properties such as LAI or leaf angle distribution also influence

reflectance in the VIS, albeit to a lower extent than leaf pigments (Jacquemoud et al., 2009). This is in accordance to previous studies that report the importance of the VIS region to discriminate between species (Fassnacht et al., 2016; Roberts et al., 2004).

VIP values indicated only a minor contribution of spectral bands located in the NIR and SWIR, which is contrary to results of previous studies using image spectroscopy (Homolová et al., 2013). According to Ollinger (2011) NIR reflectance is especially important in datasets with only little variance in the VIS reflectance. The high variance in the VIS reflectance (see supplementary material Fig. S3) observed in this study may thus be an explanation for the minor contribution of NIR and SWIR bands. Additionally, any signal in the infrared reflectance may be strongly disturbed, by the high variability of canopy gaps in the field plots used for this study (Ollinger, 2011).

For mapping N_{mass}, important LiDAR-derived variables were mainly connected to the horizontal variation of canopy cover (fcover_6_10_sd, fcover_6_60_sd, fcover_2_6_sd). These three variables represent the variation of the fractional vegetation cover between different height thresholds, in one $24\,\mathrm{m} \times 24\,\mathrm{m}$ pixel. They can thus be interpreted as indicators for spatial heterogeneity of the canopy. The most important LiDAR-derived variable for predicting canopy level N_{mass} was the spatial variation of fractional vegetation cover between 6 and $10\,\mathrm{m}$ height (fcover_6_10_sd), which is related to the occurrence of shrubs or small trees in the understory. Low values either indicate little vegetation present between 6 and $10\,\mathrm{m}$ height, as it can be observed in mature forest stands with closed canopies, or very dense homogeneous vegetation, as it can be observed in earlier successional stages. High values indicate heterogeneous, typically old-grown forest stands with gaps that are filled by young trees. Similarly, fcover_6_60_sd is related to the horizontal heterogeneity of the tree canopy cover, that was highest in *P. sylvestris* stands (supplementary material, Fig. S5). Moreover fcover_2_6 also was highest in *P. sylvestris* stands, indicating that LiDAR-derived variables helped to accentuate differences in N_{mass} between *P. sylvestris* and broadleaved species.

In summary, N_{mass} predictions were strongly dependent on the presence of the only coniferous tree species, *P. sylvestris.* Stands of *P. sylvestris* were characterized by lower N_{mass} and higher spatial variation of canopy cover compared to broadleaved forest stands. These structural differences could be well captured by LiDAR data (supplementary material, Fig. S5). Hence, integrating LiDAR-derived information improved models based on imaging spectroscopy data solely. The poor performance of models, using hyperspectral data solely, can be attributed to the high structural heterogeneity in the study area, in terms of LAI and stand ages. Our results suggest, that LiDAR data can help to diminish the effect of canopy heterogeneity when mapping forest N_{mass} using imaging spectroscopy.

Mapping P$_{mass}$

Mapping leaf phosphorus with remote sensing has received much less attention compared to N$_{mass}$. Earlier mapping attempts were based on hyperspectral indices (Mirik et al., 2005), radiative transfer models (Porder et al., 2005) and empirical models (Asner et al., 2015; Gökkaya et al., 2015). Gökkaya et al. (2015) achieved excellent predictive performances mapping P$_{mass}$ in a boreal mixed forest using Hyperion imaging spectroscopy data. Asner et al. (2015) successfully mapped P$_{mass}$ along a broad environmental gradient using airborne hyperspectral data and partial least squares regression. Contrary to N$_{mass}$, P$_{mass}$ has no characteristic absorption features in the used wavelength range and thus the success of mapping P$_{mass}$ can be rather attributed to correlations to other canopy properties. For many plant species, P$_{mass}$ is positively correlated with N$_{mass}$ (Elser et al., 2010; Güsewell, 2004) or leaf mass per area (Wright et al., 2004). For temperate tree species, Sardans et al. (2015) found a negative correlation between above ground biomass and leaf N:P ratio, due to higher P retention with increasing age.

Important bands for the prediction of P$_{mass}$ were located throughout the whole range of the spectra. Asner et al. (2015) and Gökkaya et al. (2015) found similar results with important bands located in the VIS, SWIR and NIR regions. The most important selected LiDAR-derived variables were related to the cover of shrubs and the cover of trees (fcover_2_6_mean, fcover_6_60_mean). While the shrub cover was positively related to P$_{mass}$, tree canopy cover had an negative relationship, both indicating higher P$_{mass}$ in very young and very open stands. We furthermore observed a negative relation between P$_{mass}$ and LiDAR-derived variables related to vegetation height (e.g. max_h_mean, perc90_h_mean, mean_h_mean). These variables are correlated to the mean height of all LiDAR vegetation points and indicate that taller stands are related to lower P$_{mass}$. The observation of higher P$_{mass}$ in younger stands reflects the observation that earlier successional stages are often characterized by higher P$_{mass}$ (Chai et al., 2015; Eichenberg et al., 2015). Relations between important LiDAR-derived variables and P$_{mass}$ can also be well explained by species-specific differences within the study area. *Prunus serotina*, for which we observed highest P$_{mass}$ values, is a characteristic species of young and early-succesional stands in the forest of Compiègne. The observed negative relation between canopy cover and P$_{mass}$ can also be explained by species -specific differences, particularly between *P. serotina*, *P. sylvestris* and *F. sylvatica* (see supplementary material, Fig. S5). *Fagus sylvatica*, for which we observed smallest P$_{mass}$, is forming most dense canopies in Mid-Europe, while *P. sylvestris*, characterized by higher P$_{mass}$ than most of the native broadleaved species, is forming very sparse canopies. *Prunus serotina* most frequently occurred in forest stands with sparse canopy cover and good light conditions (Starfinger et al., 2003).

In summary, P$_{mass}$ predictions were driven by one tree species occurring in young or open forest stands. Existing covariation between canopy structure and P$_{mass}$ was better captured by LiDAR data than by imaging spectroscopy. The relative importance of structural

properties for mapping P$_{mass}$ is not surprising, as phosphorus is not expected to be directly represented in the spectral signal of plant canopies.

2.1.5 Conclusion

In this study we used a combination of imaging spectroscopy and airborne LiDAR data for mapping canopy N$_{mass}$ and P$_{mass}$ in a forest characterized by a high structural heterogeneity. For both, N$_{mass}$ and P$_{mass}$, LiDAR-derived variables improved predictions based on imaging spectroscopy solely. This highlights the importance of structural properties for remote sensing of biochemical variation in forest canopies. For N$_{mass}$ the poor performance of hyperspectral data alone can be attributed to the high structural heterogeneity in the study area, in terms of LAI and stand ages. LiDAR data helped to capture this heterogeneity and hence improve model performances. Both, N$_{mass}$ and P$_{mass}$ results were strongly influenced by the presence of only two tree species featuring structural and biochemical properties different from their co-occurring tree species. This limits the transferability of identified linkages between canopy structure and biochemistry to other study settings. However, in the case of N$_{mass}$, the known covariation with structural properties existing at the leaf and canopy level suggests that canopy structure used as proxy, can support the mapping of N$_{mass}$ also for different study settings. Information on canopy structure derived from airborne LiDAR can help to understand existing functional links.

2.1.6 Supplementary material

Table 2.3 Characteristics of the field plots. LAI: leaf area index measured at 1 m height above ground; Canopy gaps: estimated percentage of canopy gaps; Stand height: Dominant canopy height; Forest type: forest type represented by the dominant tree species covering at least half of the total basal area; # tree species: number of tree species in the overstory; # sampled species: number of species considered for leaf sampling

Plot ID	LAI	Canopy gaps [%]	Stand height [m]	Forest type	# tree species	# sampled species
I1082W	4.7	40	22	*P. sylvestris*	3	3
I1091E	4.7	15	22	Mixed broadleaf	4	4
I1112E.	5.4	5	29	*F. sylvatica*	4	3
I1262NE.	5.5	10	32	*F. sylvatica*	3	2
I1313SE	2.7	35	23	*F. sylvatica*	4	3
I1323E	4.6	35	34	*F. sylvatica*	2	2
I1451NE.	2.5	55	21	*P. sylvestris*	7	3
I1481E	2.1	65	13	*P. serotina*	4	1
I1510E	5.3	5	18	*C. betulus*	3	2
I1520S	4.7	20	33	Mixed broadleaf	5	5
I2041S	NA	15	22	*C. betulus*	7	3
I2151S	3.8	35	18	*C. betulus*	4	2
I2152S	3.4	50	24	*Q. robur*	4	3
I2161C	5	20	13	*F. sylvatica*	5	3
I3221S	4.9	5	29	Mixed broadleaf	4	3
I3282SE.	3.8	50	3	*P. serotina*	3	1
I3291SE	1.7	50	25	*Q. robur*	4	2
I3431NW	5.1	15	40	Mixed broadleaf	5	5
I3481E	5.9	40	21	Mixed broadleaf	6	4
I3482SE	5.2	45	25	Mixed broadleaf	6	2
I4021M	4	25	36	*Q. robur*	4	1
I4031W	4.8	10	20	*F. sylvatica*	4	2
I4050W	2.6	20	23	*F. sylvatica*	2	2
I7042E	3.6	20	27	*Q. robur*	5	3
I7061SE.	4.1	0	9	*P. sylvestris*	2	2
I7081SE	2.1	35	27	*P. sylvestris*	4	2
I7162W	2.9	10	28	*P. serotina*	2	2
I7193NW	3.7	40	28	*F. sylvatica*	6	2
I9012SW	2.1	40	28	*Q. robur*	5	3
I9012W	2.2	20	29	*Q. robur*	5	2
I9032SE.	3	30	2	*P. serotina*	3	1

| Plot ID	LAI	Canopy gaps [%]	Stand height [m]	Forest type	# tree species	# sampled species
N1452SW	5.2	0	19	*F. sylvatica*	2	1
N5171W	3.5	20	33	*Q. robur*	3	2
N5182S	3.5	15	34	*F. sylvatica*	1	1
N5191S	1.8	75	36	*F. sylvatica*	1	1
N6021S	4.6	30	34	*F. sylvatica*	3	2
N6152W	1.3	70	25	*Q. robur*	1	1
N6192N	1.1	60	26	*Q. robur*	2	1
N7301E	NA	25	28	Mixed broadleaf	5	3
N7301SE	4.7	5	22	*F. sylvatica*	3	1
N7391NE	5.8	20	26	*F. sylvatica*	1	1
N7392NW	3.8	10	25	*F. sylvatica*	2	2
N7392W	5.7	15	22	Mixed broadleaf	4	3
N7403W	6.1	30	28	*F. sylvatica*	4	3
N8092S	2.6	40	24	*P. sylvestris*	5	1
N8113S	5.8	5	18	*F. sylvatica*	5	2
N9161C	2.7	35	22	*P. sylvestris*	5	2
N9191SE	3.6	10	32	*Q. robur*	3	3
N9192SE	4.5	15	29	Mixed broadleaf	4	3
N9222E	4.6	10	31	*Q. robur*	3	2
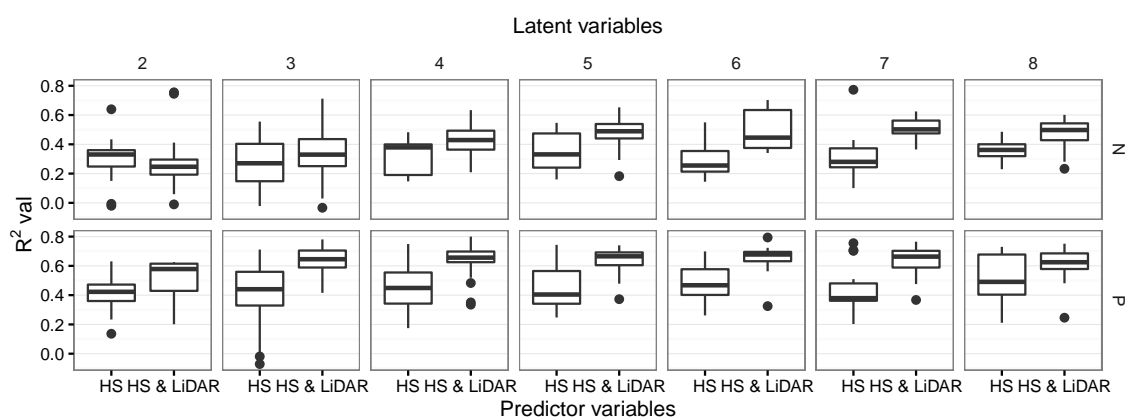
Figure 2.12 R^2 in leave-one-out cross-validation depending on the selected number of latent variables (displayed above) for N_{mass} (upper row) and P_{mass} (lower row) for PLSR models including hyperspectral bands (HS) or a combination of hyperspectral bands and LiDAR derived variables as predictors.

Table 2.4 Ranges of N_{mass} and P_{mass} of sampled tree species

Species	N_{mass} [g/kg]	P_{mass} [g/kg]
Acer pseudoplatanus	16.2 - 27.3	1.69 - 1.94
Carpinus betulus	22.9 - 26.9	0.75 - 1.46
Fagus sylvatica	15.4 - 27.7	0.61 - 1.33
Fraxinius excelsior	21.0 - 30.6	0.81 - 1.43
Pinus sylvestris	12.5 - 19.8	1.02 - 1.52
Prunus serotina	17.4 - 29.9	0.82 - 3.05
Quercus petrea	17.9 - 21.8	0.88 - 1.47
Quercus robur	12.5 - 25.4	0.72 - 1.68
Salix caprea	23.4 - 25.2	1.18 - 1.25

Table 2.5 Results of pairwise Kruskal-Wallis tests to compare N_{mass} and P_{mass} between most dominant tree species. Significant differences are displayed in bold.

| Species pair	N_{mass} Chi-squared	p	P_{mass} Chi-squared	p
Carpinus betulus - Fagus sylvatica	2.847	0.091	26.808	**< 0.001**
Carpinus betulus - Pinus sylvestris	38.297	**< 0.001**	7.5924	0.006
Carpinus betulus - Prunus serotina	24.679	**< 0.001**	51.909	**< 0.001**
Carpinus betulus - Quercus robur	0.43495	0.51	1.2066	0.272
Fagus sylvatica - Pinus sylvestris	37.285	**< 0.001**	29.574	**< 0.001**
Fagus sylvatica - Prunus serotina	33.156	**< 0.001**	80.598	**< 0.001**
Fagus sylvatica - Quercus robur	0.11386	0.736	18.343	**< 0.001**
Pinus sylvestris - Prunus serotina	40.074	**< 0.001**	15.29	**< 0.001**
Pinus sylvestris - Quercus robur	30.51	**< 0.001**	11.252	**< 0.001**
Prunus serotina - Quercus robur	25.035	**< 0.001**	56.801	**< 0.001**
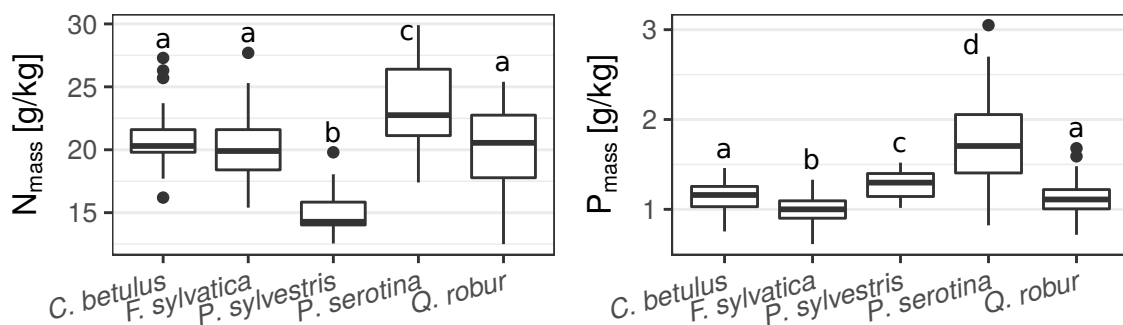
Figure 2.13 Measured leaf N_{mass} and P_{mass} of the most dominant tree species. Characters show significant differences between the species resulting from pairwise Kruskal-Wallis tests.
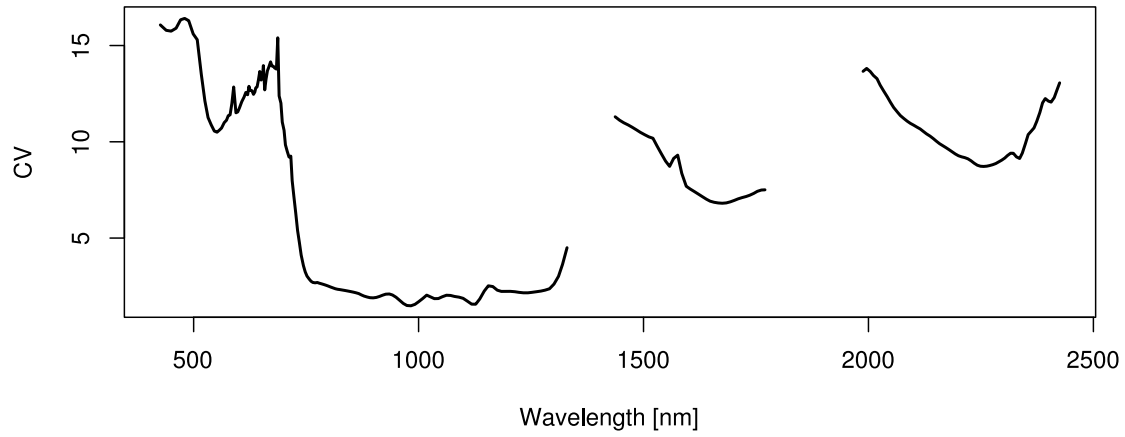
Figure 2.14 Coefficient of variation (CV) of 50 canopy spectra used for model calibration. Values display the canopy spectra after brightness normalization.
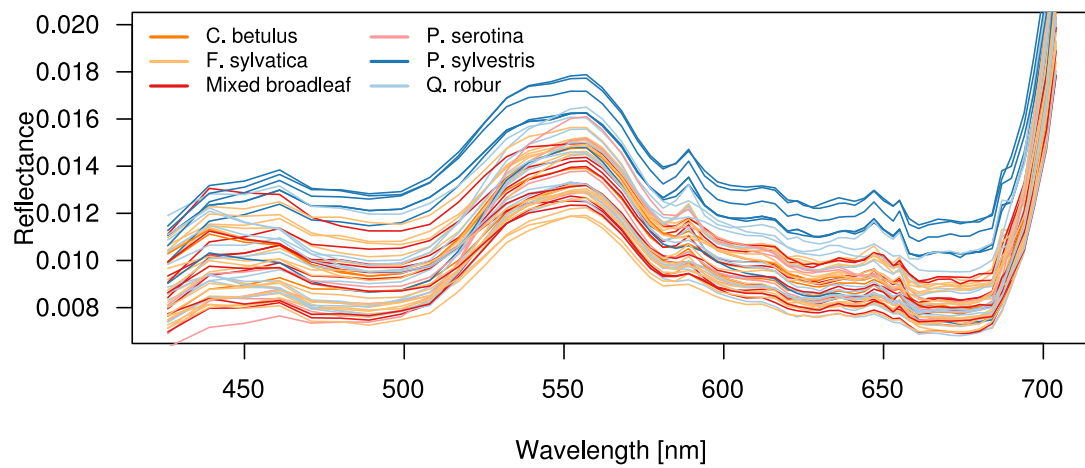

Figure 2.15 Canopy spectra after brightness normalization of field plots in the visible wavelength range. Colors indicate different forest types represented by the dominant tree species.
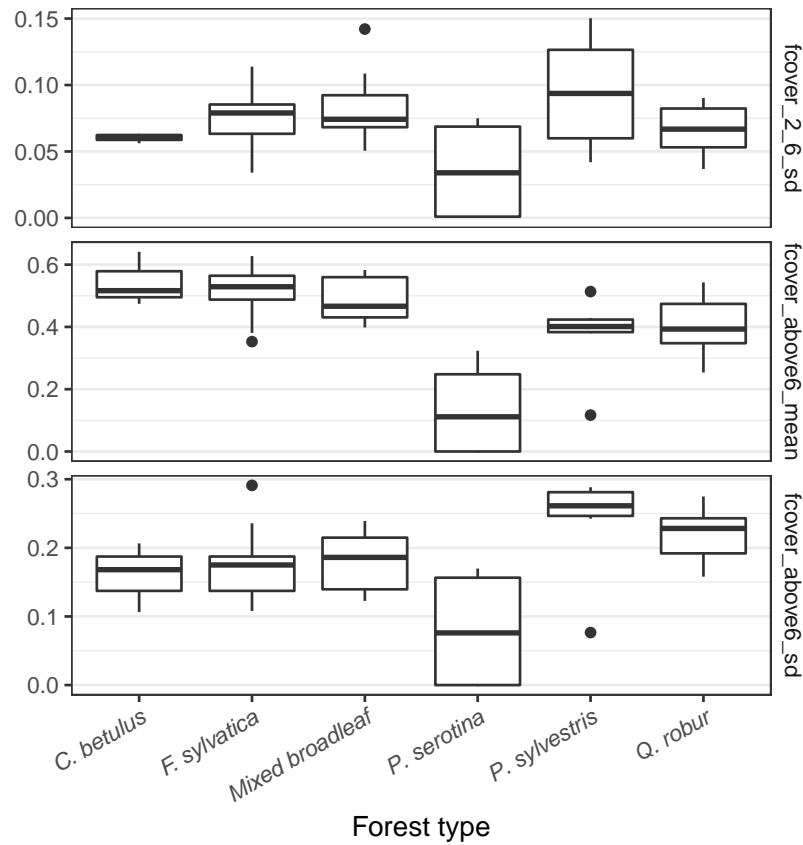
Figure 2.16 Differences of selected LiDAR-variables between forest types. Values are shown for used field plots. fcover_2_6_sd: standard deviation of fractional vegetation cover between 2 m and 6 m above ground; fcover_above6_mean: mean fractional vegetation cover above 6 m; fcover_above6_sd; standard deviation of fractional vegetation cover above 6 m

Figure 2.17 Selection frequency of 245 hyperspectral bands used in models for the prediction of canopy N_{mass} in 200 variable selection procedures. Frequencies are displayed for models using hyperspectral bands only (HS) and for models using a combination of hyperspectral bands and LiDAR-variables (HS & LiDAR).
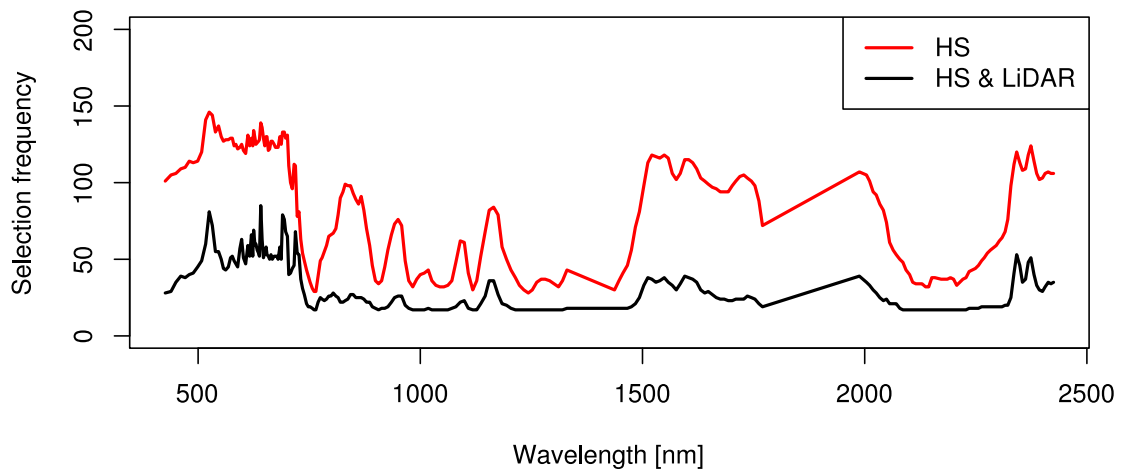
Figure 2.18 Selection frequency of 245 hyperspectral bands used in models for the prediction of canopy P_{mass} in 200 variable selection procedures. Frequencies are displayed for models using hyperspectral bands only (HS) and for models using a combination of hyperspectral bands and LiDAR-variables (HS & LiDAR).
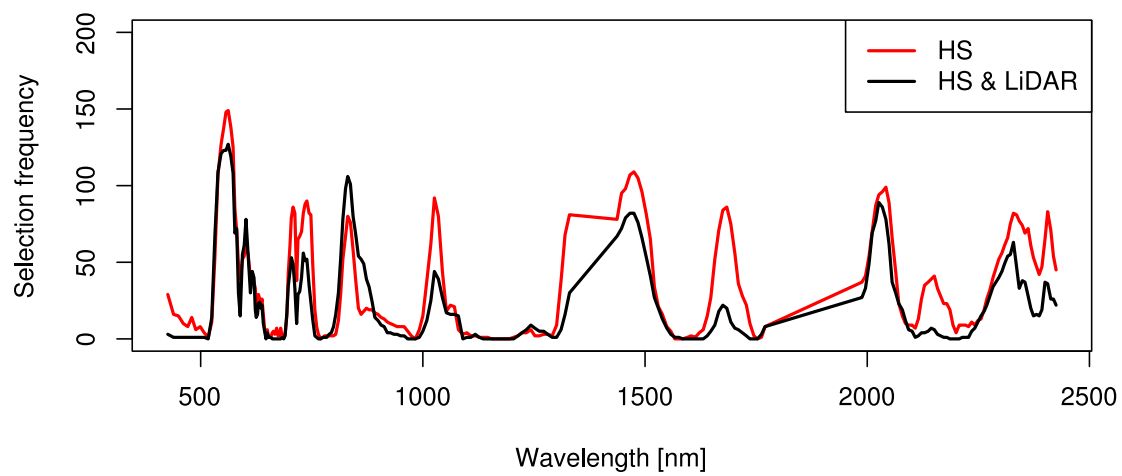
2.2 Analyzing remotely sensed structural and chemical canopy traits of a forest invaded by *Prunus serotina* over multiple spatial scales

Michael Ewald, Sandra Skowronek, Raf Aerts, Klara Dolos, Jonathan Lenoir, Manuel Nicolas, Jens Warrie, Tarek Hattab, Hannes Feilhauer, Olivier Honnay, Carol X. Garzón-López, Guillaume Decocq, Ruben Van De Kerchove, Ben Somers, Duccio Rocchini, Sebastian Schmidtlein

Abstract

Non-native invasive plant species can influence ecosystem functioning over broad spatial scales, but most research on ecosystem impacts has focused on the plot level covering sampling units of only a few square meters or less.

We used a multi-scale approach to analyze structural and leaf chemical vegetation traits depending on the presence of non-native American black cherry (*P. serotina*) in a mixed deciduous forest at the plot level and at the forest stand level. Trait data were derived from remotely sensed maps of leaf area index (LAI), wood volume as well as canopy leaf nitrogen content (N_{mass}), phosphorus content (P_{mass}), and N:P ratio. Differences in these traits were compared between invaded and non-invaded areas at the plot level using 264 sampling units with a size of $25\,m \times 25\,m$ and in 4119 forest management units (mean area: $7.6 \pm 5.1\,ha$).

Observed patterns between invaded and non-invaded areas were similar at both spatial scales. Invaded areas were characterized by less wood volume, indicating that lower standing biomass promotes the occurrence of *P. serotina*. In contrast, LAI did not differ between invaded and non-invaded areas. Furthermore, the presence of *P. serotina* trees had an impact on the chemical composition of the forest canopy by decreasing leaf N:P. While for P_{mass}, we found no differences between invaded and non-invaded areas, for N_{mass} we observed an invasion effect, though only at the plot level. Using remotely sensed trait data proved valuable to evaluate the relevance of invasion impacts at broader scales.

2.2.1 Introduction

Non-native invasive plant species can have manifold impacts on ecosystems, by changing biotic or abiotic conditions through many different pathways (Ehrenfeld, 2010; Weidenhamer and Callaway, 2010; Gaertner et al., 2014). Due to effective spreading and fast growth they are often found to build up dense populations and can thus change the composition of native plant communities and locally decrease biodiversity (Powell et al., 2011; Vilà et al., 2011; Pyšek et al., 2012). Besides altering community composition, invasive plant species can also influence ecosystem properties or processes (Stricker et al., 2015). For instance, the presence of non-native invasive plant species has often been associated with an increase in above-ground biomass, above ground nutrient stocks, and nutrient concentrations in the topsoil (Liao et al., 2008; Dassonville et al., 2008; Weidenhamer and Callaway, 2010; Vilà et al., 2011).

Changes in ecosystem properties are often related to increased primary production (Vilà et al., 2011) that can be attributed to the fast growing character of many invasive plant species (van Kleunen et al., 2010). Fast growth is generally related to low investments of carbon in leafs associated with higher leaf N and P concentrations (Wright et al., 2004). Hence, many invasive plant species are characterized by higher leaf N and P concentrations (e.g. Thorpe et al., 2006; Kurokawa et al., 2010; Jäger et al., 2013) or increased total N and P uptake (e.g. Windham and Ehrenfeld, 2003; Chapuis-Lardy et al., 2006; Aguilera et al., 2010) compared to co-occurring native species. Changes in community level above-ground nutrient contents can be caused by direct or indirect effects. An direct effect can be for example an increase of community level above-ground nitrogen, due to high uptake by an invasive species. Indirect effects can include increased nitrogen or phosphorus concentrations in the leaves of co-occurring native species due to nutrient mobilization (Fisher et al., 2006; Kurten et al., 2008). However, invasive plants can also reduce nutrient concentrations in the leaves of co-occurring species (Aerts et al., 2017), presumably as an effect of resource competition (Vilà and Weiner, 2004).

The majority of studies dealing with ecosystem impacts of invasive plants have been limited to plot based observations or experiments, in which each sampling unit is covering areas of only few square meters (Parker et al., 1999; Stricker et al., 2015). While this is a valid approach to understand effects of invasion processes it provides little information about the spatial relevance of such impacts. Besides the per capita or per biomass impact of an invasive species, its broad scale ecosystem impact depends on its range size and its occurrence prevalence within the area of interest (Parker et al., 1999; Thiele et al., 2009). Moreover, the spatial distribution patters of invasive plant species can differ across spatial scales, and similarly also their ecological effects (Pauchard and Shea, 2006). Plot level studies of invasion effects thus provide only part of the information needed to evaluate its overall ecosystem impact. Evaluating the impact of an invader at multiple spatial scales

will provide a more comprehensive picture of its impact (Parker et al., 1999; Pauchard and Shea, 2006), and therefore also valuable information for prioritizing management actions.

Remote sensing offers great opportunities to support ecological research addressing multiple spatial scales by providing spatial explicit projections of vegetation traits. Such projections include structural vegetation traits such as biomass or LAI (Zheng and Moskal, 2009; Fassnacht et al., 2014; Kumar et al., 2015), chemical leaf traits such as chlorophyll or nitrogen content (Asner et al., 2015; Singh et al., 2015) and plant functional types (Ustin and Gamon, 2010; Kattenborn et al., 2017). Applications of remote sensing in invasion ecology have mainly focused on mapping and monitoring the distribution of invasive plant species (Bradley, 2014) holding potential to detect early invasion stages (Rocchini et al., 2015; Skowronek et al., 2017b). However, remote sensing data can also be used to detect invasion impacts on ecosystem functioning over large areas in a spatially continuous manner (Asner and Vitousek, 2005; Vicente et al., 2013).

In this study, we applied a multi-scale approach to investigate the impact of an invasive tree species on structural and chemical vegetation traits in a mixed deciduous forest using sampling units of different size. Impacts were analyzed at the plot level and at the level of forest management units, hereafter referred to as stand level. Our target species was *Prunus serotina*, an alien invasive tree species in Western and Central Europe. In its non-native range *P. serotina* mainly occurs on nutrient poor acidic soils within oak and pine forests (Starfinger et al., 2003; Closset-Kopp et al., 2010) and is promoted by high light availability in canopy gaps or in forests characterized by sparse canopies (Vanhellemont et al., 2008; Terwei et al., 2013). Reported impacts of *P. serotina* outside of its native range include changes of soil conditions and understory plant communities in forest ecosystems (Halarewicz and Pruchniewicz, 2015). Especially as a shrub, *P. serotina* can form very dense populations and dramatically reduce understory light availability (Starfinger et al., 2003). *P. serotina* is characterized by higher leaf nitrogen and phosphorus contents than most of the co-occurring native tree species (Aerts et al., 2017), thereby showing potential to alter nutrient cycling in forest ecosystems. At the plot level, *P. serotina* has been found to decrease leaf nitrogen content of co-occurring European beech (*Fagus sylvatica*) and to increase leaf phosphorus contents of co-occurring Scots pine (*Pinus sylvestris*) (Aerts et al., 2017). Differences in structural and chemical traits were analyzed dependent on stand type, stand age, soil pH and the presence of *P. serotina* in the tree layer at the plot level and at the forest stand level. Using this multi scale approach we aimed to get a more comprehensive picture of ecosystem changes caused by *P. serotina*.

2.2.2 Materials and methods

2.2.2.1 Study area

The forest of Compiégne (northern France, coordinates: N 49.370, W 2.886), covering an area of $144.2\,km^2$, is located in the oceanic climate zone with a mean annual temperature of 10.3°Cand a mean annual precipitation of 677 mm. Soils are formed of nutrient-poor sandy substrate in the northern part of the forest and nutrient rich calcareous substrate in the southern part (Chabrerie et al., 2008). The forest is mainly managed as even-aged stands of beech (*Fagus sylvatica*), oaks (*Quercus robur*, *Quercus petrea*) and pine (*Pinus sylvestris*), which often also occur in mixed stands. These stands are frequently intermingled with European hornbeam (*Carpinus betulus*) and ash (*Fraxinius excelsior*). Stands can reach ages of more than 200 years (Chabrerie et al., 2008). *P. serotina* was introduced to the area around 1850 and has since then spread across a substantial part of the forest (Fig. 2.19) (Chabrerie et al., 2008). Although *P. serotina* is affected by frequent thinning, it is often highly abundant in the shrub layer and can locally become the dominant tree species within the forest canopy.
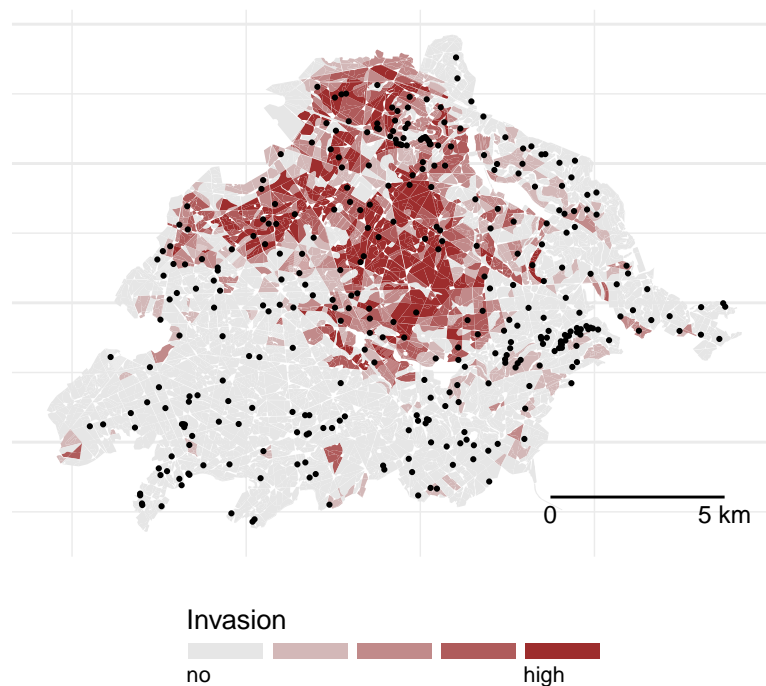

Figure 2.19 Study area with forest management units and presence-absence locations used for analyses at the stand and plot level respectively. Colors indicate estimated frequency of *P. serotina* trees within the management units (Data from Chabrerie et al. (2007))

2.2.2.2 Data

Spatial forest stand information

We used forest inventory maps from the year 2009, providing polygons with information on stand age (9 different classes ranging from "0-20 years" to "older than 200 years") and up to four dominant tree species for each of the 2846 forest management units (Tab. 2.6, supplementary material Fig. 2.26). We classified stand types according to the most dominant tree species of each forest stand. Stands consisting of three or more tree species exceeding 20 % of total canopy cover were classified as mixed stands.

Table 2.6 Overview of data used as basis for response and predictor variables.

	Variable	Data type	Variable type	Data source
Response	LAI	raster	continuous	Combination of remote sensing and field data
	Wood volume	raster	continuous	Combination of remote sensing and field data
	N_{mass}	raster	continuous	Combination of remote sensing and field data
	P_{mass}	raster	continuous	Combination of remote sensing and field data
	N:P ratio	raster	continuous	Combination of remote sensing and field data
Predictors	Soil pH	raster	continuous	(Hattab et al., 2017)
	P. serotina presence *	point	factor (2 levels)	Field acquisition
	P. serotina presence **	polygon	factor (5 levels)	(Chabrerie et al., 2007)
	Stand type	polygon	factor (4 levels)	Forest inventory data
	Stand age	polygon	factor (9 levels)	Forest inventory data

∗ only used for analyses at the plot level
∗∗ only used for analyses at the stand level

Soil pH map

Information on soil pH was obtained from a soil pH map at $25\,\text{m} \times 25\,\text{m}$ resolution covering the entire study area (Tab. 2.6, supplementary material Fig. 2.26). This map was generated through regression-kriging using 161 point measurements of topsoil pH and including soil type, elevation, slope, bedrock geology and a litter quality index as predictors (for more information see Hattab et al. (2017)).

Data on *P. serotina* presence

For the analysis of differences between invaded and non-invaded parts of the forest at the plot level we sampled information on presence-absence of *P. serotina* in the tree canopy within 336 field plots with a size of $25\,\text{m} \times 25\,\text{m}$ (Tab. 2.6, Fig. 2.19). Presence-absence data were recorded between July and October 2015 throughout the whole forest area combining random sampling with an environmental systematic mapping (Hattab et al., 2017).

For the stand level we used 6432 polygons with information on the occurrence of *P. serotina* in the tree layer in 6 discrete classes ranging from 0 to 5 (0: no *P. serotina*, 1: isolated individuals, 2: scattered aggregates of individuals, 3: fragmented populations, 4: large, continuous population, 5: dominant canopy tree species over the entire stand) based on field sampling between the years 2003 and 2004 (Chabrerie et al., 2007). Because of its low sample size, class 5 was merged with class 4. In order to join information on stand type/age and occurrence of *P. serotina* trees we calculated a spatial overlay of the two polygon maps.

Remotely sensed maps of structural and chemical traits

To compare structural and chemical vegetation traits within invaded and non-invaded parts of the forests we used maps for leaf area index (LAI), wood volume, canopy nitrogen content (N_{mass}), canopy phosphorus content (P_{mass}), and canopy N:P ratio, based on a combination of field derived trait and remote sensing data (Tab. 2.6). Remote sensing data consisted of airborne imaging spectroscopy data (248 bands, 380 — 2500 nm) acquired in July 2014 by the Airborne Prism Experiment (APEX) spectrometer (Schaepman et al., 2015) with a spatial resolution of 3 m × 3 m, and airborne discrete return LiDAR data with an average point density of 23 points m^{-2}. (for detailed information on remote sensing data, and its processing see supplementary material Data S1). For mapping LAI, wood volume, N_{mass}, P_{mass} and N:P, we used partial least squares regression models that were calibrated by field-derived trait data (Fig. 2.20, for more information see supplementary material Data S2). In order to get more robust predictions, model calculations were embedded in a repeated data splitting procedure with 200 repetitions. For each iteration a random set of 10 out of 50 field plots was not included in model calibration. Predictive models resulted in mean Pearson r^2 values of 0.48, 0.72, 0.41, 0.63 and 0.61 in leave-one-out cross-validation for LAI, wood volume, N_{mass}, P_{mass} and N:P respectively. Spectral bands and LiDAR-derived variables were used to predict 200 maps for LAI, wood volume, N_{mass}, P_{mass} and N:P from the resulting models of each data split. Finally, for each trait, we calculated median maps representing the median value for each pixel from those 200 prediction maps (supplementary material Fig. 2.27).

2.2.2.3 Data processing

We created two different datasets: one for the analysis of impacts by *P. serotina* at the plot level and one for the analyses at the stand level (Fig. 2.20). For both datasets we extracted information on stand type, stand age, soil pH, LAI, wood volume, N_{mass}, P_{mass} and N:P from the available set of maps. Information from raster maps (pH, LAI, wood volume, N_{mass}, P_{mass}, N:P) was extracted for all pixels intersecting with an square of 25 m × 25 m around the presence-absence locations and all pixels intersecting with the polygons representing forest stands, respectively. For soil pH we calculated median values for each
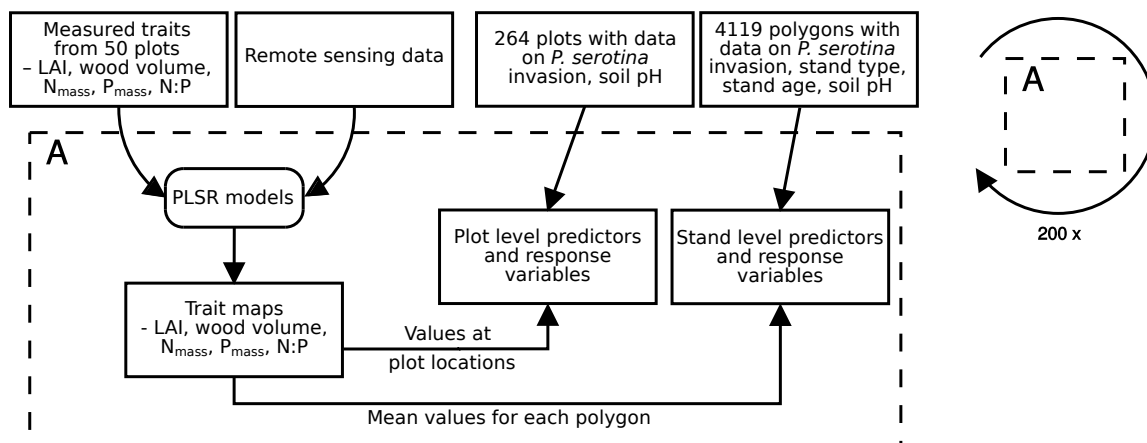
Figure 2.20 Work-flow illustrating the retrieval of response and predictor datasets at the plot and at the stand level (for more information on used variables see Tab. 2.6). Trait maps were generated using predictions from partial least squares regression (PLSR) models.

location and forest stand. Extracted pixel values of the remaining variables were averaged. For LAI, wood volume, N_{mass}, P_{mass} and N:P this procedure was repeated for each of the 200 predicted maps and the median map. We only considered mixed stands and stands dominated by *F. sylvatica, Q. robur* or *P. sylvestris* for the subsequent analyses. Mixed stands were usually only represented by broadleaved tree species. Other stand types were excluded from the analyses because of their small sample size. Furthermore, for the analyses at the stand level polygons smaller than 0.5 ha were not considered as stands and thus discarded from the data set. This resulted in 264 samples for analyses at the plot level and 4119 polygons (mean area: 7.6 ha, maximum area: 34.5 ha, standard error: ± 5.1 ha) for analyses at the stand level.

2.2.2.4 Statistical analyses

We aimed to analyze the four vegetation traits (LAI, wood volume, N_{mass}, P_{mass}, N:P) depending on *P. serotina* presence (plot level) or invasion degree (stand level) and stand type (Tab. 2.6), considering the confounding effects of soil pH and stand age. Both plot and stand level data were analyzed using the same procedure (Fig. 2.21). We ran mixed effects models using each of the four studied vegetation traits as response variables, whereas stand type, soil pH and invasion by *P. serotina* were used as fixed effects and stand age class was integrated as a grouping factor. In a first step we built preliminary models for each response variable using values extracted from the median prediction maps. These models were used to select an appropriate model type (model family) and link function by visual examination of quantile-quantile plots. Additionally, preliminary models were used to test for spatial autocorrelation (SAC) in the residuals. For this purpose we calculated the centroids of polygons representing forest stands. SAC was tested calculating the Moran's I value between residuals ordered by distance in uniformly distributed distance classes. Class

width was 200 m for plot level models and 50 m for stand level models. For all response variables we observed considerable SAC.
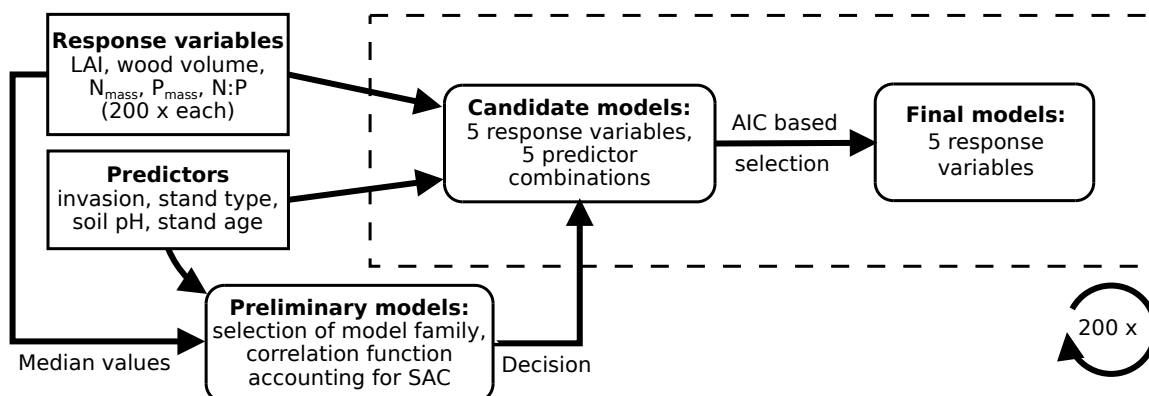

Figure 2.21 Work-flow illustrating the steps of statistical analyses of structural and chemical canopy traits depending on the presence of *P. serotina*, stand type and soil pH and stand age (for more information on response and predictor variables see Tab. 2.6). The presented procedure was used for analyses at both the plot and stand level. SAC: Spatial autocorrelation.

We chose linear mixed effects models with identity link and a Gaussian error distribution (LMM) as quantile-quantile plots suggested this for all variables at the plot level as well as for LAI, wood volume, N_{mass} and N:P ratio at the stand level. We accounted for SAC by integrating a correlation function into the model (Dormann et al., 2007). For all response variables an exponential correlation function was chosen based on visual examination of the residual's correlogram (Dormann et al., 2007).

To select the best set of predictors we successively calculated five candidate models. Each candidate model included different predictor variable combinations (see Tab. 2.7, Fig. 2.21) for each of the four response variables. This procedure was repeated 200 times for each dataset resulting from the 200 prediction maps respectively. For each of the response variables, we selected the final conceptual model according to lowest median AIC values resulting from 200 model repetitions (Tab. 2.7).

To test for differences between included fixed effects we extracted parameter coefficients and calculated the differences between the coefficients of all possible factor combinations for each of the 200 calculated models. In a second step we checked if these differences were significantly different from zero by calculating the 95 % confidence intervals.

Data processing and statistical analyses were performed using R 3.3.1 (R Core Team, 2016). SAC was tested using the package ncf 1.1 (Bjornstad, 2016) and LMMs were calculated using the package nlme 3.1 (Pinheiro et al., 2016).

2.2.3 Results

In all LMMs stand type was included as predictor variable, irrespective of the response variable for both plot and stand level (Tab. 2.7). This indicated a high influence of species-

Table 2.7 Median AIC and Pearson r^2 values of the five candidate linear mixed effect models for LAI, wood volume, N_{mass}, P_{mass} and N:P. Results are presented for analyses at the plot level and the forest stand level. Bold values indicate lowest AIC values. pH: soil pH, stand type: forest stand.type defined by dominating tree species, stand.age: stand age comprising 9 age classes, invasion.tree: Invasion of *P. serotina* in the tree layer (presence-absence for plot level data and five classes for stand level data)

Response	Model	Fixed effects	Grouping factor	r^2 plot	r^2 stand	AIC plot	AIC stand
LAI	M1	pH	stand.age	0.41	0.24	711.2	6843
	M2	invasion.tree + pH	stand.age	0.41	0.24	714.7	6845
	M3	stand.type + pH	stand.age	0.52	0.39	**675.4**	**6430**
	M4	invasion.tree + stand.type + pH	stand.age	0.52	0.40	679.3	6447
	M5	invasion.tree + stand.type + invasion.tree:stand.type + pH	stand.age	0.53	0.40	681.1	6479
Wood volume	M1	pH	stand.age	0.22	0.27	2159	29314
	M2	invasion.tree + pH	stand.age	0.23	0.29	2155	29286
	M3	stand.type + pH	stand.age	0.23	0.30	2150	29257
	M4	invasion.tree + stand.type + pH	stand.age	0.24	0.32	2145	29226
	M5	invasion.tree + stand.type + invasion.tree:stand.type + pH	stand.age	0.26	0.32	**2131**	**29187**
N_{mass}	M1	pH	stand.age	0.18	0.04	1132	13223
	M2	invasion.tree + pH	stand.age	0.19	0.08	1129	13225
	M3	stand.type + pH	stand.age	0.32	0.33	1088	**12534**
	M4	invasion.tree + stand.type + pH	stand.age	0.33	0.34	1088	12543
	M5	invasion.tree + stand.type + invasion.tree:stand.type + pH	stand.age	0.35	0.34	**1082**	12569
P_{mass}	M1	pH	stand.age	0.22	0.22	-122	-6349
	M2	invasion.tree + pH	stand.age	0.23	0.24	-119.3	-6343
	M3	stand.type + pH	stand.age	0.33	0.29	**-139.4**	**-6499**
	M4	invasion.tree + stand.type + pH	stand.age	0.34	0.30	-132.8	-6477
	M5	invasion.tree + stand.type + invasion.tree:stand.type + pH	stand.age	0.34	0.29	-121	-6414
N:P	M1	pH	stand.age	0.12	0.03	1388	17335
	M2	invasion.tree + pH	stand.age	0.15	0.07	1380	17351
	M3	stand.type + pH	stand.age	0.37	0.33	1306	16751
	M4	invasion.tree + stand.type + pH	stand.age	0.39	0.34	1302	**16751**
	M5	invasion.tree + stand.type + invasion.tree:stand.type + pH	stand.age	0.40	0.33	**1296**	16760

specific differences in the variation of observed canopy traits, LAI, wood volume, N_{mass}, P_{mass} and N:P ratio. Best models after AIC-based model selection also included invasion by *P. serotina* for wood volume, N:P and N_{mass} (Tab. 2.7). However, for N_{mass} an influence of *P. serotina* was only apparent at plot level and not at the stand level. Furthermore, for N:P models at the stand level integration of *P. serotina* invasion reduced AIC values only moderately (16751.1 vs. 16750.7). LAI and P_{mass} did not differ between invaded and non-invaded parts of the forest, irrespective of the spatial scale. Final models resulted in mean Pearson r^2 values between 0.26 and 0.52 at the plot level and between 0.29 and 0.39 at the stand level (Tab. 2.7).

While the presence of *P. serotina* in the tree layer was connected to lower wood volume at the stand level for all forest types, we observed no clear trend at the plot level (Figs. 2.22 and 2.23). Here, wood volume was higher at sites with *P. serotina* trees in *Q. robur*

and mixed stands, whereas it was lower in *F. sylvatica* and *P. sylvestris* stands, though not significant for the latter two. At the plot level, presence of textitP. serotina trees was connected to significantly lower N_{mass} in mixed deciduous stands and higher N_{mass} in *P. sylvestris* stands (Figs. 2.22 and 2.23). Canopy N:P ratios observed at the plot level were lower in *F. sylvatica* and mixed deciduous stands when *P. serotina* trees were present. When looking at the stand level, *P. serotina* presence was related to decreased N:P ratios for all stand types, but only for invasion classes 3 and 4, representing large fragmented up to continuous populations of *P. serotina* trees (Figs. 2.22 and 2.23).
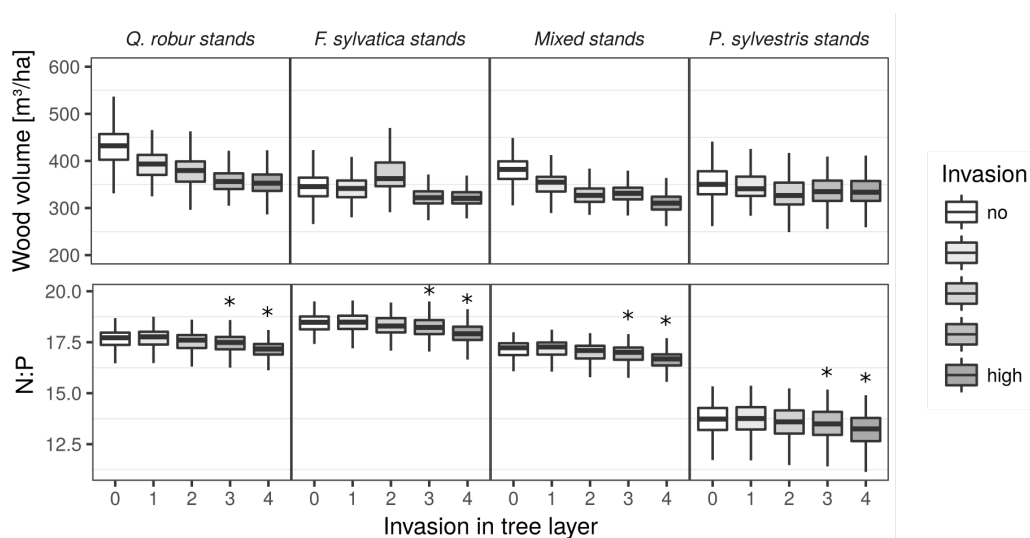

Figure 2.22 Predicted values of 200 repeated model calculations for wood volume and canopy N:P depending on the occurrence of *P. serotina* trees at the stand level for different stand types characterized by the dominant tree species. *P. serotina* occurrence is grouped into 5 classes (0: no *P. serotina*, 1: isolated individuals, 2: scattered aggregates of individuals, 3: fragmented populations, 4: large, continuous population). Asterisks indicate significant differences from areas without presence of *P. serotina* trees resulting from a comparison of model coefficients from 200 model repetitions. Results are displayed for stands with an age of 90-100 years and a soil pH value of 5.96.

Stand type specific differences of canopy traits were similar across fine and broad spatial scales for LAI, N_{mass}, P_{mass} and N:P ratio (Fig. 2.24 and 2.25). Most apparent was a lower LAI and lower N_{mass} in pine stands, depicting the functional differences between broadleaved tree species and the coniferous *P. sylvestris*. Despite the observation of lowest P_{mass} and highest N:P values in beech dominated stands, differences between broadleaved forest stands were low. For wood volume we observed no consistent pattern between the stand types, when comparing plant and stand level results (Fig. 2.24).

2.2.4 Discussion

Influences of *P. serotina* on canopy chemical traits

Regarding leaf N:P, our results suggest that *P. serotina* has the potential to alter forest canopy chemical stoichiometry across scales. While previous field studies found evidence
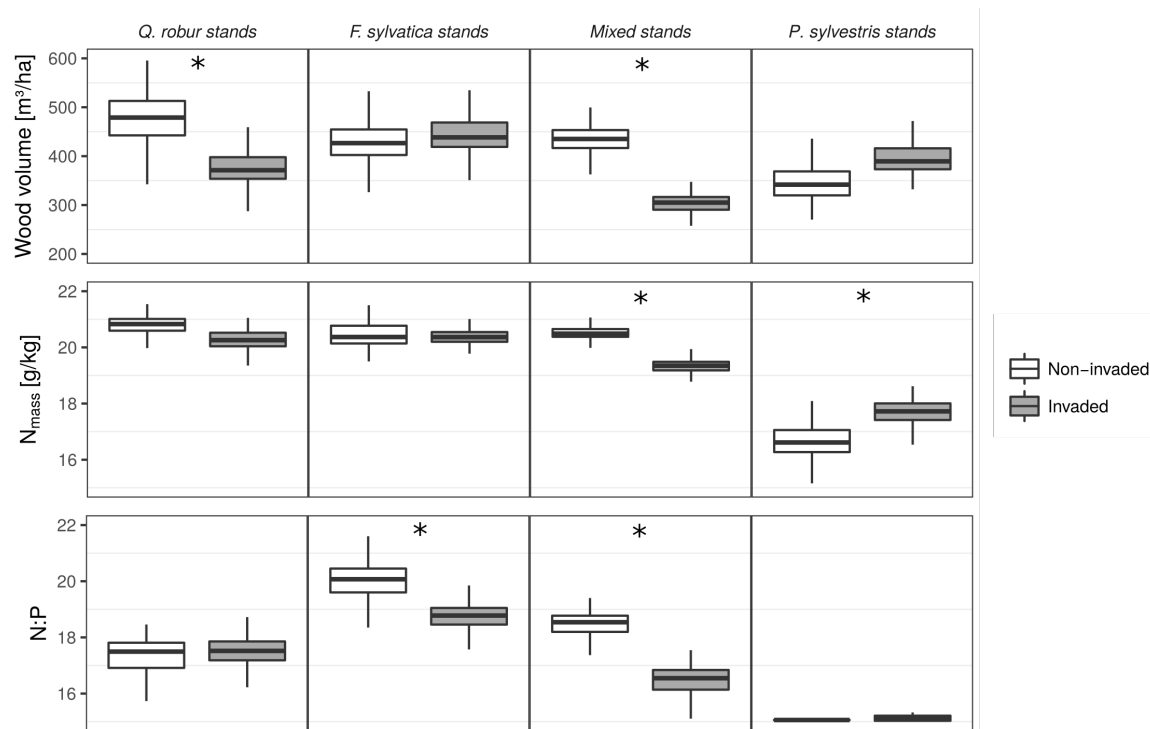
Figure 2.23 Predicted values of 200 repeated model calculations for Wood volume, N_{mass} and N:P depending on the presence of *P. serotina* trees at the plot level (based on presence-absence locations) for different stand types characterized by the dominant tree species. Soil pH was kept constant. Asterisks indicate significant differences between invaded and non-invaded sites resulting from a comparison of model coefficients from 200 model repetitions. Results are displayed for stands with an age of 90-100 years and a soil pH value of 5.96.

for ecosystem impacts of *P. serotina* at the plot level (Halarewicz and Pruchniewicz, 2015; Aerts et al., 2017) we could now demonstrate the relevance of impacts on forest ecosystems also at larger scales. Observed differences in leaf chemical composition between invaded and non invaded areas can be explained by direct and indirect effects of *P. serotina*. We can assume that *P. serotina* directly influenced canopy N:P due to its leaf chemical stoichiometry differing from the resident species (Aerts et al., 2017). This also conforms to the results of a recent meta-study by Lee et al. (2017), which showed that impacts of invasive plant species on N cycling were mainly driven by trait differences between invaders and native plant communities.

An indirect way of altering canopy chemistry would presuppose that *P. serotina* was able to influence leaf chemical traits of the co-occurring resident tree species. In fact, Aerts et al. (2017) observed that *P. serotina* increased P_{mass} of co-occuring *P. sylvestris* and decreased N_{mass} of co-occuring *F. sylvatica*. One possible driver is resource competition causing reduced soil nutrient availability for the resident species and consequently also reduced leaf nutrient contents. This is one possible reason for the reduced N_{mass} in invaded areas at the plot level and for reduced N:P ratios observed at the stand level. Another possible pathway is improved soil nutrient availability through alterations of litter chemical composition.
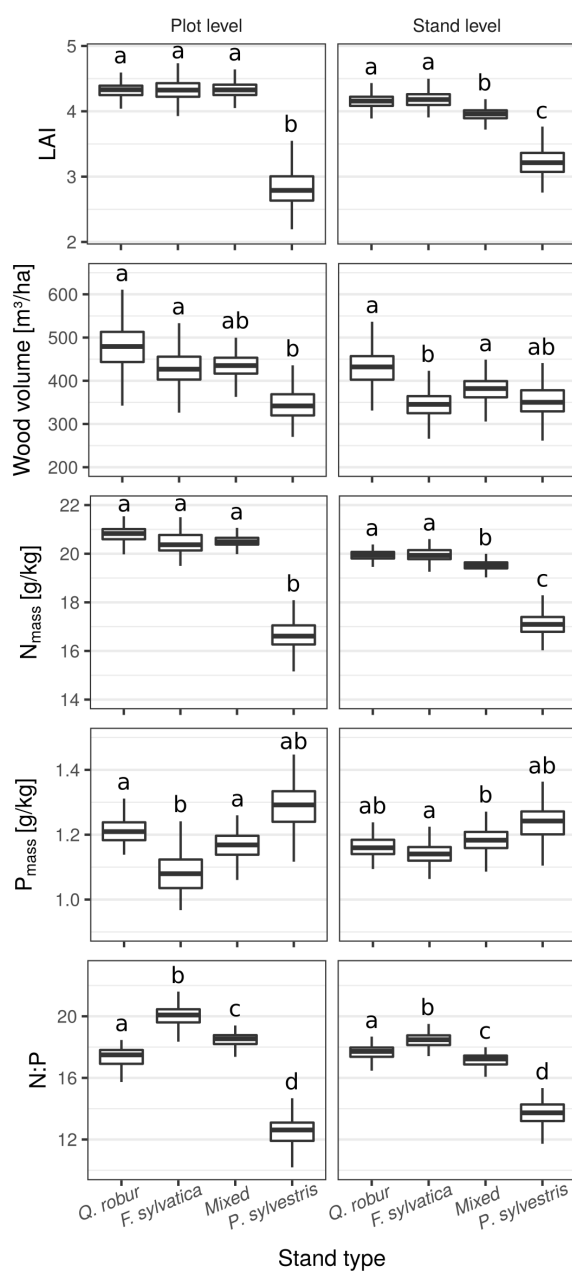
Figure 2.24 Predicted values of 200 repeated model calculations for LAI, wood volume, canopy N_{mass}, P_{mass} and N:P depending on stand types characterized by the dominant tree species. Predictions from plot level models are displayed on the left, predictions from stand level models on the right. Characters indicate significant differences between stand types resulting from a comparison of model coefficients from 200 model repetitions. Results are displayed for non-invaded stands with an age of 90-100 years and a soil pH value of 5.96.

Early successional fast-growing tree species like *P. serotina* are often characterized by lower resorption rates of leaf nutrients from senescent leaves (Sardans et al., 2015) that are also depicted in higher litter nutrient contents (Richardson et al., 2005) accelerating litter decomposition. Likewise, *P. serotina* has been found to accelerate litter decomposition
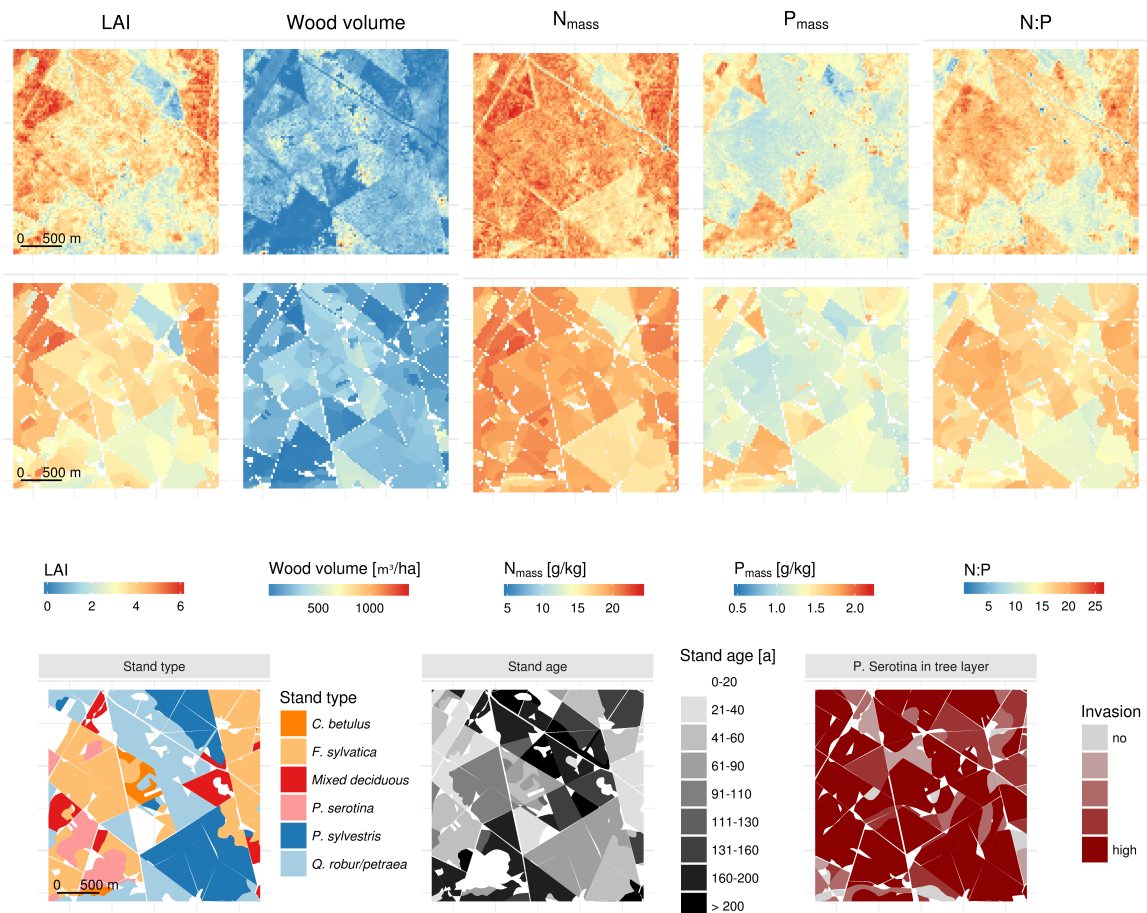
Figure 2.25 Map segments showing trait values derived from remote sensing at the original resolution with 24 m pixel size (above) and aggregated to the single forest management units as used for the analyses at the stand level (center). Polygon maps at the bottom display stand-level information on stand type, stand age and *P. serotina* occurrence.

(Aerts et al., 2017) which may have increased nutrient availability in the topsoil resulting in higher N$_{mass}$ of the co-occurring trees species, like observed in invaded *P. sylvestris* stands.

The leaf N:P ratio can be used as an indicator for plant nutrient status giving information on productivity and tree vitality (Güsewell, 2004). In the last decades leaf N:P ratios have increased across European forests presumably resulting from high nitrogen deposition (Jonard et al., 2015; Talkner et al., 2015; Sardans et al., 2016). Mean observed N:P ratios in our study area (20.5, 18.3 and 11.7 in the leaves of *F. sylvatica*, *Q. robur* and *P. sylvestris* respectively), already exceeded the tolerable ranges suggested by (Mellert and Göttlein, 2012), indicating P deficiency. In that respect, a potential reduction of leaf N:P ratios by *P. serotina* can be rather considered positive.

Structural differences between invaded an non-invaded areas

Invaded mixed deciduous and *Q. robur* stands were characterized by less wood volume than non-invaded ones. In contrast, invaded *P. sylvestris* stands showed slightly higher wood volume at the plot level, though not significant. This pattern can be attributed to the strong demand for light of *P. serotina* (Vanhellemont et al., 2008; Terwei et al., 2013) and different light conditions in broad-leaved and pine stands. Broad-leaved stands in our study area were characterized by lower light availability at the forest floor compared to pine stands (see Fig. 2.24). Therefore, in broadleaved stands *P. serotina* establishment is constrained to canopy gaps caused by natural and anthropogenic disturbances (Chabrerie et al., 2008; Closset-Kopp et al., 2010). As a result, stands with less wood volume were characterized by a higher infestation of *P. serotina*. In pine stands, light availability at forest floor is usually sufficient for *P. serotina* establishment and therefore we did not observe significant differences between invaded and non-invaded stands.

Contrary to differences in wood volume, we found no differences in LAI between invaded and non-invaded areas. As discussed above, *P. serotina* establishment is promoted by high light availability which is related to lower LAI values. Our finding suggests that *P. serotina* is able to quickly compensate lower LAI needed for its establishment by its own biomass. This agrees with previous studies reporting dense cover of *P. serotina* in the shrub layer and reduced light availability at the forest floor. The latter is regarded as most influential factor for inhibiting natural forest regeneration (Starfinger et al., 2003; Halarewicz and Pruchniewicz, 2015).

Evaluating invasion impacts across scales

We found general agreement between patterns observed at the plot and the stand level. Most important, we found evidence for invasion effects on canopy nutrient-contents caused by *P. serotina* also when taking larger areas into account. Due to the fact, that in many cases it is unknown how invasion effects on biogeochemical cycles scale up (Weidenhamer and Callaway, 2010), such information is very valuable to evaluate invasion impacts. Additionally it may be important for evaluation of invasion effects on ecosystem services, which are usually accounted for at larger spatial scales (Eviner et al., 2012). Previous studies assessing plant invasion impacts over multiple scales almost solely focused on effects on plant community composition. The results of these studies underline the importance of mulit-scale assessments (Fridley et al., 2007). While plant invasions generally tend to decrease local biodiversity when looking at the fine scale, this effect is smaller or even opposed at broader spatial scales (Gaertner et al., 2009; Powell et al., 2011, 2013). Besides the evidence for spatial relevance, also the observation that invasion impacts were dependent from the occurrence frequency of *P. serotina* delivered valuable information. This result suggests that *P. serotina* can influence leaf nutrient stoichiometry already when forest stands are affected by fragmented populations of individuals present in the tree layer. Interpreting this result, it is important

to consider that at the moment single individuals reach the tree layer in many cases there is already subsequent recruitment present in the shrub layer, that may also influence canopy nutrient stoichiometry indirectly. Our results confirm that consideration of the spatial distribution patterns of species abundances or prevalences are an important aspect for evaluating invasion impacts (Thiele et al., 2009).

Contrary to leaf N:P ratio, for N_{mass} we found an invasion effect only at the plot, but not at the forest stand level. This finding indicates, that the influence of *P. serotina* on canopy leaf N contents alone is less substantial than its influence on N:P rations. The interpretation of observed differences between scales is strongly limited due to the high temporal mismatch between *P. serotina* occurrence data used for the plot and the stand level analysis. Since 2004 *P. serotina* further spread within the forest area, but was also partly removed in some management units in the course of thinning activities. Apart from the temporal mismatch in used data, differences between the two scales, may be also caused by strongly decreased variability at the stand level, by calculation mean values. This may have lead to smaller differences between invaded and non invaded areas compared to the plot level (Wiens, 1989). This effect at least can be observed when comparing differences between stand types at the plot and the stand level (see Fig. 2.24).

Remote sensing data proved useful to characterize differences between invaded and non invaded areas beyond the plot level, thereby highlighting its potential for quantification of invasion impacts across scales. This includes impacts on vegetation or ecosystem properties that otherwise are only hard to obtain across large areas. It is important to note that many plant functional traits, like N_{mass} and P_{mass} are not directly represented in the spectral signal of plant canopies (Ollinger, 2011). Thus, relationships between such traits and canopy reflectance can be established only via empirical models, which have to be calibrated with field data (Verrelst et al., 2015). Limitations of empirical relationships arise from their strong site specificity making predictions of traits under novel environmental conditions difficult (Ollinger, 2011).

Apart from providing maps of vegetation traits, applications of remote sensing in invasion ecology most commonly relate to mapping distributions of invasive plant species (Huang and Asner, 2009). Resulting maps can be used to study spatial distribution patterns of invasive plant species across scales and thus provide valuable information for the management of invasive species. Similar to traits, transferring models for mapping species distributions to other study areas is challenging, but feasible when focusing on distinct habitat types (Skowronek et al., 2018). Such model transfer is an important prerequisite for efficient early detection of invasive plant species. One major limitation for the use of remote sensing in invasion ecology evolves from the trade-off between resolution and coverage. Depending on the size of the target species, monitoring plant invasions requires fine resolution remote sensing particularly for the purpose of early detection (Bradley, 2014). Such fine resolution

data have become readily available by the use of sensors mounted on unmanned areal vehicles (UAV), but usually only over limited spatial extents.

2.2.5 Conclusion

We assessed differences in structural and chemical forest canopy traits between invaded and non-invaded areas at the plot and the stand level. Using this multi scale approach provided a more comprehensive picture on patterns and impacts of *P. serotina* invasions. Particularly, the assessment of invasion impacts over larger areas beyond the plot level provided valuable additional information on the spatial relevance of invasion impacts. Such information can help to prioritize management actions, by focusing on species that affect ecosystems over large areas. For the evaluation of potential impacts of plant invasions we thus recommend observations at a coarser spatial grain to supplement plot-level observations. Remotely sensed vegetation trait maps proved useful for this kind of multi-scale assessments.

Acknowledgements

2.2.6 Supplementary material

Figure 2.26 Maps displaying stand type, stand age (source: Office National des Forêts) and pH (Hattab et al., 2017) in the forest of Compiégne (France).
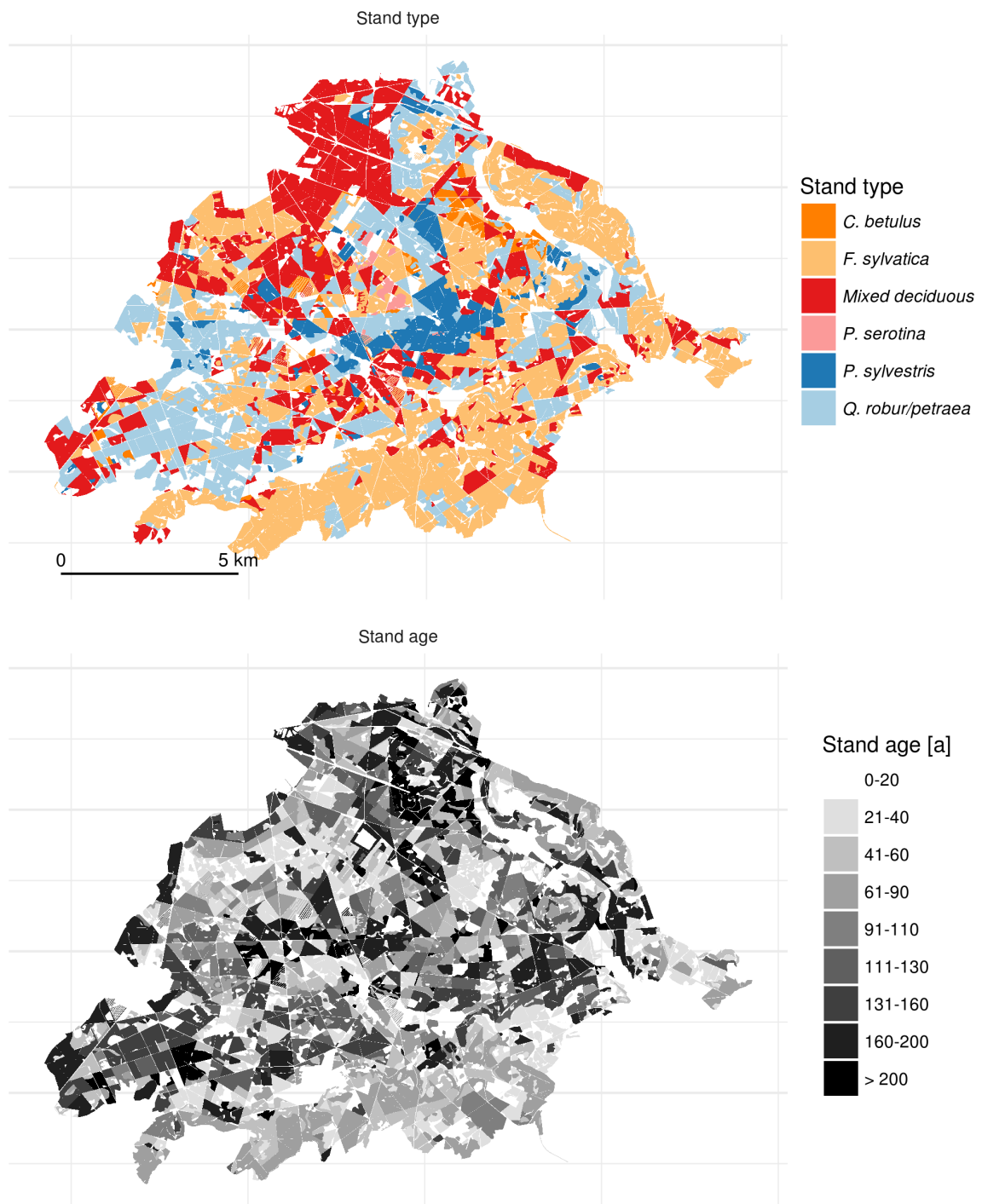
soil pH

Figure 2.26 Maps displaying stand type, stand age (source: Office National des Forêts) and pH (Hattab et al., 2017) in the forest of Compiégne (France).

LAI

Figure 2.27 Vegetation trait maps derived from a combination of airborne imaging spectroscopy and LiDAR data for the forest of Compiégne (France).

Figure 2.27 Vegetation trait maps derived from a combination of airborne imaging spectroscopy and LiDAR data for the forest of Compiégne (France).

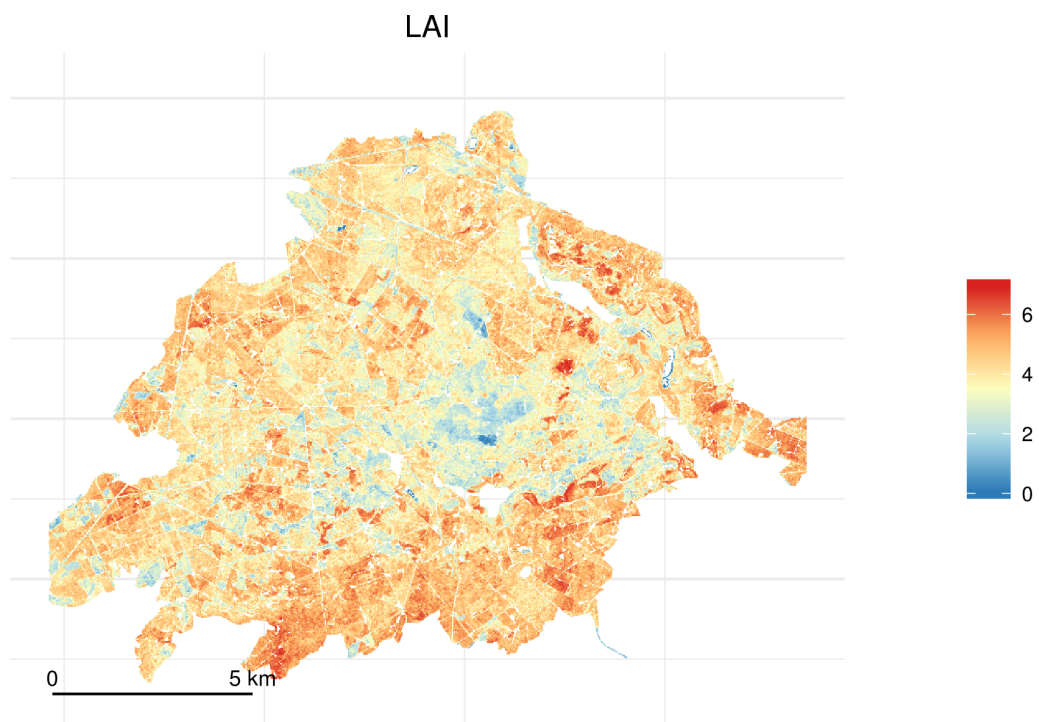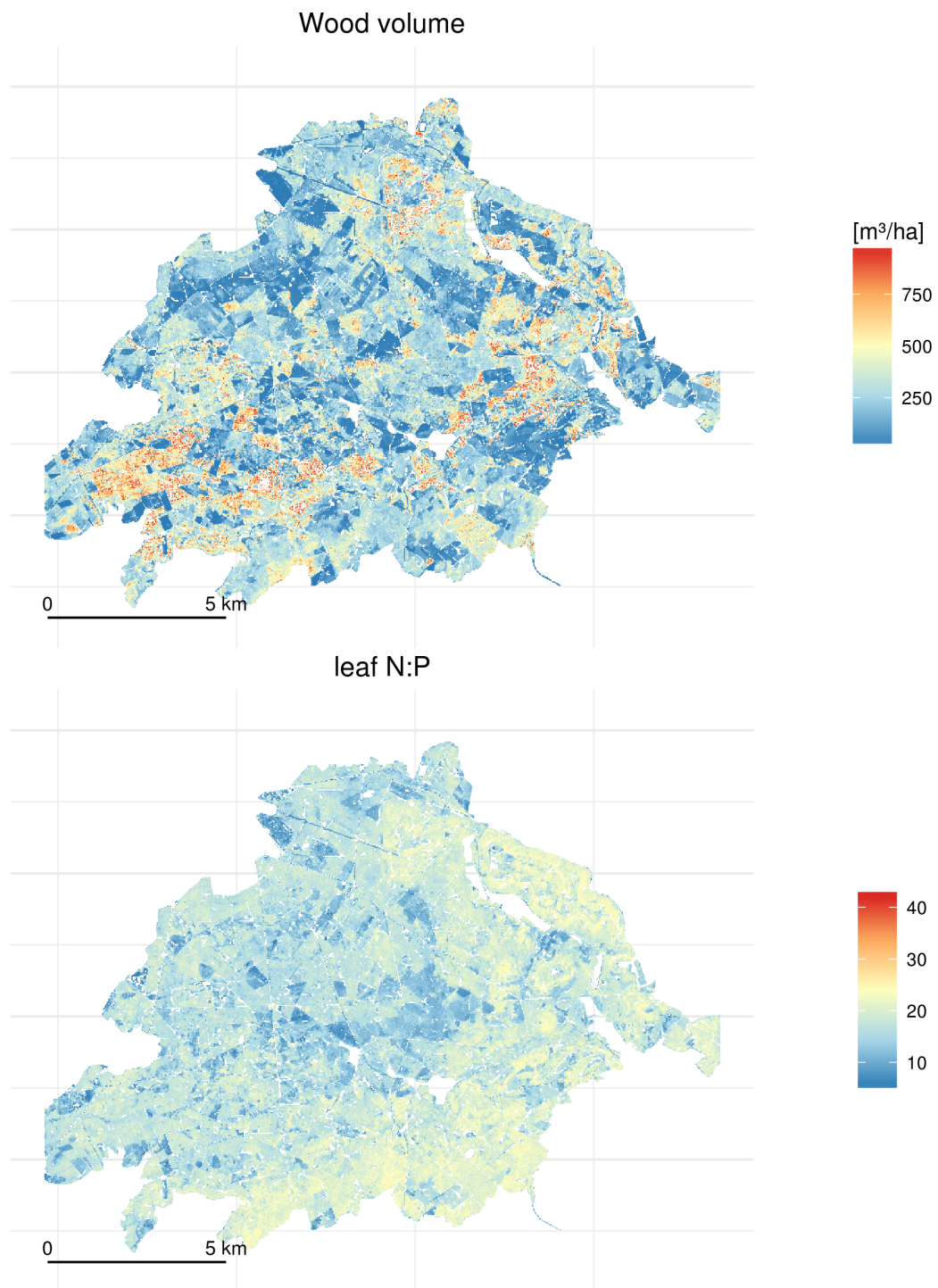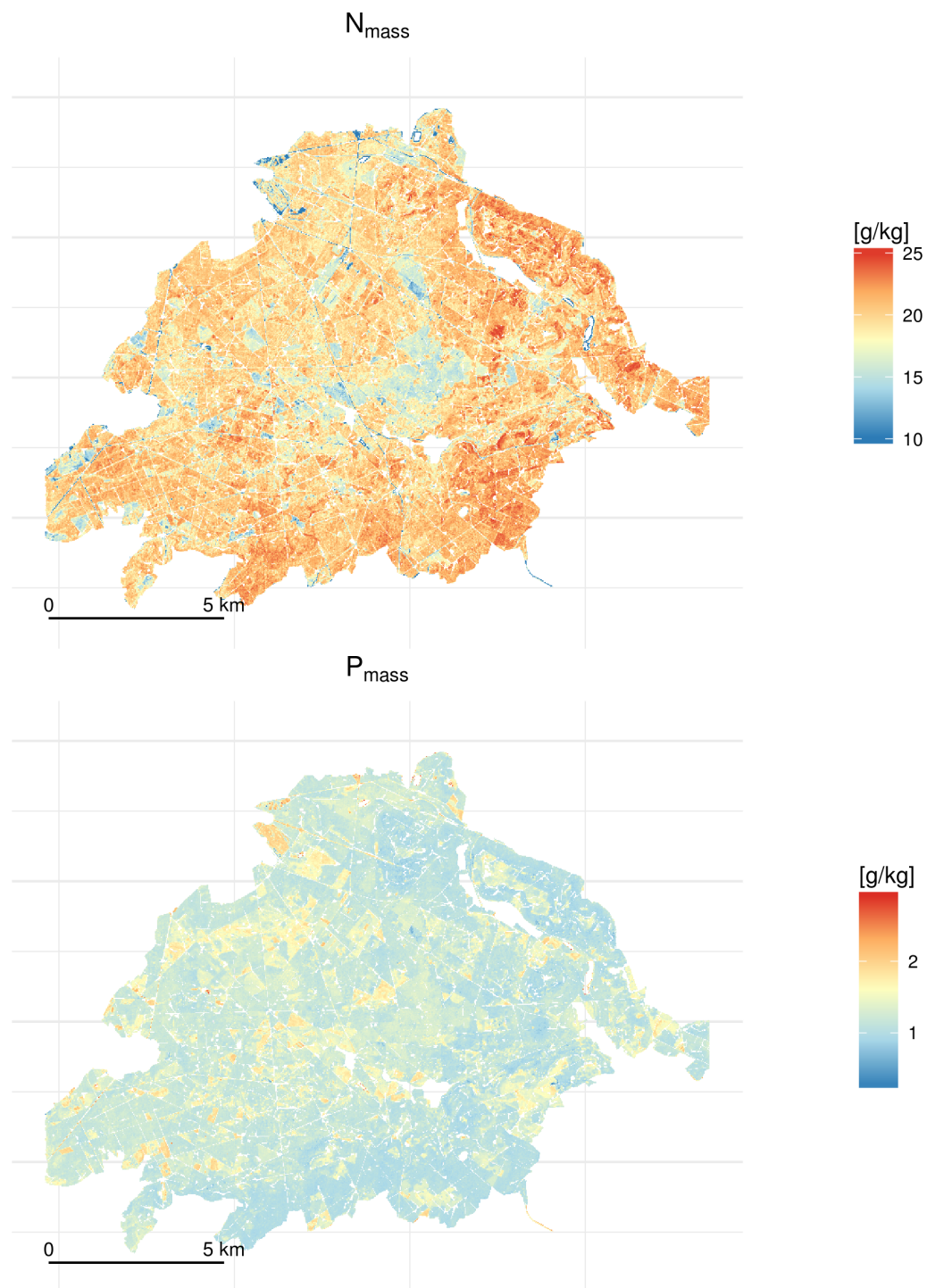**Figure 2.27** Vegetation trait maps derived from a combination of airborne imaging spectroscopy and LiDAR data for the forest of Compiégne (France).

Data S1: Acquisition and processing of remote sensing data

Airborne Imaging spectroscopy data of $3\,\text{m} \times 3\,\text{m}$ resolution was acquired in July 24, 2014 (9:56 – 11:25 UTC + 2h) at a flight height of 5400 m using the Airborne Prism EXperiment

(APEX) sensor (Schaepman et al., 2015). The data consisted of 284 bands in the wavelength range between 380 nm and 2500 nm and were recorded in 12 flight lines covering the whole study area. Recorded images were geometrically and atmospherically corrected according to the standard precessing chain applied to APEX recorded images (Sterckx et al., 2016; Vreys et al., 2016). Spectral bands affected by atmospheric water absorption and noisy bands at the beginning and end of the spectral range were removed. The final dataset consisted of 245 spectral bands between 426 nm and 2425 nm. From the resulting images we calculated the normalized difference vegetation index (NDVI) for the entire study area. Pixels with an NDVI value below 0.7 were excluded from subsequent analyses to remove information from non-vegetated areas. In order to reduce effects caused by different illumination we applied a brightness normalization (Feilhauer et al., 2010).

Airborne discrete-return LiDAR data was acquired in February 2014 during the leaf-off period at a flight height of 530 m using a RIEGL LMS-680i Lasersccanner (RIEGL Laser Measurement Systems GmbH, Horn, Austria). Point clouds were recorded with an maximum scan angle of 30°and a 65 % lateral overlap of neighboring flight lines resulting in an average point density of 23 points/m^2. The data were acquired and delivered by Aeredata (Lille, France) including a classification in ground and vegetation returns and a digital terrain model (DTM). Vegetation returns were normalized by subtracting them from the underlying DTM and then aggregated into a 3 m × 3 m grid using the imaging spectroscopy data as reference grid. For each grid cell we calculated 18 LiDAR metricss representing the vertical canopy structure (Tab. 2.8, see Ewald et al. (2014) for more information).

For the subsequent modelling we extracted data from hyperspectral images and maps of LiDAR derived variables at 50 plot locations. Values from pixels overlapping the plot area, were extracted for each plot. From extracted values we calculated weighted mean values for each plot, using the percentage overlap of each pixel with the plot area as weight. For all LiDAR derived variables we repeated this procedure calculating the weighted standard deviation as a measure for the horizontal heterogeneity of the forest canopy. This resulted in a dataset consisting of 281 predictor variables, 245 derived from imaging spectroscopy and 36 from airborne LiDAR.

For the calculation of prediction maps we aggregated hyperspectral images and LiDAR derived maps to a resolution of 24 m × 24 m to fit the size of used calibration plots. Resulting pixel values were derived by calculating mean values. LiDAR derived maps were additionally aggregated to the same resolution by calculating the standard deviation. This resulted in 281 raster-layers used for calculation of prediction maps.

Table 2.8 Predictor variables calculated from LiDAR point clouds.

LiDAR Metric	Description
Minimum	Basic statistics based on the height values of
Maximum	vegetation LiDAR points
Mean	
Standard deviation	
Variance	
Coefficient of variation	
10th percentile	
25th percentile	
50th percentile	
75th percentile	
90th percentile	
Fractional cover 0.5 m – 2 m	Inverse penetration ratios representing an estimate
Fractional cover 0.5 m – 60 m	for fractional cover of the vegetation within given
Fractional cover 2 m – 6 m	height thresholds
Fractional cover 2 m – 60 m	
Fractional cover 6 m – 10 m	
Fractional cover 6 m – 60 m	
Fractional cover 10 m – 20 m	
Fractional cover 20 m – 60 m	

Data S2: Generation of trait maps from remote sensing data

For mapping LAI, wood volume, N_{mass}, P_{mass} and N:P ratio, we used partial least squares regression models that were calibrated by field-derived trait data. For this purpose we collected trait data in a subset of the 336 field plots described above, consisting of 50 plots covering the range of invasion from non-invaded to fully invaded sites as well as all main forest types. Plot level LAI values were averaged from five measurements taken in each plot using a LAI-2200C Plant Canopy Analyzer (LI-COR Inc., Lincoln, USA). Reference measurements of light conditions were taken simultaneously at the nearest available clearing. Wood volume representing the total volume of woody standing biomass was calculated for each tree via the following allometric equation (Deleuze et al., 2014):

$$Vol = \frac{a \cdot h \cdot c^2}{4 \cdot pi \cdot \frac{1-1.3}{h}} \tag{2.2}$$

where h is the tree height, c the stem circumference at breast height and a represents a constant factor depending on the tree species. Constants determined using models calibrated within France were available for the most dominant of the 15 present tree species. For the seven remaining species we used constants from the same genus or one of the two universal constants available for broadleaved and coniferous trees (Tab. 2.9). Plot level values were calculated by summing up wood volumes of each tree and shrub including *P. serotina* individuals. N_{mass} and P_{mass} representing the community weighted mean of mass based leaf nitrogen and phosphorus content respectively was derived from analysis of canopy leaf samples. Leaf sampling included the most dominant tree species making up at least 80 % of

the total basal area in each plot. For each species and plot we sampled leaves from three different locations from the sunlit part of the canopy, if possible from different individuals. Depending on the species each sample consisted of 10 to 15 undamaged and healthy leaves. Sampled leaves were stored in sealed plastic bags and dried at 80°Cfor 48 h at the end of each field work day. Dried leaves were milled for subsequent analyses. Mass-based nitrogen was measured using a vario MACRO element analyzer (Elementar Analysensysteme, Hanau, Germany). Mass-based phosphorus content was measured using an inductively coupled plasma-optical emission spectrometer (ICP-OES) (Varian 725ES, Varian Inc., Palo Alto, CA, USA). For calculating community weighted mean values we used the relative basal areas of the occurring tree species as weights. To calculate N:P ratios, N_{mass} was divided by P_{mass} for each plot respectively.

For the prediction of vegetation traits maps we calculated partial least squares regression (PLSR) models using remote sensing data extracted at plot locations as predictors. Field-measured LAI, wood volume, N_{mass}, P_{mass} and N:P were used as response variables. We used a stepwise-backward model selection procedure to reduce the number of predictor variables in our models. Best models in each step were selected on the basis of the lowest root mean squared error (RMSE) in leave one out cross validation (Schmidtlein et al., 2012). Prior to model calculations predictors were standardized and centered. The modelling was embedded in a repeated data splitting procedure with 200 repetitions. In each repetition we randomly selected data from a subset of 40 out of 50 plots for model calibrations. From each of the 200 resulting models a prediction map was calculated for each response variable. From the resulting 200 maps we calculated median values for all pixels resulting in one median prediction map for each vegetation trait. Mean Pearson r-squared and RMSE in LOO validation were used to assess the predictive performance of each model set.

Table 2.9 Tree species, number of individuals, mean diameter at breast height (DBH) and species-specific constants used in the allometric equation for the calculation of wood volume in 50 calibration plots (Deleuze et al., 2014). For seven tree species no reference constants were available. In these cases we selected constants from species of the same genus or universal constants, available for broadleaved and deciduous tree species.

Species	# Individuals	Mean DBH [cm]	Constant
Acer campestre	1	12.1	0.509
Acer platanoides ∗	1	31.8	0.486
Acer pseudoplatanus	34	13.0 ± 9.1	0.486
Betula pendula	4	34.2 ± 8.3	0.472
Carpinus betulus	407	18.4 ± 9.2	0.503
Crataegus monogyna ∗∗	11	16.6 ± 4.0	0.496
Fagus sylvatica	498	23.8 ± 17.4	0.515
Fraxinus excelsior	20	32.9 ± 10.5	0.497
Malus sylvestris ∗∗	1	31.5	0.496
Picea abies	3	26.7 ± 11.0	0.486
Pinus sylvestris	56	41.3 ± 15.5	0.473
Prunus avium	4	32.1 ± 8.4	0.497
Prunus serotina ∗∗∗	483	9.4 ± 4.9	0.497
Quercus robur	121	53.9 ± 21.2	0.512
Salix caprea ∗∗	5	24.3 ± 4.7	0.496
Sorbus aucuparia ∗∗	1	11.8	0.496

∗ Constant for *A. pseudoplatanus*
∗∗ Universal constant for broadleaved tree species
∗∗∗ Constant for *P. avium*

Table 2.10 Evaluation results of Partial least squares regression models from 200 repeated model calculations based on permutations of the calibration dataset for LAI, Wood volume, N_{mass}, P_{mass}, and N:P ratio. Each calibration dataset permutation consisted of 40 observations. # LV: mean number of latent variables, # Var: mean number of selected predictor variables, R^2_{cal} : mean coefficient of determination in calibration, R^2_{cv} : mean coefficient of determination in leave-one-out cross-validation, $RMSE_{cal}$: mean root mean squared error in calibration, $RMSE_{cv}$: mean average root mean squared error in leave-one-out cross-validation

Response	# LV	# Var	R^2_{cal}	R^2_{cv}	$RMSE_{cal}$	$RMSE_{cv}$
LAI	7.5	20	0.57 ± 0.08	0.48 ± 0.09	0.87 ± 0.07	0.96 ± 0.07
Wood volume [m³/plot] *	4.7	22	0.85 ± 0.09	0.72 ± 0.07	0.32 ± 0.10	0.45 ± 1.16
N_{mass} [g/kg] *	5.7	43	0.55 ± 0.12	0.41 ± 0.16	0.08 ± 0.01	0.09 ± 0.01
P_{mass} [g/kg]	6.9	38	0.73 ± 0.08	0.63 ± 0.10	0.13 ± 0.02	0.14 ± 0.02
N:P ratio	5.9	99	0.72 ± 0.08	0.61 ± 0.10	1.91± 0.31	2.29 ± 0.32

* natural log transformed

Table 2.11 Median values and interquartile ranges of regression coefficients resulting from 200 repeated calculations of final plot level models. Stand type: Stand type represented by dominant tree species (factor with four levels: *Q. robur*, *F. sylvatica*, *P. sylvestris* and mixed broadleaved stands); pH: soil pH; Invasion: Presence/absence of *P. serotina* trees

Predictors	Response variables				
	LAI	Wood volume	N_{mass}	P_{mass}	N:P
Intercept	2.88 (0.42)	27.94 (6.89)	19.43 (0.85)	1.17 (0.07)	17.87 (1.49)
Stand type (*F. sylvatica*)	-0.01 (0.26)	-3.16 (5.41)	-0.46 (0.70)	-0.13 (0.08)	2.54 (1.20)
Stand type (Mixed)	0.00 (0.11)	-2.79 (3.73)	-0.31 (0.30)	-0.04 (0.05)	0.99 (0.57)
Stand type (*P. sylvestris*)	-1.53 (0.38)	-8.25 (5.55)	-4.14 (0.83)	0.07 (0.09)	-4.74 (1.21)
pH	0.23 (0.06)	-0.57 (1.59)	0.22 (0.14)	0.02 (0.01)	-0.13 (0.25)
Invasion	-	-6.33 (2.90)	-0.45 (0.75)	-	0.06 (0.81)
Invasion : Stand type (*F. sylvatica*)	-	7.63 (3.41)	0.50 (0.59)	-	-1.40 (0.90)
Invasion : Stand type (Mixed)	-	-1.78 (2.15)	-0.53 (0.70)	-	-2.01 (0.70)
Invasion : Stand type (*P. sylvestris*)	-	9.77 (3.82)	1.60 (0.70)	-	0.64 (1.07)

Table 2.12 Median values and interquartile ranges of regression coefficients resulting from 200 repeated calculations of final plot level models. Stand type: Stand type represented by dominant tree species (factor with four levels: *Q. robur*, *F. sylvatica*, *P. sylvestris* and mixed broadleaved stands); pH: soil pH; Invasion: Occurrence of *P. serotina* trees (factor with five levels ranging from no invasion in the tree layer (0) to continuous populations)

| Predictors	Response variables				
	LAI	Wood volume	N_{mass}	P_{mass}	N:P
Intercept	3.54 (0.16)	24.17 (3.99)	19.56 (0.44)	1.20 (0.05)	17.67 (0.49)
Stand type (*F. sylvatica*)	0.02 (0.10)	-5.65 (2.34)	-0.01 (0.18)	-0.02 (0.03)	0.83 (0.56)
Stand type (Mixed)	-0.19 (0.05)	-3.09 (1.73)	-0.44 (0.11)	0.02 (0.02)	-0.50 (0.18)
Stand type (*P. sylvestris*)	-0.95 (0.31)	-4.77 (5.15)	-2.82 (0.61)	0.07 (0.07)	-3.86 (0.77)
pH	0.12 (0.03)	-0.18 (0.77)	0.08 (0.09)	0.00 (0.01)	-0.04 (0.11)
Invasion (1)	-	-2.02 (1.28)	-	-	0.03 (0.05)
Invasion (2)	-	-2.89 (1.45)	-	-	-0.13 (0.11)
Invasion (3)	-	-4.46 (1.93)	-	-	-0.22 (0.13)
Invasion (4)	-	-4.63 (1.97)	-	-	-0.55 (0.15)
Invasion (1) : Stand type (*F. sylvatica*)	-	2.04 (1.15)	-	-	-
Invasion (2) : Stand type (*F. sylvatica*)	-	4.32 (5.35)	-	-	-
Invasion (3) : Stand type (*F. sylvatica*)	-	3.09 (1.52)	-	-	-
Invasion (4) : Stand type (*F. sylvatica*)	-	3.16 (1.31)	-	-	-
Invasion (1) : Stand type (Mixed)	-	0.61 (0.75)	-	-	-
Invasion (2) : Stand type (Mixed)	-	-0.30 (0.81)	-	-	-
Invasion (3) : Stand type (Mixed)	-	1.46 (1.00)	-	-	-
Invasion (4) : Stand type (Mixed)	-	0.34 (1.03)	-	-	-
Invasion (1) : Stand type (*P. sylvestris*)	-	1.53 (1.84)	-	-	-
Invasion (2) : Stand type (*P. sylvestris*)	-	1.49 (1.59)	-	-	-
Invasion (3) : Stand type (*P. sylvestris*)	-	3.13 (3.28)	-	-	-
Invasion (4) : Stand type (*P. sylvestris*)	-	4.09 (2.07)	-	-	-
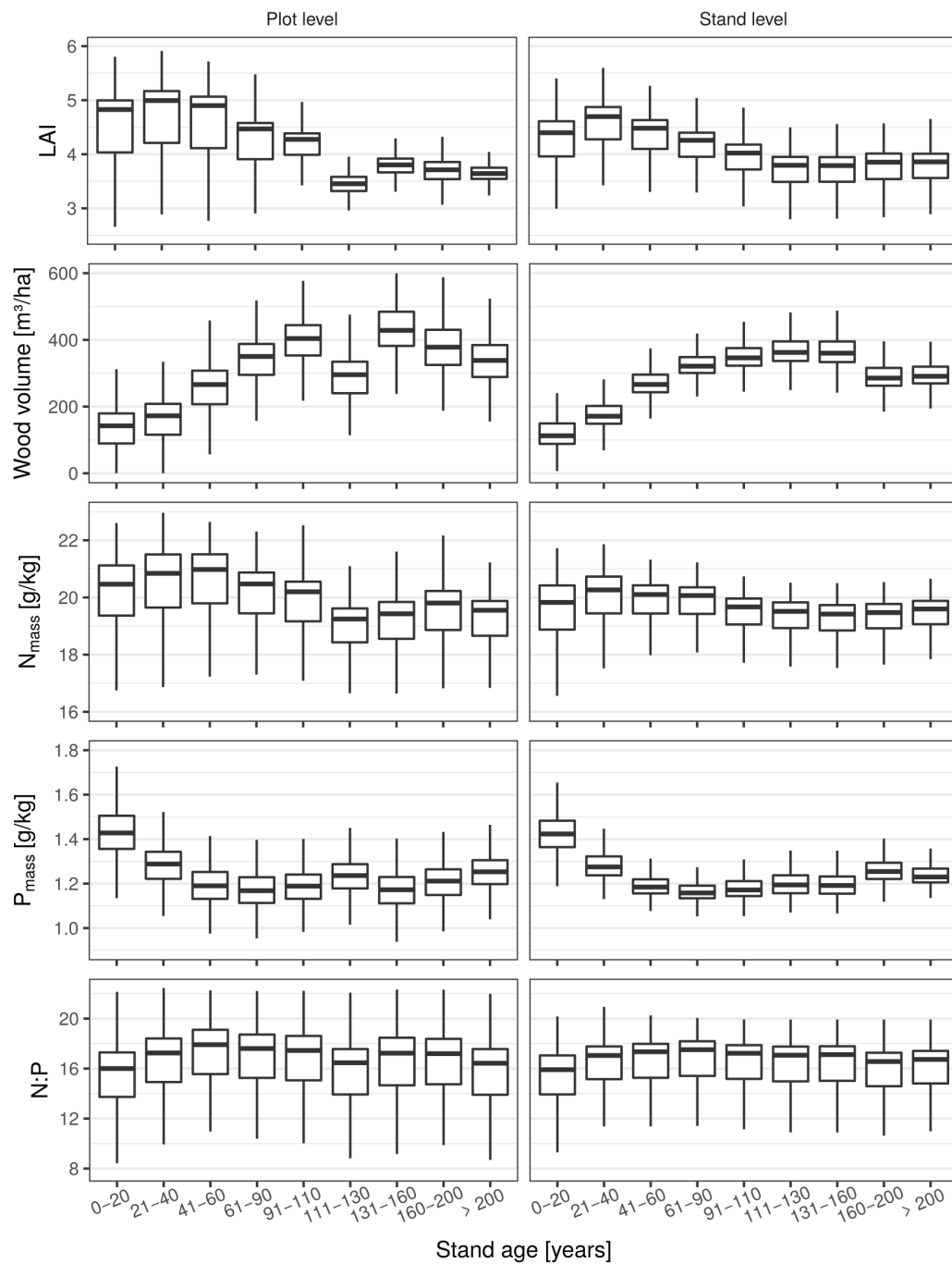
Figure 2.28 Predicted values of 200 repeated model calculations for LAI, wood volume, N_{mass}, P_{mass}, and leaf N:P shown for different age classes. Predictions from plot level models are displayed on the left, predictions from stand level models on the right. Displayed value ranges include all stand types included in the models.

2.3 Evaluating the ecosystem impact of an invasive moss using high resolution imaging spectroscopy

Michael Ewald, Sandra Skowronek, Raf Aerts, Jonathan Lenoir, Hannes Feilhauer, Ruben Van De Kerchove, Olivier Honnay, Ben Somers, Carol X. Garzón-López, Duccio Rocchini, Sebastian Schmidtlein

Abstract

Remote sensing has frequently been used to map the presences of alien invasive plant species. While most of these studies target the presence-absence of such species, remote sensing has an underutilized potential to predict fractional covers across large areas, which are more closely linked to the ecosystem impact of invasive plant species.

Here, we aimed at mapping the fractional cover of the invasive Heath Star Moss (*Campylopus introflexus*) using high resolution imaging spectroscopy (233 bands, 490 nm - 2430 nm, $3\,m \times 3\,m$ pixel size). Combining cover maps with field investigations, we further aimed to evaluate the impact of *C. introflexus* on plant diversity in different habitat types within a coastal dune ecosystem. Using cover information from 266 field plots we ran generalized partial least squares (gPLS) regression models to estimate the cover of *C. introflexus* from imaging spectroscopy. Models were calibrated using different training datasets, following a spatially blocked subsampling design. Additionally, the influence of *C. introflexus* fractional cover on the plant α-diversity was evaluated based on field data.

Fractional cover estimates from gPLS models resulted in R^2_{cv} values of 0.64 ± 0.17 and a RMSE of 0.14 ± 0.02 in independent validation. Results from our field investigations suggested a negative relationship between C. introflexus fractional cover and plant species α-diversity when the covers exceeded $44\,\%$ in one pixel. According to the remotely sensed cover maps this threshold was exceeded in $4.3\,\%$ to $7.1\,\%$ of the area in the studied habitats. Grey dunes were the most seriously affected habitat.

Our study demonstrates that apart from mapping occurrences, remote sensing can also be used to map fractional covers of alien invasive plant species indicating the impact magnitude. Cover maps can be used to highlight high impact areas or evaluate the susceptibility of different habitat types to invasion impacts and thus can help to prioritize management of established non-native invaders.

2.3.1 Introduction

Invasive alien plant species can have various unwanted consequences, including adverse effects on human health (Shackleton et al., 2019) and ecosystem functioning (Pyšek et al., 2012; Vilà et al., 2011). Impacts on ecosystems include alterations of species richness and composition (Powell et al., 2013), changes in disturbance regimes (Pauchard et al., 2008), or in ecological processes like carbon and nutrient cycling (Aerts et al., 2017; Liao et al., 2008). Once an invasive plant species has established within a new range, it is often extremely difficult to eradicate (Rejmanek and J. Pitcairn, 2002). Therefore, the management of established alien species focuses on limiting the most adverse effects (Kumschick et al., 2012). This requires prioritizing management efforts towards the most harmful species and the most valuable habitats (Gaertner et al., 2014; McGeoch et al., 2016). One prerequisite to prioritize these management efforts is the detection and monitoring of invasive plant species (Latombe et al., 2016).

Remote sensing techniques have high potential for monitoring invasive plants across vast areas (Rocchini et al., 2015). Many studies have demonstrated the capability of remote sensing approaches to detect invasive plant species and to map their distribution (Vaz et al., 2018). These studies covered a variety of growth forms including trees and shrubs (Lopatin et al., 2019; Somers and Asner, 2013) herbs or grasses (Müllerová et al., 2016; Skowronek et al., 2017a) and even cryptogams (Skowronek et al., 2018). Most commonly, these mapping approaches use classifiers, delivering maps with information on the target species presence and absence. Yet, remote sensing can also be used to acquire quantitative information on abundance measures such as the fractional cover of a plant species (e.g. Falkowski et al., 2017; Huang and Geiger, 2008; Miao et al., 2006; Peerbhay et al., 2016). As the ecosystem impact of an invasive plant species is considerably influenced by its local abundance (Parker et al., 1999), remote sensing is offering high potential not only to map invasive plant species, but also to indicate impact magnitudes across large areas (section 2.2. However, the potential to link abundance maps with potential invasion impacts has not been fully explored, yet. For, example abundance information can be used to compare the susceptibility of different habitat types to invasion impacts. Furthermore, abundance maps can be used in combination with abundance-impact relationships, displaying linkages between the abundance of an invader and specific ecosystem properties. This combination can be used as spatially explicit indicator for invasion impacts. Here, we aim to explore this potential.

The ability to retrieve plant species covers using imaging remote sensing techniques depends on the size of plant individuals or populations and the pixel-size of the images. Broadly speaking, two scenarios are possible. First, the outline of the target individual or population is exceeding the pixel size of the image. This is often the case, when using very high resolution remote sensing data in combination with large target individuals, such as shrubs and trees, or large monospecific stands (Gil et al., 2013; Guirado et al., 2017;

Kattenborn et al., 2019). Suitable mapping approaches for this scenario include classification approaches, delivering pixel-wise presence-absence information, and object or texture based approaches (Bradley, 2014). These approaches allow species covers to be calculated from resulting maps across larger areas (Falkowski et al., 2017). In the second scenario, the outline of the target individuals or stands are smaller than the pixel size of the used image. In this case spectral unmixing approaches and regression techniques can be used to predict plant species covers for single pixels (Asner and Martin, 2008; Miao et al., 2006; Peterson, 2005).

Here, we used airborne imaging spectroscopy to map the fractional cover of the invasive bryophyte *Campylopus introflexus*. We used generalized partial least squares (gPLS) regression, addressing a case with cover variation at the subpixel level. Using the fractional cover as a proxy for local abundance, we aimed to evaluate the ecosystem impact of *C. introflexus* within a dune habitat. The specific research questions were:

1. How accurate can the fractional cover of the invasive moss *C. introflexus* be mapped in different habitats using airborne imaging spectroscopy data?

2. Which are the most important wavelength bands for predicting fractional cover?

3. Which habitat type is most susceptible to invasion impacts?

4. At which fractional cover can we expect impacts on plant species diversity?

2.3.2 Materials and Methods

2.3.2.1 Study area

The study area covers the coastal dune ecosystem in the western part of the island of Sylt (54°55'00" N, 8°20'00" E) located in Northern Germany (Fig. 2.29). The climate is temperate oceanic with a mean annual temperature of 9° C and annual precipitation of 715 mm. The western coastline of Sylt has a north-to-south distance of approximately 35 km with protected dunes covering an area of 27.7 km^2. Habitats are characterized by a narrow belt of shifting dunes along the shoreline and vast areas of decalcified fixed dunes with herbaceous or dwarf shrub vegetation. In the northern part of the island, dunes are grazed by sheep. The predominant soil types are sandy loose immature soils and podsolized regosols both characterized by low organic matter content. The vegetation in the shifting dunes is characterized by grassland dominated by *Ammophila arenaria* (European Habitat Directive number 2120, Shifting dunes along the shoreline with *Ammophila arenaria*; further referred to as white dunes). Decalcified fixed dunes are characterized by heath vegetation dominated by *Empetrum nigrum* (2140, Decalcified fixed dunes with *Empetrum nigrum*; further referred to as crowberry heath), or by herbaceous vegetation with *Carex arenaria*, *Corynephorus canescens* and *Hypochoeris radicata* as the characteristic species (2130, Fixed dunes with herbaceous vegetation; further regarded as grey dunes). Frequently occurring dune slacks

which are periodically flooded by precipitation water floristically present the most valuable habitats (2190, Humid dune slacks). The vegetation in dune slacks is characterized by *Erica tetralix* and *Vaccinium uliginosum* with frequent occurrences of red listed plant species like *Drosera rotundifolia*, *Drosera intermedia* and *Pedicularis sylvatica*. *Campylopus introflexus* is present across the entire island, mainly occurring in the fixed dunes with little windblown sand intake. The species is locally forming huge and dense populations with growth heights up to 8 cm.
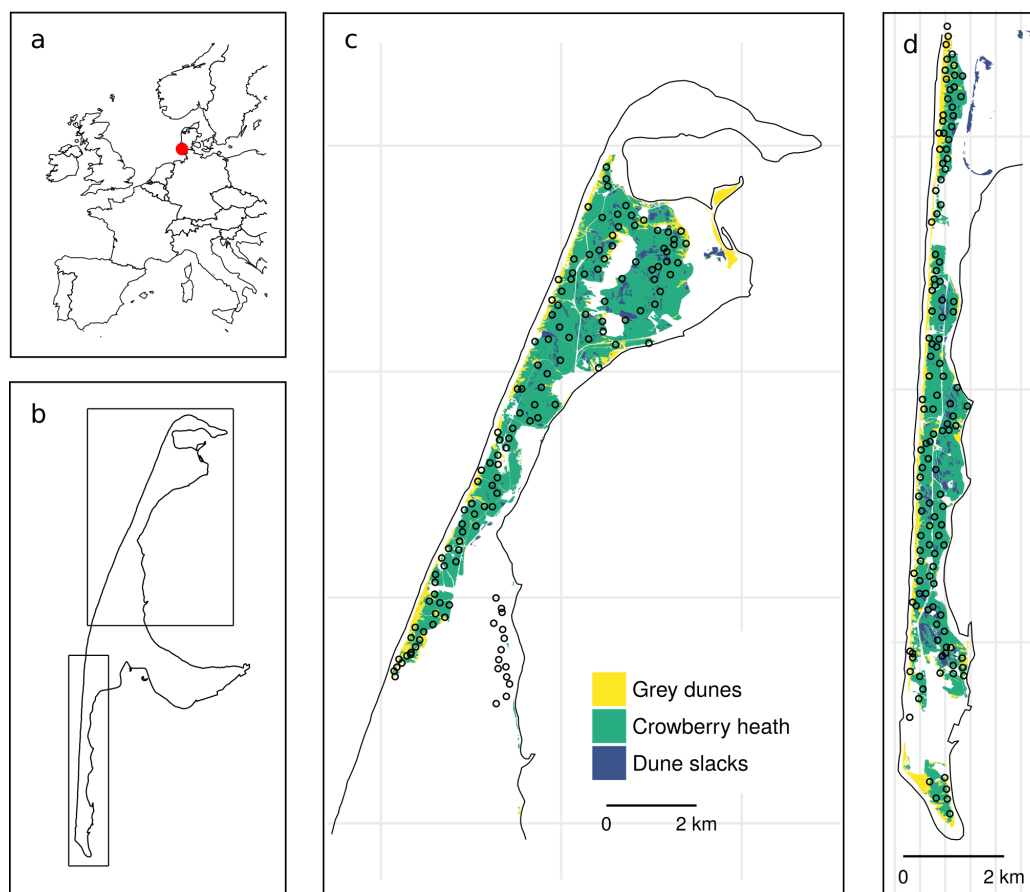
Figure 2.29 Location of the study area (a), outline of the island of Sylt (b) and habitat maps including plot locations for the northern (c) and southern part of the island (d).

Study species

Campylopus introflexus was first observed in Europe in 1941 and has by now spread across major parts of the continent (Hassel and Soderstrom, 2005). On the neighboring island of Römö it was first noticed in 1970 (Frahm, 1971), and probably also introduced on the island of Sylt around the same time. Growing on bare sand *C. introflexus* is predominately present in coastal dunes (Essl et al., 2014). When present, *C. introflexus* can form dense mats and may suppress native plant species (Biermann and Daniels, 1997; Hasse, 2007).

Vegetation data

Field data were acquired between June and November 2014 across 287 plots of $3\,\mathrm{m} \times 3\,\mathrm{m}$ surface area. Ninety of these plots were selected in-situ in order to cover sites with no presence (n = 30), low ($\leq 30\%$, n = 31) and medium to high fractional cover ($> 30\%$, n = 29) of *C. introflexus*. Hundred sixty additional plots were randomly sampled to cover all relevant habitat types in the study area. For each of the 287 plots we recorded the center coordinates and estimated the percentage cover of *C. introflexus*. In 90 plots we acquired additional field data including estimations of the percentage cover of all occurring vascular plant and moss species. In addition to the field data, for each plot, habitat types according to the Habitats Directive of the European union were derived from biotope maps of the year 2012 (Fig. 2.29, Tab. 2.13) (Leguan, 2012).

Table 2.13 Habitat types included in this study and total coverage across the Island of Sylt. # Training plots: number of plots included in the dataset used for model calibration. The remaining plots covered other habitat types.

Used Acronym	Description	Area (km²)	# Training plots
Grey dunes	Fixed coastal dunes with herbaceous vegetation	3.3	44
Crowberry dunes	Decalcified fixed dunes with Empetrum nigrum	15.1	167
Dune slacks	Humid dune slacks	1.6	13

Remote sensing data

Airborne imaging spectroscopy data were acquired on July 16th 2014, between 12:21 and 13:13 local time (UTC+2), using the APEX (Airborne Prism EXperiment) sensor at a flight height of $2270\,\mathrm{m}$ with flight lines in north-to-south direction. The data included images of 285 spectral bands covering the spectral range between $412\,\mathrm{nm}$ and $2432\,\mathrm{nm}$ with a pixel size of $1.8\,\mathrm{m} \times 1.8\,\mathrm{m}$. Imaging spectroscopy data was geometrically and atmospherically corrected using the standard procedures applied to APEX data (Sterckx et al., 2016; Vreys et al., 2016). For atmospheric correction ground reference samples were taken in September 2014 at 15 different locations at the beach and at large parking lots respectively using a full range field spectrometer (FieldSpec 4JR, ASD Inc., Longmont, USA).

Noisy bands between $410\,\mathrm{nm}$ and $480\,\mathrm{nm}$, and bands in the range between $1320\,\mathrm{nm}$ and $1450\,\mathrm{nm}$ and between $1670\,\mathrm{nm}$ and $1990\,\mathrm{nm}$, being affected by atmospheric water absorption were excluded from subsequent analyses. This resulted in a total of 233 predictor variables. To minimize the influence of shadows, we subjected the spectra to brightness normalization (Feilhauer et al., 2010). To meet the size of the field plots, the spatial resolution of spectral images was resampled to a pixel size of $3\,\mathrm{m} \times 3\,\mathrm{m}$.

For each of the 287 plots, we extracted the brightness normalized reflectance values from all pixels overlapping with the plot area. This resulted in up to four spectra originating from different neighboring pixels per plot. From these values we calculated the weighted

mean for each band using the percentage overlap of each pixel with the respective plot area as weight.

Generalized partial least squares regression

To model *C. introflexus* fractional covers we ran generalized partial least squares (gPLS) regression models using a logit link function. Models were calculated using the package plsRglm 1.1.1 (Bertrand et al., 2014) in R 3.4.4 (R Core Team, 2018). The northern end of the island was excluded from modeling because the specific vegetation community was underrepresented in the dataset. We therefore also dropped data from 21 field plots located in that area. This resulted in a total of 266 plots including 162 absence plots used in the final training dataset. All predictor variables were scaled to a mean value of 0 and a standard deviation of 1 to allow direct comparisons among estimated coefficients.

To prevent a possible underestimation of the prediction errors, model calculations were ran repeatedly using 10 different data subsets resulting from a spatially blocked subsampling procedure (Roberts et al., 2017). Based on their coordinates, field plots were divided into ten clusters using k-means clustering. For each dataset 20 % of the field plots were held out for independent validation, each time selecting the plots closest to the center coordinates of the respective clusters.

For the selection of relevant spectral bands, model calculations were additionally embedded in a 10-fold cross validation procedure. Bands were selected based on a stepwise backward variable selection procedure using the standardized coefficients as selection criteria. In each step we dropped ten percent of the predictor variables using the following procedure: We implemented a non-parametric bootstrap with 250 bootstrap replicates. For each bootstrap sample we recalculated gPLS regression models. Standardized coefficients for each predictor variable resulting from the 250 bootstraps were then tested for significant difference from zero using a confidence interval of $p < 0.05$. Using the test results we dropped predictor variables with insignificant standardized coefficient starting with those having the smallest mean absolute value.

For all models calculated in each step the optimal number of latent variables was selected based on the lowest AIC (Akaike Information Criterion) value. To prevent overfitting, we additionally limited the maximum number of latent variables to five. The procedure stopped when less than 10 percent of the remaining predictor variables showed insignificant standardized coefficients. From all steps the model associated with the lowest RMSE in 10-fold cross validation was selected as final model.

For each model calculated with different data subsets, we calculated prediction maps representing covers of *C. introflexus* in each pixel. From these maps we calculated median maps representing pixel-wise medians of predicted values.

Model evaluation

The model's predictive performances were evaluated by calculating two sets of Pearson R^2 values and root mean square error (RMSE) values based on the training and the independent validation dataset for each model respectively. To obtain the overall predictive performance we calculated the mean and standard error for both, R^2 and RMSE values.

The relative importance of each spectral band was derived by calculating model predictions with permuted predictor datasets. For each model, permuted datasets were created by successively randomizing the values of each predictor variable. For each permuted dataset, we re-calculated model predictions based on the original response data. Predicted values calculated from permuted datasets were then compared to the predictions from the non-permuted dataset, calculating the Pearson correlation coefficient. A high correlation coefficient here indicates that a band is not better than a random variable to predict fractional covers of *C. introflexus*. In contrast, a small coefficient indicates high relevance. Accordingly, the inverse correlation coefficient was then used as variable importance for each predictor variable.

Model residuals were used to compare prediction errors for different habitat types. To get a picture from all model residuals, we ran a linear mixed model (LMM) using the residuals from all models as response variable and habitat type as fixed effect. The used data subsets were numbered from 1 to 10 and included as random intercepts. We ran LMMs using the nlme 3.1 (Pinheiro et al., 2018) package in R.

Evaluating the impact of *C. introflexus*

To evaluate the abundance of *C. introflexus* in different habitat types, we calculated mean fractional covers and the total coverage for each type. First, average covers were calculated from each of the 10 prediction maps for each habitat type. As a second step, we calculated the mean and standard error from these values. Total coverages were derived by multiplying mean fractional covers with the total area of each habitat type, respectively.

To assess the impact of *C. introflexus* on native plant communities, we evaluated the relationship between its fractional cover and the plant α-diversity given by the Simpson diversity index (Simpson, 1949) calculated for 90 field plots. This cover-impact relationship was analyzed by fitting a linear model. The plot level α-diversity was used as response and the percentage cover of *C. introflexus* and its quadratic term as explaining variable. To identify existing break points in this relationship we ran a piecewise regression using the segmented 3.0 package in R (Muggeo, 2008, 2003).

2.3.3 Results

Using generalized partial least squares regression we were able to predict the fractional cover of *C. introflexus* at the subpixel level (Fig. 2.30). Models resulted in mean R^2 values of 0.71 (standard error: $\pm$ 0.03), and 0.64 $\pm$ 0.17 as well as mean RMSE values of 0.12 $\pm$

0.01 and 0.14 ± 0.02 based on the training and independent validation datasets respectively (Supplementary material Tab. 2.15).
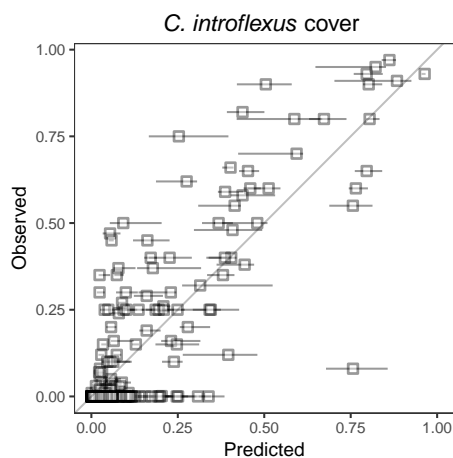

C. introflexus cover

Figure 2.30 Median predicted values retrieved from generalized partial least squares regression models vs. observed values for the fractional cover of *C. introflexus* in 3 m × 3 m plots from 10 training datasets. Error bars represent ranges between the 25 % quantile and the 75 % quantile of model predictions.

The ten final models included a range of 7 to 183 selected bands after variable selection. All models included bands situated in the shortwave-infrared region (SWIR) between 2150 nm and 2160 nm as well as between 2240 nm and 2250 nm (Fig. 2.31). The bands located around 2242 nm and 2248 nm had highest mean variable importances. Prediction errors differed between the habitat types, indicating highest prediction accuracy for crowberry heath and lowest accuracy for dune slacks (Fig. 2.32).
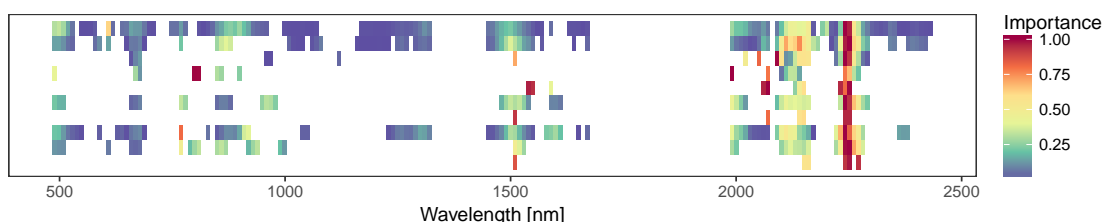

Figure 2.31 Relative importances of spectral bands included in 10 gPLS models using different training dataset.

Based on the median predictions *C. introflexus* total coverage across the island of Sylt reached 2.08 km^2. Mean covers of *C. introflexus* estimated for the three habitat types ranged from 10.2 ± 0.9 % in crowberry heath and 11.1 ± 1.0 % in grey dunes (Tab. 2.14).

The linear model relating fractional cover of *C. introflexus* to plot level α-diversity resulted in a R^2 value of 0.10. The predicted curve peaks at medium cover of *C. introflexus* (Fig. 2.33). Piecewise regression resulted in a break point at a fractional cover of 44 %. Above this break point increasing cover of *C. introflexus* is related to decreasing plant diversity at the level of 3 m × 3 m plots. The application of this break point on the prediction maps
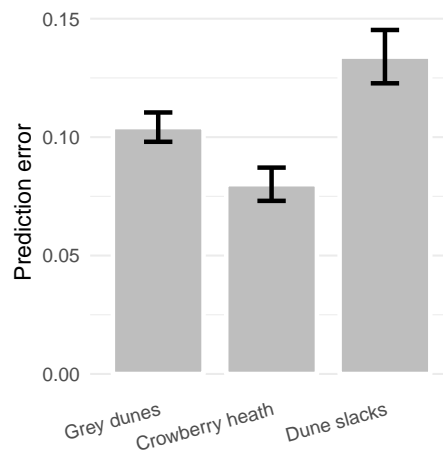
Figure 2.32 Prediction error of *C. introflexus* fractional cover for different habitat types. Displayed values represent absolute deviations of predicted covers from observed covers calculated using a linear mixed effects model including all deviations resulting from repeated gPLS model calculations.

Table 2.14 Fractional covers of *C. introflexus* for different habitat types based on predicted maps. Mean cover represents mean pixel values for each habitat type averaged for all calculated maps. The total coverage is giving the total area covered by *C. introflexus*.

Habitat	Mean cover (%)	Total coverage (km^2)
Grey dunes	11.1 ± 1.0	0.37
Crowberry heath	10.2 ± 0.9	1.54
Dune slacks	10.6 ± 1.9	0.17

indicated that 7.1 %, 4.3 % and 6.8 % of the pixels were characterized by fractional covers of 44 % or above, for grey dunes, crowberry heath and dune slacks respectively (Fig. 2.34).
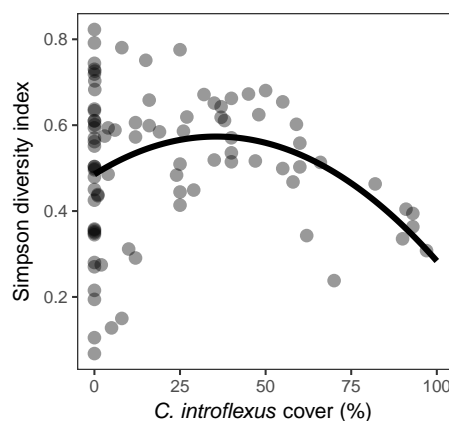

Figure 2.33 Relationship between *C. introflexus* cover and the α-diversity of plant species given by the Simpson diversity index observed for 90 field plots (3 m × 3 m) and predicted using a linear model.
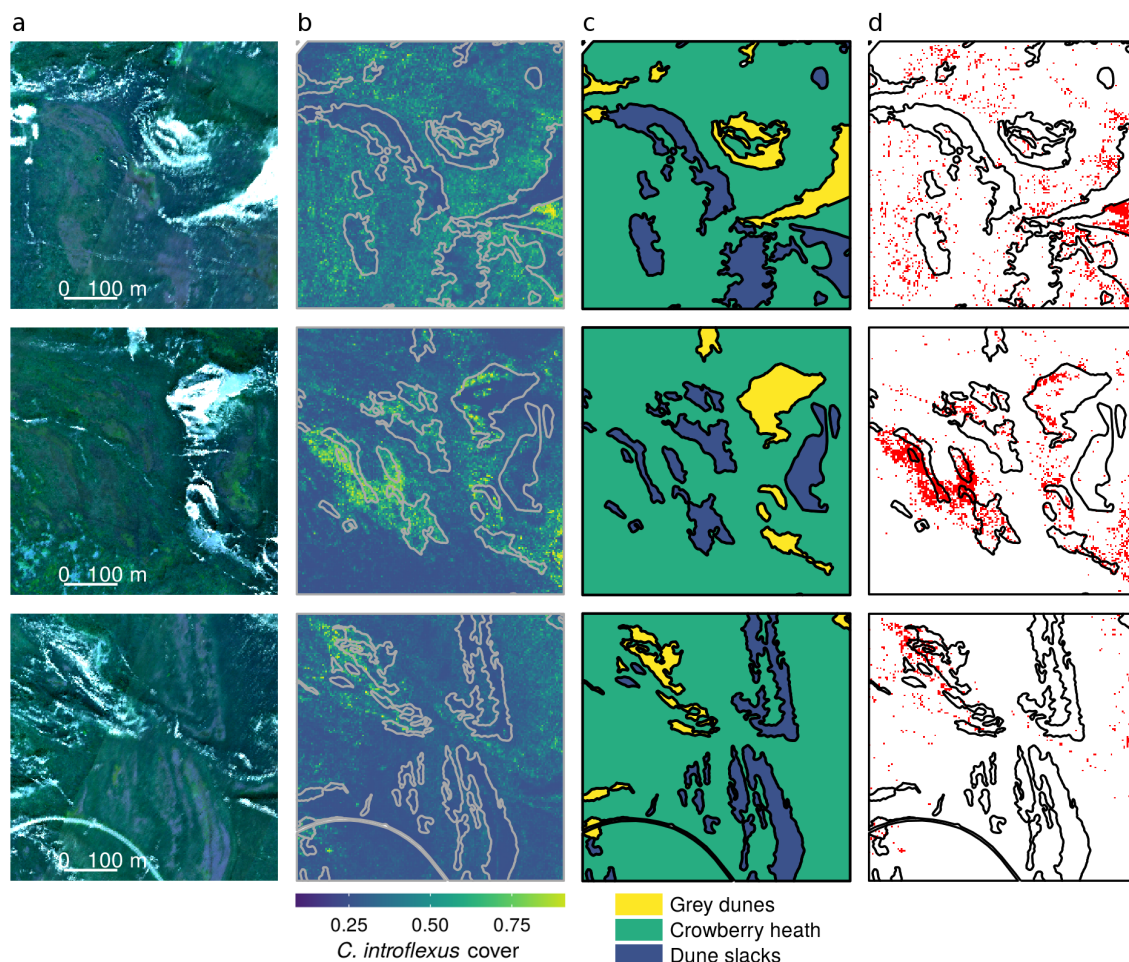
Figure 2.34 Map examples showing an RGB image (a), the predicted fractional cover of C. introflexus (b), a map of habitat types (c) and potential high impact areas (in red) concerning local α-diversity (d).

2.3.4 Discussion

Mapping the fractional cover of *C. introflexus*

We demonstrated that imaging spectroscopy can be used to map fractional covers of an invasive alien moss. Similar results for mapping invasive alien plant species covers have been found by previous studies, however in different contexts. For example, Peterson (2005) used multi-seasonal Landsat 7 images to map the cover of a grass species using different regression approaches. Guo et al. (2018), predicted the fractional cover of an invasive grass species using hyperspectral data derived from field spectroscopy using partial least squares regression. As alternative to regression approaches spectral mixture analyses can be used in scenarios where pixel size is exceeding the size of target species individuals or stands (Andrew and Ustin, 2008; Somers et al., 2011). This approach models reflectance spectra dependent on the fractional covers of different endmembers in one pixel. By inversion of such a model spectral mixture analyses can predict the covers of included endmembers, for

example dominant plant species occurring in a specific study area. This way, Asner and Martin (2008) predicted the covers of several non-native tree species in a rainforest using imaging spectroscopy.

Similar to presence-absence mapping one major requirement for the success of mapping species covers is that the spectral signal of the target species differs from that of the background vegetation (Bradley, 2014). In our study, plots with high *C. introflexus* covers were spectrally different from those without presence (Supplementary material Fig. 2.35). *C. introflexus* reflectance spectra are characterized by higher reflectance in the short wave infrared (SWIR) and lower reflectance in the near infrared (NIR) compared to the dominating species of the included habitat types. In contrast, differences in the visible region were far less pronounced. Although differences were present across large parts of the spectrum, variable importances indicated that only distinct sections were important for modeling fractional covers. The high importance of bands in the SWIR for the prediction of *C. introflexus* cover can be attributed to differences in leaf structural properties or water content (Jacquemoud et al., 2009; Kokaly et al., 2009). It is important to note that Skowronek et al. (2018) found different bands to be important for predicting presence and absence of *C. introflexus*. This study located important bands in the 1700 nm - 1750 nm region and around 2000 nm. This suggests that discriminating abundances of one species may require different spectral information than discriminating presences and absences.

Prediction accuracies differed for the habitat types included in this study, indicating less accurate cover predictions for dune slacks and grey dunes in comparison to crowberry heath. Lower accuracies for dune slacks can probably be attributed to the small sample size. For grey dunes lower accuracies can presumably be attributed to the spectral variability, that was highest in this habitat type (Supplementary material Fig. 2.36). Previous studies showed that the mapping accuracy of species is influenced by the spectral variability of the studied habitat (Andrew and Ustin, 2008; Somers et al., 2011). Besides the high variability, grey dune and *C. introflexus* canopy spectra seem to be less different compared to the other habitat types (Supplementary material Fig. 2.36). This may also influence prediction accuracies negatively (Andrew and Ustin, 2008). Apart from found differences in prediction accuracies, our results indicate that imaging spectroscopy is suited for cover predictions in different habitat types and hence also for comparing impacts of invasive plant species in these habitat types.

Evaluating the impact of *C. introflexus*

This study demonstrates the potential of remote sensing data to evaluate the susceptibility different habitat types to invasion impacts. Our results indicate that *C. introflexus* is most abundant in grey dunes which agrees with the findings of Klinck (2009). As the impact of a species is strongly related to its local abundance our cover maps can directly be used as

indicator for the impact magnitude of *C. introflexus*. Such information covering different habitat types can be used to prioritize limited management resources.

In our specific case, average fractional covers for *C. introflexus* were in the same order of magnitude for the three habitat types. Cover values derived from prediction maps were slightly higher than observed in the 160 randomly placed field plots (mean fractional covers of 9 %, 5 % and 6 % for crowberry heath, grey dunes and dune slacks, respectively). This may be because the discrete field sampling missed relevant spatial variation of *C. introflexus* fractional covers. Furthermore, differences may be caused by uncertainties of the used mapping approach. Potential difficulties may arise from its unreliability to detect low cover occurrences at the sub-pixel level (Bradley, 2014). For example Skowronek et al. (2017b) found, that the detection of *C. introflexus* becomes unreliable, when the species is covering less than one third of the pixel size. We therefore do not expect, that the used approach can be used to differentiate between low covers and absences. However, it has high potential to discriminate between low, medium or high abundance areas, and thus can indicate the magnitude of invasion effects.

In combination with abundance-impact relationships cover maps can be used to highlight high impact areas. Our results suggest a cover threshold of 44 % above which increasing cover of *C. introflexus* is related to decreasing α-diversity of vascular species. So far there exist only few studies that link ecosystem properties based with invasive alien plant species abundances (Panetta and Gooden, 2017). Those who did, found variable relationships strongly depending on the target species and studied variables (e.g. Fried and Panetta, 2016; Gooden et al., 2009; McAlpine et al., 2015). Deriving thresholds is only possible for non-linear relationships. Such thresholds should be applied with caution because they not necessary imply a causal link between invasive species abundances and a specific ecosystem property. For our case study it should also be considered that invasive species may affect sensitive species or functional types already, when occurring with lower abundances, than indicated by the threshold (Panetta and Gooden, 2017). In our case, particularly, interactions of *C. introflexus* with other mosses and lichens are not displayed in the threshold defined in this study and should be subject to further studies. Still abundance or cover threshold are meaningful particularly to prioritize the control of established invaders in valuable habitats (Panetta and Gooden, 2017).

2.3.5 Conclusion

In this study, we successfully mapped the fractional cover of an invasive alien moss species at the using imaging spectroscopy. Important spectral bands for the prediction of covers were situated in the SWIR, suggesting that variation in covers was related to differences in leaf and canopy structural properties. Resulting maps can be used to indicate ecosystem impacts, because the impact magnitude of alien species is strongly determined by their local abundances. We showed that cover maps can be used to evaluate the susceptibility of different

habitat types to potential invasion impacts. Furthermore, cover maps in combination with thresholds derived from cover-impact relationships might be useful to highlight areas of particular concern. Both outputs represent valuable information to prioritize management of established invasive alien species.

Acknowledgements

2.3.6 Supplementary material

Table 2.15 Results of generalized partial least squares models for predicting the fractional cover of C. introflexus using different training data subsets (sample size always n=212). $RMSE_{cal}$: root mean squared error in calibration, R^2_{cal}: coefficient of determination in calibration, $RMSE_{val}$: root mean squared error in independent validation; R^2_{val}: coefficient of determination in independent validation; # LV: number of latent variables; # Var: number of predictor variables.

Model	$RMSE_{cal}$	R^2_{cal}	$RMSE_{val}$	R^2_{val}	# LV	# Var
1	0.14	0.66	0.12	0.69	3	7
2	0.12	0.75	0.17	0.43	5	56
3	0.13	0.70	0.11	0.85	5	118
4	0.13	0.69	0.13	0.65	4	8
5	0.12	0.71	0.17	0.62	5	69
6	0.11	0.77	0.18	0.44	4	15
7	0.12	0.73	0.15	0.68	5	34
8	0.12	0.74	0.16	0.38	5	41
9	0.13	0.69	0.13	0.81	5	121
10	0.13	0.70	0.13	0.80	5	183
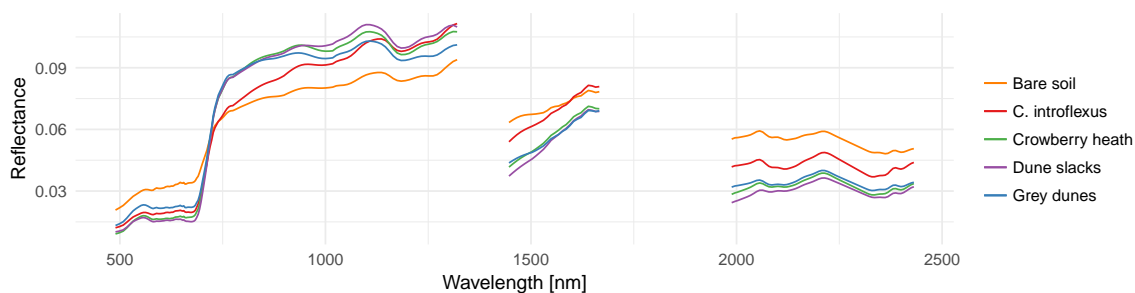
Figure 2.35 Mean spectra after brightness normalization for field plots located in the included habitat types (vegetation cover ≥ 90 %, up to 1 % *C. introflexus* presence), plots with high *C. introflexus* covers (≥ 80 %) and plots with high fractions of bare soil (≥ 85 %).

Figure 2.36 Mean spectra after brightness normalization for field plots located in the included habitat types (vegetation cover $\geq 90\,\%$, up to $1\,\%$ *C. introflexus* presence) and plots with high *C. introflexus* covers ($\geq 80\,\%$). Shaded areas represent the range between the 25 th and 75 th percentile of included spectra.
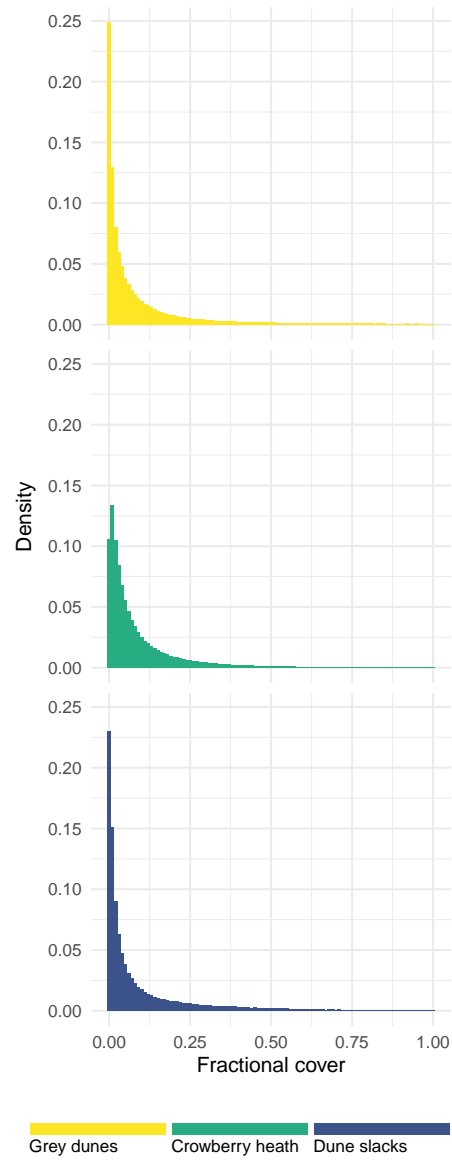
Figure 2.37 Histograms representing the relative frequency of predicted pixel values for different habitat types.
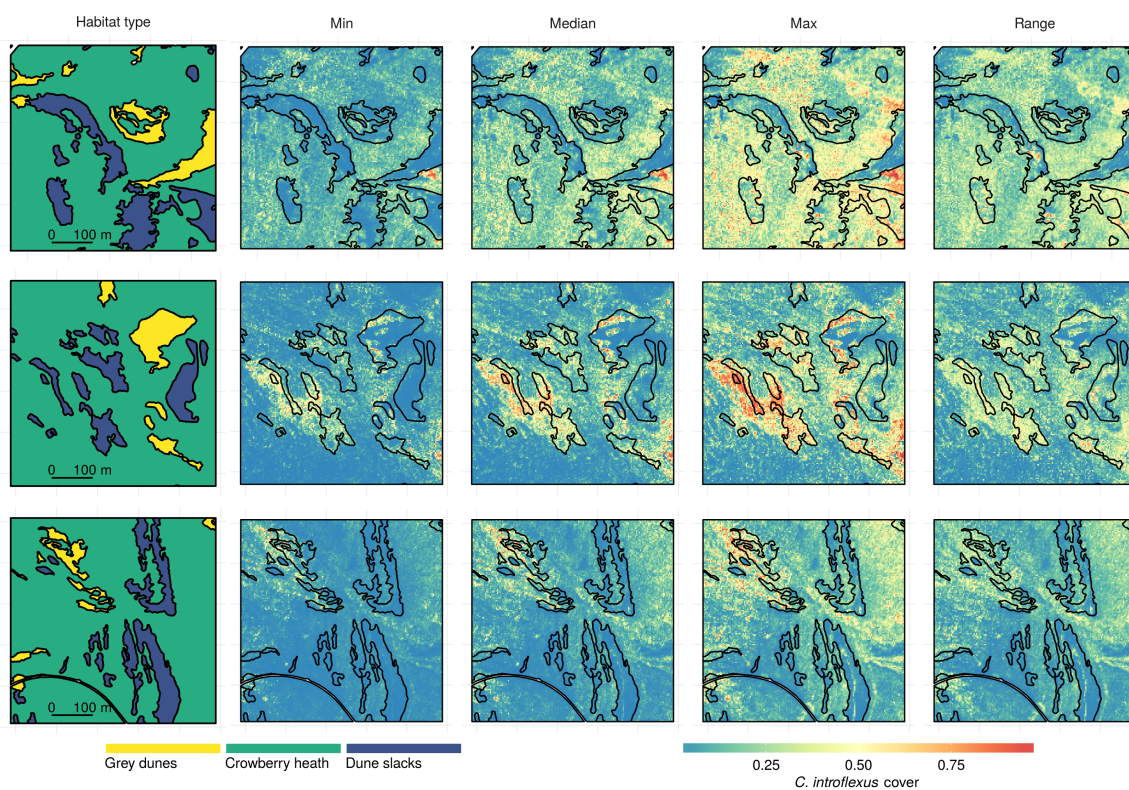
Figure 2.38 Map example showing median, minimum, maximum and the range of predicted values for the fractional cover *C. introflexus* including different habitat types within the dunes of the island Sylt. Median, minimum and maximum prediction as well as prediction ranges were derived from 10 repeated model calculation using different training datasets.

3 Synthesis and outlook

3.1 Synthesis

Invasive plant species can affect ecosystems in many ways. Detailed knowledge on the distribution and potential impacts of present species is a prerequisite to avoid undesired consequences. One way for remote sensing to contribute to a better understanding of invasive species habitat preference and impact is by delivering spatially explicit information. On this topic, remote sensing techniques have been mainly used to map distributions of invasive plant species, but rarely to assess impact. This thesis is breaking new ground by demonstrating and evaluating methods to assess invasive plant species impact using remote sensing.

The first research paper tested the potential of imaging spectroscopy to map chemical leaf constituents related to important ecosystem processes. Such maps can be used to display large-scale ecosystem changes caused by invasive plants. However, the retrieval of chemical canopy properties is difficult for structurally complex canopies. To tackle this problem canopy structure information, derived from airborne LiDAR data, was included in empirical models to link mass-based canopy N and P with imaging spectroscopy data. The results from paper 1 confirmed that a heterogeneous canopy structure is hampering the ability to map canopy N. One the other hand, a considerable part of variation in canopy P was explained by LiDAR-derived structural information. Paper 1 demonstrates that leaf chemical traits can also be mapped for structurally complex canopies. In such a case, successful mapping is achieved through the co-variation between structure and chemistry, rather than by a direct influence of N and P on canopy reflectance.

In paper 2, maps from paper 1 were combined with maps of the canopy N:P ratio, leaf area index (LAI), and wood volume. This set of maps was used to asses canopy traits in a temperate forest ecosystem and how they were related to the presence of black cherry (*Prunus serotina*). Here, canopy N and N:P ratio for invaded and non-invaded sites indicated that the presence of *P. serotina* affected canopy chemical composition. This result agrees with findings of a previous field study (Aerts et al., 2017), and thus highlights the potential of remote sensing to assess impact of invasive plant species. Moreover, paper 2 revealed that forest structural properties differed for invaded and non-invaded sites, providing insight into the site preference of *P. serotina*. These differences were detected for discrete locations and at the forest stand level. At the stand level, however, differences in canopy chemistry were only detected for the N:P ratio, and only when *P. serotina* was abundant. This highlights

the importance of the observational scale when assessing the ecosystem impact of invasive plant species. These results further underline the high potential of remote sensing to assess large scale ecosystem changes caused by invasive plant species. Remote sensing can thus be used to evaluate the relevance of invasion impacts for large areas.

Paper 3 demonstrates the use of imaging spectroscopy to map fractional cover of the invasive heath star moss *Campylopus introflexus* in an dune ecosystem. It represents the first study using remote sensing data to map the abundance of a bryophyte. By using local abundance as an indicator of impact magnitude the resulting maps provided a basis to evaluate the potential impact of *C. introflexus* in various habitat types. Additionally, plot-level plant diversity was analyzed in relation fractional cover of *C. introflexus*. From this cover-impact relationship we identified a threshold, above which increasing cover *C. introflexus* was negatively related to plant species diversity. This threshold was subsequently used to identify potential high impact areas. Although studies using remote sensing to map plant species abundances and studies evaluating the abundance-impact relationships of selected invasive plant species exist both, these approaches have never been combined.

In summary, this thesis identified and applied two major approaches to assess ecosystem impacts of invasive plant species using remote sensing techniques.

1. The first approach links remotely sensed information on ecosystem properties to invasive species occurrences (paper 2). This approach can be used to assess impacts at multiple spatial scales and, perhaps most important, can prove the relevance of impacts detected in small scale studies also for larger areas (paper 2). Here, remote sensing can deliver valuable information on vegetation properties which are related to ecosystem functioning such as biochemical leaf constituents or aboveground biomass (paper 1 & 2). Moreover, it is possible to identify also indirect links between vegetation properties and canopy reflectance using empirical models (paper 1). Remote sensing can therefore also be used to map vegetation attributes that do not influence canopy reflectance directly. One major drawback is that deriving information on many ecosystem properties using remote sensing is still far from being straight forward. This is particularly true for canopy chemical properties like demonstrated in paper 1.

2. The second approach refers to mapping the abundance, such as the fractional cover, of a particular species within a defined area, and using the abundance as an indicator of impact. Since the overall ecosystem impact of an invasive species strongly depends on its spatial distribution and local abundance (Parker et al., 1999), this approach allows to quantify impact magnitude across large areas. As shown in paper 3, abundance can also be directly linked to impact, regarding selected ecosystem properties, using the abundance-impact relationship. This allows to identify high impact areas concerning these ecosystem properties. Paper 3 demonstrates that mapping the abundance of a single species is feasible using very high resolution imaging spectroscopy. The importance of distinct bands in the SWIR, as observed in paper 3, indicates that it

is recommended to use hyperspectral remote sensing for this purpose. One major advantage of this approach is that it can be easily adapted for different species and habitats. It thus provides a means to compare impact severity between habitats.

3.2 Outlook

This thesis identified and applied two major approaches to assess ecosystem impacts of invasive plant species using remote sensing. The first approach— relating remotely sensed maps of ecosystem properties to the presence of invasive species—can substantially increase the understanding of biological invasions, particularly by evaluating the relevance of invasion impact over large areas. Despite the promising outcome of numerous previous studies, the retrieval of information on ecosystem properties from remote sensing remains difficult due to the complexity of natural ecosystems, and is still a topic under basic research. Therefore, giving reliable forecasts on which particular properties can be mapped successfully for a given study area is hardly possible. This makes it difficult to design studies to answer specific research questions related to invasion impact. Mapping accuracy is expected to be highest for vegetation attributes directly influencing the canopy reflectance. These include in particular structure-related variables such as the LAI, but also leaf pigments such as chlorophyll. To deliver reliable predictions of traits for different points in time and across different vegetation types, future research needs to improve the understanding of linkages between important functional vegetation traits and reflectance patters. Moreover, time series of ecosystem properties are highly suitable to detect and monitor changes related to plant invasions, particularly to disentangle cause and effect relationships between invasive species and environmental change. Invasion ecology research should use existing remote sensing products more often to study the broad scale relevance of various invasion impacts.

The second approach—mapping the abundance of invasive species as an indicator of ecological impact—is easier to implement and thus more promising to deliver information relevant for management practice. It can be used to highlight hotspot areas in which management is necessary, and to monitor occurrence over time. Furthermore, maps can be linked with the outcomes of risk assessments, providing information on a invasive species local impact related to its fractional cover. Field studies therefore need to consider recording invasion impacts in relation to the abundance of the target species; ideally its fractional cover. Future remote sensing studies should focus on mapping invasive plant fractional covers. To ensure a broad application, there is a need to develop approaches that are universally applicable and do not require sampling of new training data when moving to another study area. New machine-learning pattern-recognition algorithms hold promise to be capable of detecting species in multiple contexts (Wäldchen and Mäder, 2018). Such approaches can map fractional covers from RGB-images which can be acquired with little effort. Despite various methods for pattern recognition are readily available, only few have been applied

to detect vegetation characteristics from remote sensing data (Wagner et al., 2019). Here, further research is essential. Independent from the used method, future applications will strongly depend on the availability of very high resolution imaging data. Images acquired from UAV platforms represent a very flexible and cost-efficient alternative to cover smaller areas, as compared to images captured from an aircraft. Such data can, for example, be used to monitor invasion impact in conservation areas where invasive species are causing significant undesirable ecological impact.

Bibliography

Aerts, R., Ewald, M., Nicolas, M., Piat, J., Skowronek, S., Lenoir, J., Hattab, T., Garzón-López, C.X., Feilhauer, H., Schmidtlein, S., Rocchini, D., Decocq, G., Somers, B., Van De Kerchove, R., Denef, K., Honnay, O., 2017. Invasion by the alien tree *Prunus serotina* alters ecosystem functions in a temperate deciduous forest. Frontiers in Plant Science 8, 179. doi:`10.3389/fpls.2017.00179`.

Aguilera, A.G., Alpert, P., Dukes, J.S., Harrington, R., 2010. Impacts of the invasive plant *Fallopia japonica* (Houtt.) on plant communities and ecosystem processes. Biological Invasions 12, 1243–1252. doi:`10.1007/s10530-009-9543-z`.

Alberternst, B., Nawrath, S., 2018. Bewertungsansatz für die Priorisierung von Managementmaßnahmen an weit verbreiteten invasiven Pflanzenarten. Natur und Landschaft 93, 439–445. doi:`10.17433/9.2018.50153625.439-445`.

Albrecht, M., Ramis, M.R., Traveset, A., 2016. Pollinator-mediated impacts of alien invasive plants on the pollination of native plants: the role of spatial scale and distinct behaviour among pollinator guilds. Biological Invasions 18, 1801–1812. doi:`10.1007/s10530-016-1121-6`.

Ali, A.M., Darvishzadeh, R., Skidmore, A.K., van Duren, I., 2016. Effects of canopy structural variables on retrieval of leaf dry matter content and specific leaf area from remotely sensed data. IEEE Journal of Selected Topics in Applied Earth Observations and Remote Sensing 9, 898–909. doi:`10.1109/JSTARS.2015.2450762`.

Andrew, M.E., Ustin, S.L., 2008. The role of environmental context in mapping invasive plants with hyperspectral image data. Remote Sensing of Environment 112, 4301–4317. doi:`10.1016/j.rse.2008.07.016`.

Andrew, M.E., Ustin, S.L., 2009. Habitat suitability modelling of an invasive plant with advanced remote sensing data. Diversity and Distributions 15, 627–640. doi:`10.1111/j.1472-4642.2009.00568.x`.

Andrew, M.E., Wulder, M.A., Nelson, T.A., 2014. Potential contributions of remote sensing to ecosystem service assessments. Progress in Physical Geography 38, 328–353. doi:`10.1177/0309133314528942`.

de Araujo Barbosa, C.C., Atkinson, P.M., Dearing, J.A., 2015. Remote sensing of ecosystem services: A systematic review. Ecological Indicators 52, 430–443. doi:`10.1016/j.ecolind.2015.01.007`.

Asner, G.P., 1998. Biophysical and biochemical sources of variability in canopy reflectance. Remote Sensing of Environment 64, 234–253. doi:`10.1016/S0034-4257(98)00014-5`.

Asner, G.P., Martin, R.E., 2008. Spectral and chemical analysis of tropical forests: Scaling from leaf to canopy levels. Remote Sensing of Environment 112, 3958–3970. doi:`10.1016/j.rse.2008.07.003`.

Asner, G.P., Martin, R.E., Anderson, C.B., Knapp, D.E., 2015. Quantifying forest canopy traits: Imaging spectroscopy versus field survey. Remote Sensing of Environment 158, 15–27. doi:`10.1016/j.rse.2014.11.011`.

Asner, G.P., Martin, R.E., Suhaili, A.B., 2012. Sources of canopy chemical and spectral diversity in lowland bornean forest. Ecosystems 15, 504–517. doi:`10.1007/s10021-012-9526-2`.

Asner, G.P., Vitousek, P.M., 2005. Remote analysis of biological invasion and biogeochemical change. Proceedings of the National Academy of Sciences of the United States of America 102, 4383–4386. doi:`10.1073/pnas.0500823102`.

Badgley, G., Field, C.B., Berry, J.A., 2017. Canopy near-infrared reflectance and terrestrial photosynthesis. Science Advances 3, e1602244. doi:`10.1126/sciadv.1602244`.

Baker, R.H.A., Black, R., Copp, G.H., Haysom, K.A., Hulme, P.E., Thomas, M.B., Brown, A., Brown, M., Cannon, R.J.C., Ellis, J., Ellis, M., Ferris, R., Glaves, P., Gozlan, R.E., Holt, J., Howe, L., Knight, J.D., MacLeod, A., Moore, N.P., Mumford, J.D., Murphy, S.T., Parrott, D., Sansford, C.E., Smith, G.C., St-Hilaire, S., Ward, N.L., 2008. The UK risk assessment scheme for all non-native species., in: Rabitsch, W., Essl, F., Klingenstein, F. (Eds.), Biological Invasions: from Ecology to Conservation. NEOBIOTA 7, pp. 46–57.

Barbosa, J.M., Asner, G.P., Hughes, R.F., Johnson, M.T., 2017. Landscape-scale GPP and carbon density inform patterns and impacts of an invasive tree across wet forests of Hawaii. Ecological Applications 27, 403–415. doi:`10.1002/eap.1445`.

Bellard, C., Cassey, P., Blackburn, T.M., 2016. Alien species as a driver of recent extinctions. Biology Letters 12, 20150623. doi:`10.1098/rsbl.2015.0623`.

Bertrand, F., Meyer, N., Maumy-Bertrand, M., 2014. Partial least squares regression for generalized linear models, R package version 1.1.1.

Biermann, R., Daniels, F.J.A., 1997. Changes in a lichen-rich dry sand grassland vegetation with special reference to lichen synusiae and *Campylopus introflexus*. Phytocoenologia 27, 257–273. doi:`10.1127/phyto/27/1997/257`.

Birnbaum, C., Morald, T.K., Tibbett, M., Bennett, R.G., Standish, R.J., 2018. Effect of plant root symbionts on performance of native woody species in competition with an invasive grass in multispecies microcosms. Ecology and Evolution 8, 8652–8664. doi:`10.1002/ece3.4397`.

Bjornstad, O.N., 2016. ncf: Spatial nonparametric covariance functions, R package version 1.1-7.

Blackburn, T.M., Essl, F., Evans, T., Hulme, P.E., Jeschke, J.M., Kühn, I., Kumschick, S., Marková, Z., Mrugała, A., Nentwig, W., Pergl, J., Pyšek, P., Rabitsch, W., Ricciardi, A., Richardson, D.M., Sendek, A., Vilà, M., Wilson, J.R.U., Winter, M., Genovesi, P., Bacher, S., 2014. A unified classification of alien species based on the magnitude of

their environmentale impacts. PLOS Biology 12, e1001850. doi:`10.1371/journal.pbio.1001850`.

Bloom, A.J., Chapin, III, F., Mooney, H.A., 1985. resource limitation in plants-an economic analogy. Annual Review of Ecology and Systematics 16, 363–392. doi:`10.1146/annurev.es.16.110185.002051`.

Bonan, G.B., Levis, S., Kergoat, L., Oleson, K.W., 2002. Landscapes as patches of plant functional types: An integrating concept for climate and ecosystem models. Global Biogeochemical Cycles 16, 5–1. doi:`10.1029/2000GB001360`.

Bradley, B.A., 2014. Remote detection of invasive plants: a review of spectral, textural and phenological approaches. Biological Invasions 16, 1411–1425. doi:`10.1007/s10530-013-0578-9`.

Branquart, E., 2009. Alert, black and watch lists of invasive species in Belgium. Harmonia version 1.2 ed., Belgian Forum on Invasive species. URL: `http://ias.biodiversity.be`.

Cade, B.S., 1997. Comparison of tree basal area and canopy cover in habitat models: subalpine forest. The Journal of Wildlife Management 61, 326–335. doi:`10.2307/3802588`.

Castro-Díez, P., Godoy, O., Alonso, A., Gallardo, A., Saldaña, A., 2014. What explains variation in the impacts of exotic plant invasions on the nitrogen cycle? A meta–analysis. Ecology Letters 17, 1–12. doi:`10.1111/ele.12197`.

Catford, J.A., Daehler, C.C., Murphy, H.T., Sheppard, A.W., Hardesty, B.D., Westcott, D.A., Rejmánek, M., Bellingham, P.J., Pergl, J., Horvitz, C.C., Hulme, P.E., 2012. The intermediate disturbance hypothesis and plant invasions: Implications for species richness and management. Perspectives in Plant Ecology, Evolution and Systematics 14, 231–241. doi:`10.1016/j.ppees.2011.12.002`.

Cavaleri, M.A., Ostertag, R., Cordell, S., Sack, L., 2014. Native trees show conservative water use relative to invasive trees: results from a removal experiment in a Hawaiian wet forest. Conservation Physiology 2, 1–14. doi:`10.1093/conphys/cou016`.

Celesti-Grapow, L., Bassi, L., Brundu, G., Camarda, I., Carli, E., D'Auria, G., Guacchio, E.D., Domina, G., Ferretti, G., Foggi, B., Lazzaro, L., Mazzola, P., Peccenini, S., Pretto, F., Stinca, A., Blasi, C., 2016. Plant invasions on small Mediterranean islands: An overview. Plant Biosystems - An International Journal Dealing with all Aspects of Plant Biology 150, 1119–1133. doi:`10.1080/11263504.2016.1218974`.

Chabrerie, O., Roulier, F., Hoeblich, H., Sebert-Cuvillier, E., Closset-Kopp, D., Leblanc, I., Jaminon, J., Decocq, G., 2007. Defining patch mosaic functional types to predict invasion patterns in a forest landscape. Ecological Applications 17, 464–481. doi:`10.1890/06-0614`.

Chabrerie, O., Verheyen, K., Saguez, R., Decocq, G., 2008. Disentangling relationships between habitat conditions, disturbance history, plant diversity, and American black cherry *Prunus serotina* Ehrh.) invasion in a European temperate forest. Diversity and Distributions 14, 204–212. doi:`10.1111/j.1472-4642.2007.00453.x`.

Chai, Y., Yue, M., Wang, M., Xu, J., Liu, X., Zhang, R., Wan, P., 2015. Plant functional traits suggest a change in novel ecological strategies for dominant species in the stages of forest succession. Oecologia 180, 771–783. doi:`10.1007/s00442-015-3483-3`.

Chapin, F.S., 2003. Effects of plant traits on ecosystem and regional processes: a conceptual framework for predicting the consequences of global change. Annals of Botany 91, 455–463. doi:`10.1093/aob/mcg041`.

Chapuis-Lardy, L., Vanderhoeven, S., Dassonville, N., Koutika, L.S., Meerts, P., 2006. Effect of the exotic invasive plant *Solidago gigantea* on soil phosphorus status. Biology and Fertility of Soils 42, 481–489. doi:`10.1007/s00374-005-0039-4`.

Closset-Kopp, D., Saguez, R., Decocq, G., 2010. Differential growth patterns and fitness may explain contrasted performances of the invasive *Prunus serotina* in its exotic range. Biological Invasions 13, 1341–1355. doi:`10.1007/s10530-010-9893-6`.

Courchamp, F., Fournier, A., Bellard, C., Bertelsmeier, C., Bonnaud, E., Jeschke, J.M., Russell, J.C., 2017. Invasion biology: specific problems and possiblep solutions. Trends in Ecology & Evolution 32, 13–22. doi:`10.1016/j.tree.2016.11.001`.

Craven, D., Hall, J.S., Berlyn, G.P., Ashton, M.S., Breugel, M.v., 2015. Changing gears during succession: shifting functional strategies in young tropical secondary forests. Oecologia 179, 293–305. doi:`10.1007/s00442-015-3339-x`.

Curran, P.J., 1989. Remote sensing of foliar chemistry. Remote Sensing of Environment 30, 271–278. doi:`10.1016/0034-4257(89)90069-2`.

Curran, P.J., Kupiec, J.A., Smith, G.M., 1997. Remote sensing the biochemical composition of a slash pine canopy. IEEE Transactions on Geoscience and Remote Sensing 35, 415–420. doi:`10.1109/36.563280`.

Dahlin, K.M., Asner, G.P., Field, C.B., 2013. Environmental and community controls on plant canopy chemistry in a Mediterranean-type ecosystem. Proceedings of the National Academy of Sciences 110, 6895–6900. doi:`10.1073/pnas.1215513110`.

Dassonville, N., Vanderhoeven, S., Vanparys, V., Hayez, M., Gruber, W., Meerts, P., 2008. Impacts of alien invasive plants on soil nutrients are correlated with initial site conditions in NW Europe. Oecologia 157, 131–140. doi:`10.1007/s00442-008-1054-6`.

Davis, E.S., Kelly, R., Maggs, C.A., Stout, J.C., 2018. Contrasting impacts of highly invasive plant species on flower-visiting insect communities. Biodiversity and Conservation 27, 2069–2085. doi:`10.1007/s10531-018-1525-y`.

Deleuze, C., Morneau, F., Renaud, J., Vivien, Y., Rivoire, M., Santenoise, P., Longuetaud, F., MOTHE, F., Hervé, J., Vallet, P., 2014. Estimer le volume total d'un arbre, quelles que soient l'essence, la taille, la sylviculture, la station. Rendez-vous Techniques ONF , 22–32.

Denslow, J.S., 2003. Weeds in paradise: thoughts on the invasibility of tropical islands. Annals of the Missouri Botanical Garden 90, 119–127. doi:`10.2307/3298531`.

Di Palo, F., Fornara, D., 2015. Soil fertility and the carbon:nutrient stoichiometry of herbaceous plant species. Ecosphere 6, 1–15. doi:`10.1890/ES15-00451.1`.

Dormann, C.F., McPherson, J.M., Araújo, M.B., Bivand, R., Bolliger, J., Carl, G., Davies, R.G., Hirzel, A., Jetz, W., Kissling, W.D., Kühn, I., Ohlemüller, R., Peres-Neto, P.R.,

Reineking, B., Schröder, B., Schurr, F.M., Wilson, R., 2007. Methods to account for spatial autocorrelation in the analysis of species distributional data: a review. Ecography 30, 609–628. doi:`10.1111/j.2007.0906-7590.05171.x`.

Dzikiti, S., Gush, M.B., Le Maitre, D.C., Maherry, A., Jovanovic, N.Z., Ramoelo, A., Cho, M.A., 2016. Quantifying potential water savings from clearing invasive alien *Eucalyptus camaldulensis* using in situ and high resolution remote sensing data in the Berg River Catchment, Western Cape, South Africa. Forest Ecology and Management 361, 69–80. doi:`10.1016/j.foreco.2015.11.009`.

Díaz, S., Kattge, J., Cornelissen, J.H.C., Wright, I.J., Lavorel, S., Dray, S., Reu, B., Kleyer, M., Wirth, C., Colin Prentice, I., Garnier, E., Bönisch, G., Westoby, M., Poorter, H., Reich, P.B., Moles, A.T., Dickie, J., Gillison, A.N., Zanne, A.E., Chave, J., Joseph Wright, S., Sheremet'ev, S.N., Jactel, H., Baraloto, C., Cerabolini, B., Pierce, S., Shipley, B., Kirkup, D., Casanoves, F., Joswig, J.S., Günther, A., Falczuk, V., Rüger, N., Mahecha, M.D., Gorné, L.D., 2016. The global spectrum of plant form and function. Nature 529, 167–171. doi:`10.1038/nature16489`.

Ehrenfeld, J.G., 2010. Ecosystem consequences of biological invasions. Annual Review of Ecology, Evolution, and Systematics 41, 59–80. doi:`10.1146/annurev-ecolsys-102209-144650`.

Eichenberg, D., Trogisch, S., Huang, Y., He, J.S., Bruelheide, H., 2015. Shifts in community leaf functional traits are related to litter decomposition along a secondary forest succession series in subtropical China. Journal of Plant Ecology 8, 401–410. doi:`10.1093/jpe/rtu021`.

Elgersma, K.J., Ehrenfeld, J.G., 2010. Linear and non-linear impacts of a non-native plant invasion on soil microbial community structure and function. Biological Invasions 13, 757–768. doi:`10.1007/s10530-010-9866-9`.

Elser, J.J., Fagan, W.F., Kerkhoff, A.J., Swenson, N.G., Enquist, B.J., 2010. Biological stoichiometry of plant production: metabolism, scaling and ecological response to global change. New Phytologist 186, 593–608. doi:`10.1111/j.1469-8137.2010.03214.x`.

Elton, C.S., 1958. The ecology of invasions by animals and plants. Springer US, New York.

Essl, F., Lambdon, P.W., 2009. Alien bryophytes and lichens of europe, in: Handbook of Alien Species in Europe. Springer Netherlands, Dordrecht, pp. 29–41. doi:`10.1007/978-1-4020-8280-1_3`.

Essl, F., Steinbauer, K., Dullinger, S., Mang, T., Moser, D., 2014. Little, but increasing evidence of impacts by alien bryophytes. Biological Invasions 16, 1175–1184. doi:`10.1007/s10530-013-0572-2`.

EU, 2014. Regulation (EU) No 1143/2014 of the European Parliament and of the Council of 22 October 2014 on the prevention and management of the introduction and spread of invasive alien species.

European Commission, 2017. Invasive Alien Species of Union concern. Publications Office of the European Union, Luxembourg.

Eviner, V.T., Garbach, K., Baty, J.H., Hoskinson, S.A., 2012. Measuring the effects of invasive plants on ecosystem services: challenges and prospects. Invasive Plant Science and Management 5, 125–136. doi:`10.1614/IPSM-D-11-00095.1`.

Ewald, M., Dupke, C., Heurich, M., Müller, J., Reineking, B., 2014. LiDAR remote sensing of forest structure and GPS telemetry data provide insights on winter habitat selection of european roe deer. Forests 5, 1374–1390. doi:`10.3390/f5061374`.

Fajardo, A., Siefert, A., 2016. Phenological variation of leaf functional traits within species. Oecologia 180, 951–959. doi:`10.1007/s00442-016-3545-1`.

Falkowski, M.J., Evans, J.S., Naugle, D.E., Hagen, C.A., Carleton, S.A., Maestas, J.D., Khalyani, A.H., Poznanovic, A.J., Lawrence, A.J., 2017. Mapping tree canopy cover in support of proactive prairie grouse conservation in western north America. Rangeland Ecology & Management 70, 15–24. doi:`10.1016/j.rama.2016.08.002`.

Fassnacht, F.E., Hartig, F., Latifi, H., Berger, C., Hernández, J., Corvalán, P., Koch, B., 2014. Importance of sample size, data type and prediction method for remote sensing-based estimations of aboveground forest biomass. Remote Sensing of Environment 154, 102–114. doi:`10.1016/j.rse.2014.07.028`.

Fassnacht, F.E., Latifi, H., Stereńczak, K., Modzelewska, A., Lefsky, M., Waser, L.T., Straub, C., Ghosh, A., 2016. Review of studies on tree species classification from remotely sensed data. Remote Sensing of Environment 186, 64–87. doi:`10.1016/j.rse.2016.08.013`.

Fassnacht, F.E., Li, L., Fritz, A., 2015. Mapping degraded grassland on the Eastern Tibetan Plateau with multi-temporal Landsat 8 data — where do the severely degraded areas occur? International Journal of Applied Earth Observation and Geoinformation 42, 115–127. doi:`10.1016/j.jag.2015.06.005`.

Feilhauer, H., Asner, G.P., Martin, R.E., Schmidtlein, S., 2010. Brightness-normalized partial least squares regression for hyperspectral data. Journal of Quantitative Spectroscopy and Radiative Transfer 111, 1947–1957. doi:`10.1016/j.jqsrt.2010.03.007`.

Fernandes, R.A., Miller, J.R., Chen, J.M., Rubinstein, I.G., 2004. Evaluating image-based estimates of leaf area index in boreal conifer stands over a range of scales using high-resolution CASI imagery. Remote Sensing of Environment 89, 200–216. doi:`10.1016/j.rse.2002.06.005`.

Fisher, J.L., Veneklaas, E.J., Lambers, H., Loneragan, W.A., 2006. Enhanced soil and leaf nutrient status of a Western Australian Banksia woodland community invaded by *Ehrharta calycina* and *Pelargonium capitatum*. Plant and Soil 284, 253–264. doi:`10.1007/s11104-006-0042-z`.

Frahm, J.P., 1971. *Campylopus introflexus* (Hedw.) Brid. neu für Dänemark. Lindbergia 1, 117–118.

Fridley, J.D., Stachowicz, J.J., Naeem, S., Sax, D.F., Seabloom, E.W., Smith, M.D., Stohlgren, T.J., Tilman, D., Holle, B.V., 2007. The invasion paradox: reconciling pattern and process in species invasions. Ecology 88, 3–17. doi:`10.1890/0012-9658(2007)88[3:TIPRPA]2.0.CO;2`.

Fried, G., Panetta, F.D., 2016. Comparing an exotic shrub's impact with that of a native life form analogue: *Baccharis halimifolia* vs *Tamarix gallica* in Mediterranean salt marsh communities. Journal of Vegetation Science 27, 812–823. doi:`10.1111/jvs.12407`.

Fuentes, N., Saldaña, A., Kühn, I., Klotz, S., 2015. Climatic and socio-economic factors determine the level of invasion by alien plants in Chile. Plant Ecology & Diversity 8, 371–377. doi:`10.1080/17550874.2014.984003`.

Gaertner, M., Biggs, R., Te Beest, M., Hui, C., Molofsky, J., Richardson, D.M., 2014. Invasive plants as drivers of regime shifts: identifying high-priority invaders that alter feedback relationships. Diversity and Distributions 20, 733–744. doi:`10.1111/ddi.12182`.

Gaertner, M., Breeyen, A.D., Hui, C., Richardson, D.M., 2009. Impacts of alien plant invasions on species richness in Mediterranean-type ecosystems: a meta-analysis. Progress in Physical Geography 33, 319–338. doi:`10.1177/0309133309341607`.

Gallardo, B., Aldridge, D.C., González-Moreno, P., Pergl, J., Pizarro, M., Pyšek, P., Thuiller, W., Yesson, C., Vilà, M., 2017. Protected areas offer refuge from invasive species spreading under climate change. Global Change Biology 23, 5331–5343. doi:`10.1111/gcb.13798`.

Gallardo, B., Zieritz, A., Aldridge, D.C., 2015. The importance of the human footprint in shaping the global distribution of terrestrial, freshwater and marine invaders. PLoS One 10, e0125801. doi:`10.1371/journal.pone.0125801`.

Garnier, E., Lavorel, S., Ansquer, P., Castro, H., Cruz, P., Dolezal, J., Eriksson, O., Fortunel, C., Freitas, H., Golodets, C., Grigulis, K., Jouany, C., Kazakou, E., Kigel, J., Kleyer, M., Lehsten, V., Lepš, J., Meier, T., Pakeman, R., Papadimitriou, M., Papanastasis, V.P., Quested, H., Quétier, F., Robson, M., Roumet, C., Rusch, G., Skarpe, C., Sternberg, M., Theau, J.P., Thébault, A., Vile, D., Zarovali, M.P., 2007. Assessing the effects of land-use change on plant traits, communities and ecosystem functioning in grasslands: a standardized methodology and lessons from an application to 11 European sites. Annals of Botany 99, 967–985. doi:`10.1093/aob/mcl215`.

Gerard, F.F., North, P.R.J., 1997. Analyzing the effect of structural variability and canopy gaps on forest BRDF using a geometric-optical model. Remote Sensing of Environment 62, 46–62. doi:`10.1016/S0034-4257(97)00070-9`.

Gibson, M.R., Pauw, A., Richardson, D.M., 2013. Decreased insect visitation to a native species caused by an invasive tree in the Cape Floristic Region. Biological Conservation 157, 196–203. doi:`10.1016/j.biocon.2012.07.011`.

Gil, A., Lobo, A., Abadi, M., Silva, L., Calado, H., 2013. Mapping invasive woody plants in Azores Protected Areas by using very high-resolution multispectral imagery. European Journal of Remote Sensing 46, 289–304. doi:`10.5721/EuJRS20134616`.

Gill, S.J., Biging, G.S., Murphy, E.C., 2000. Modeling conifer tree crown radius and estimating canopy cover. Forest Ecology and Management 126, 405–416. doi:`10.1016/S0378-1127(99)00113-9`.

Gooden, B., French, K., Turner, P.J., Downey, P.O., 2009. Impact threshold for an alien plant invader, *Lantana camara* L., on native plant communities. Biological Conservation 142, 2631–2641. doi:`10.1016/j.biocon.2009.06.012`.

Grassi, G., Vicinelli, E., Ponti, F., Cantoni, L., Magnani, F., 2005. Seasonal and interannual variability of photosynthetic capacity in relation to leaf nitrogen in a deciduous forest plantation in northern Italy. Tree Physiology 25, 349–360.

Grossman, Y.L., Ustin, S.L., Jacquemoud, S., Sanderson, E.W., Schmuck, G., Verdebout, J., 1996. Critique of stepwise multiple linear regression for the extraction of leaf biochemistry information from leaf reflectance data. Remote Sensing of Environment 56, 182–193. doi:`10.1016/0034-4257(95)00235-9`.

Große-Stoltenberg, A., Hellmann, C., Thiele, J., Werner, C., Oldeland, J., 2018. Early detection of GPP-related regime shifts after plant invasion by integrating imaging spectroscopy with airborne LiDAR. Remote Sensing of Environment 209, 780–792. doi:`10.1016/j.rse.2018.02.038`.

Guirado, E., Tabik, S., Alcaraz-Segura, D., Cabello, J., Herrera, F., 2017. Deep-learning versus OBIA for scattered shrub detection with google earth imagery: *Ziziphus lotus* as case study. Remote Sensing 9, 1220. doi:`10.3390/rs9121220`.

Guo, Y., Graves, S., Flory, S.L., Bohlman, S., 2018. Hyperspectral measurement of seasonal variation in the coverage and mipacts of an invasive grass in an experimental setting. Remote Sensing 10, 784. doi:`10.3390/rs10050784`.

Gökkaya, K., Thomas, V., Noland, T.L., McCaughey, H., Morrison, I., Treitz, P., 2015. Prediction of macronutrients at the canopy level using spaceborne imaging spectroscopy and LiDAR data in a mixedwood boreal forest. Remote Sensing 7, 9045–9069. doi:`10.3390/rs70709045`.

Güsewell, S., 2004. N : P ratios in terrestrial plants: variation and functional significance. New Phytologist 164, 243–266. doi:`10.1111/j.1469-8137.2004.01192.x`.

Halarewicz, A., Pruchniewicz, D., 2015. Vegetation and environmental changes in a Scots pine forest invaded by *Prunus serotina*: what is the threat to terricolous bryophytes? European Journal of Forest Research 134, 793–801. doi:`10.1007/s10342-015-0890-2`.

Hale, A.N., Lapointe, L., Kalisz, S., 2016. Invader disruption of belowground plant mutualisms reduces carbon acquisition and alters allocation patterns in a native forest herb. New Phytologist 209, 542–549. doi:`10.1111/nph.13709`.

Han, W., Fang, J., Guo, D., Zhang, Y., 2005. Leaf nitrogen and phosphorus stoichiometry across 753 terrestrial plant species in China. New Phytologist 168, 377–385. doi:`10.1111/j.1469-8137.2005.01530.x`.

Hasse, T., 2007. *Campylopus introflexus* invasion in a dune grassland: succession, disturbance and relevance of existing plant invader concepts. Herzogia 20, 305–315.

Hassel, K., Soderstrom, L., 2005. The expansion of the alien mosses *Orthodontium lineare* and *Campylopus introflexu*s in Britain and continental Europe. Journal of the Hattori Botanical Laboratory , 183–194.

Hattab, T., Garzón-López, C.X., Ewald, M., Skowronek, S., Aerts, R., Horen, H., Brasseur, B., Gallet-Moron, E., Spicher, F., Decocq, G., Feilhauer, H., Honnay, O., Kempeneers, P., Schmidtlein, S., Somers, B., Van De Kerchove, R., Rocchini, D., Lenoir, J., 2017. A unified

framework to model the potential and realized distributions of invasive species within the invaded range. Diversity and Distributions 23, 806–819. doi:`10.1111/ddi.12566`.

Homolová, L., Malenovský, Z., Clevers, J.G.P.W., García-Santos, G., Schaepman, M.E., 2013. Review of optical-based remote sensing for plant trait mapping. Ecological Complexity 15, 1–16. doi:`10.1016/j.ecocom.2013.06.003`.

Huang, C.y., Asner, G.P., 2009. Applications of remote sensing to alien invasive plant studies. Sensors 9, 4869–4889. doi:`10.3390/s90604869`.

Huang, C.y., Geiger, E.L., 2008. Climate anomalies provide opportunities for large-scale mapping of non-native plant abundance in desert grasslands. Diversity and Distributions 14, 875–884. doi:`10.1111/j.1472-4642.2008.00500.x`.

Huber, S., Kneubühler, M., Psomas, A., Itten, K., Zimmermann, N.E., 2008. Estimating foliar biochemistry from hyperspectral data in mixed forest canopy. Forest Ecology and Management 256, 491–501. doi:`10.1016/j.foreco.2008.05.011`.

Jacquemoud, S., Verhoef, W., Baret, F., Bacour, C., Zarco-Tejada, P.J., Asner, G.P., François, C., Ustin, S.L., 2009. PROSPECT+SAIL models: A review of use for vegetation characterization. Remote Sensing of Environment 113, S56–S66. doi:`10.1016/j.rse.2008.01.026`.

Jonard, M., Fürst, A., Verstraeten, A., Thimonier, A., Timmermann, V., Potočić, N., Waldner, P., Benham, S., Hansen, K., Merilä, P., Ponette, Q., de la Cruz, A.C., Roskams, P., Nicolas, M., Croisé, L., Ingerslev, M., Matteucci, G., Decinti, B., Bascietto, M., Rautio, P., 2015. Tree mineral nutrition is deteriorating in Europe. Global Change Biology 21, 418–430. doi:`10.1111/gcb.12657`.

Jones, H.G., Vaughan, R.A., 2010. Remote sensing of vegetation: principles, techniques, and applications. Oxford University Press, Oxford, New York.

Jäger, H., Alencastro, M.J., Kaupenjohann, M., Kowarik, I., 2013. Ecosystem changes in Galápagos highlands by the invasive tree *Cinchona pubescens*. Plant and Soil 371, 629–640. doi:`10.1007/s11104-013-1719-8`.

Kattenborn, T., Fassnacht, F.E., Pierce, S., Lopatin, J., Grime, J.P., Schmidtlein, S., 2017. Linking plant strategies and plant traits derived by radiative transfer modelling. Journal of Vegetation Science 28, 717–727. doi:`10.1111/jvs.12525`.

Kattenborn, T., Fassnacht, F.E., Schmidtlein, S., 2018. Differentiating plant functional types using reflectance: which traits make the difference? Remote Sensing in Ecology and Conservation 5, 5–19. doi:`10.1002/rse2.86`.

Kattenborn, T., Lopatin, J., Förster, M., Braun, A., Fassnacht, F.E., 2019. UAV data as alternative to field sampling to map woody invasive species based on combined Sentinel-1 and Sentinel-2 data. Remote Sensing of Environment 227, 61–73. doi:`10.1016/j.rse.2019.03.025`.

Kimberley, A., Alan Blackburn, G., Duncan Whyatt, J., Smart, S.M., 2014. Traits of plant communities in fragmented forests: the relative influence of habitat spatial configuration and local abiotic conditions. Journal of Ecology 102, 632–640. doi:`10.1111/1365-2745.12222`.

Klinck, J., 2009. The alien invasive moss Campylopus introflexus in the Danish coastal dune system. Masterarbeit ed., Copenhagen University.

Knyazikhin, Y., Schull, M.A., Stenberg, P., Mõttus, M., Rautiainen, M., Yang, Y., Marshak, A., Carmona, P.L., Kaufmann, R.K., Lewis, P., Disney, M.I., Vanderbilt, V., Davis, A.B., Baret, F., Jacquemoud, S., Lyapustin, A., Myneni, R.B., 2013. Hyperspectral remote sensing of foliar nitrogen content. Proceedings of the National Academy of Sciences 110, E185–E192. doi:`10.1073/pnas.1210196109`.

Kokaly, R.F., Asner, G.P., Ollinger, S.V., Martin, M.E., Wessman, C.A., 2009. Characterizing canopy biochemistry from imaging spectroscopy and its application to ecosystem studies. Remote Sensing of Environment 113, 78–91. doi:`10.1016/j.rse.2008.10.018`.

Korhonen, L., Korpela, I., Heiskanen, J., Maltamo, M., 2011. Airborne discrete-return LIDAR data in the estimation of vertical canopy cover, angular canopy closure and leaf area index. Remote Sensing of Environment 115, 1065–1080. doi:`10.1016/j.rse.2010.12.011`.

Koutika, L.S., Vanderhoeven, S., Chapuis-Lardy, L., Dassonville, N., Meerts, P., 2007. Assessment of changes in soil organic matter after invasion by exotic plant species. Biology and Fertility of Soils 44, 331–341. doi:`10.1007/s00374-007-0210-1`.

Kumar, L., Sinha, P., Taylor, S., Alqurashi, A.F., 2015. Review of the use of remote sensing for biomass estimation to support renewable energy generation. Journal of Applied Remote Sensing 9, 097696. doi:`10.1117/1.JRS.9.097696`.

Kumschick, S., Bacher, S., Dawson, W., Heikkilä, J., Sendek, A., Pluess, T., Robinson, T., Kühn, I., 2012. A conceptual framework for prioritization of invasive alien species for management according to their impact. NeoBiota 15, 69–100. doi:`10.3897/neobiota.15.3323`.

Kumschick, S., Gaertner, M., Vilà, M., Essl, F., Jeschke, J.M., Pyšek, P., Ricciardi, A., Bacher, S., Blackburn, T.M., Dick, J.T.A., Evans, T., Hulme, P.E., Kühn, I., Mrugała, A., Pergl, J., Rabitsch, W., Richardson, D.M., Sendek, A., Winter, M., 2015. Ecological impacts of alien species: quantification, scope, caveats, and recommendations. BioScience 65, 55–63. doi:`10.1093/biosci/biu193`.

Kurokawa, H., Peltzer, D.A., Wardle, D.A., 2010. Plant traits, leaf palatability and litter decomposability for co-occurring woody species differing in invasion status and nitrogen fixation ability. Functional Ecology 24, 513–523. doi:`10.1111/j.1365-2435.2009.01676.x`.

Kurten, E.L., Snyder, C.P., Iwata, T., Vitousek, P.M., 2008. *Morella cerifera* invasion and nitrogen cycling on a lowland Hawaiian lava flow. Biological Invasions 10, 19–24. doi:`10.1007/s10530-007-9101-5`.

Kusumoto, B., Shiono, T., Miyoshi, M., Maeshiro, R., Fujii, S.j., Kuuluvainen, T., Kubota, Y., 2015. Functional response of plant communities to clearcutting: management impacts differ between forest vegetation zones. Journal of Applied Ecology 52, 171–180. doi:`10.1111/1365-2664.12367`.

Lamarque, P., Lavorel, S., Mouchet, M., Quétier, F., 2014. Plant trait-based models identify direct and indirect effects of climate change on bundles of grassland ecosystem services.

Proceedings of the National Academy of Sciences 111, 13751–13756. doi:`10.1073/pnas.1216051111`.

Latombe, G., Pyšek, P., Jeschke, J.M., Blackburn, T.M., Bacher, S., Capinha, C., Costello, M.J., Fernández, M., Gregory, R.D., Hobern, D., Hui, C., Jetz, W., Kumschick, S., McGrannachan, C., Pergl, J., Roy, H.E., Scalera, R., Squires, Z.E., Wilson, J.R.U., Winter, M., Genovesi, P., McGeoch, M.A., 2016. A vision for global monitoring of biological invasions. Biological Conservation 213, 295–308. doi:`10.1016/j.biocon.2016.06.013`.

Lavorel, S., Grigulis, K., Lamarque, P., Colace, M.P., Garden, D., Girel, J., Pellet, G., Douzet, R., 2011. Using plant functional traits to understand the landscape distribution of multiple ecosystem services. Journal of Ecology 99, 135–147. doi:`10.1111/j.1365-2745.2010.01753.x`.

Lee, M.R., Bernhardt, E.S., van Bodegom, P.M., Cornelissen, J.H.C., Kattge, J., Laughlin, D.C., Niinemets, U., Peñuelas, J., Reich, P.B., Yguel, B., Wright, J.P., 2017. Invasive species' leaf traits and dissimilarity from natives shape their impact on nitrogen cycling: a meta-analysis. New Phytologist 213, 128–139. doi:`10.1111/nph.14115`.

Lefsky, M.A., Cohen, W.B., Parker, G.G., Harding, D.J., 2002. Lidar remote sensing for ecosystem studies. BioScience 52, 19–30. doi:`10.1641/0006-3568(2002)052[0019:LRSFES]2.0.CO;2`.

Lefsky, M.A., Hudak, A.T., Cohen, W.B., Acker, S.A., 2005. Geographic variability in lidar predictions of forest stand structure in the Pacific Northwest. Remote Sensing of Environment 95, 532–548. doi:`10.1016/j.rse.2005.01.010`.

Leguan, 2012. Kartierung der Salzwiesen und Dünen an der Westküste von Schleswig-Holstein 2011 - 2012 - Biotop-Kartierung Sylt. Landesamt für Landwirtschaft, Umwelt und ländliche Räume (LLUR), Hamburg.

Liao, C., Peng, R., Luo, Y., Zhou, X., Wu, X., Fang, C., Chen, J., Li, B., 2008. Altered ecosystem carbon and nitrogen cycles by plant invasion: a meta-analysis. New Phytologist 177, 706–714. doi:`10.1111/j.1469-8137.2007.02290.x`.

Liu, Y., Oduor, A.M.O., Zhang, Z., Manea, A., Tooth, I.M., Leishman, M.R., Xu, X., van Kleunen, M., 2017. Do invasive alien plants benefit more from global environmental change than native plants? Global Change Biology 23, 3363–3370. doi:`10.1111/gcb.13579`.

Loiola, P.P., Bello, F.d., Chytrý, M., Götzenberger, L., Carmona, C.P., Pyšek, P., Lososová, Z., 2018. Invaders among locals: alien species decrease phylogenetic and functional diversity while increasing dissimilarity among native community members. Journal of Ecology 106, 2230–2241. doi:`10.1111/1365-2745.12986`.

Lopatin, J., Dolos, K., Kattenborn, T., Fassnacht, F.E., 2019. How canopy shadow affects invasive plant species classification in high spatial resolution remote sensing. Remote Sensing in Ecology and Conservation doi:`10.1002/rse2.109`.

Lopatin, J., Fassnacht, F.E., Kattenborn, T., Schmidtlein, S., 2017. Mapping plant species in mixed grassland communities using close range imaging spectroscopy. Remote Sensing of Environment 201, 12–23. doi:`10.1016/j.rse.2017.08.031`.

Lu, B., He, Y., Liu, H.H.T., 2018. Mapping vegetation biophysical and biochemical properties using unmanned aerial vehicles-acquired imagery. International Journal of Remote Sensing 39, 5265–5287. doi:`10.1080/01431161.2017.1363441`.

Mack, B., Roscher, R., Stenzel, S., Feilhauer, H., Schmidtlein, S., Waske, B., 2016. Mapping raised bogs with an iterative one-class classification approach. ISPRS Journal of Photogrammetry and Remote Sensing 120, 53–64. doi:`10.1016/j.isprsjprs.2016.07.008`.

Mack, R.N., Simberloff, D., Lonsdale, W.M., Evans, H., Clout, M., Bazzaz, F.A., 2000. Biotic invasions: causes, epidemiology, global consequences, and control. Ecological Applications 10, 689–710. doi:`10.1890/1051-0761(2000)010[0689:BICEGC]2.0.CO;2`.

Martin, M.E., Aber, J.D., 1997. High spectral resolution remote sensing of forest canopy lignin, nitrogen, and ecosystem processes. Ecological Applications 7, 431–443. doi:`10.2307/2269510`.

Martin, M.E., Plourde, L.C., Ollinger, S.V., Smith, M.L., McNeil, B.E., 2008. A generalizable method for remote sensing of canopy nitrogen across a wide range of forest ecosystems. Remote Sensing of Environment 112, 3511–3519. doi:`10.1016/j.rse.2008.04.008`.

Masek, J.G., Hayes, D.J., Joseph Hughes, M., Healey, S.P., Turner, D.P., 2015. The role of remote sensing in process-scaling studies of managed forest ecosystems. Forest Ecology and Management 355, 109–123. doi:`10.1016/j.foreco.2015.05.032`.

McAlpine, K.G., Lamoureaux, S.L., Westbrooke, I., 2015. Ecological impacts of ground cover weeds in New Zealand lowland forests. New Zealand Journal of Ecology 39, 50–60.

McGeoch, M.A., Genovesi, P., Bellingham, P.J., Costello, M.J., McGrannachan, C., Sheppard, A., 2016. Prioritizing species, pathways, and sites to achieve conservation targets for biological invasion. Biological Invasions 18, 299–314. doi:`10.1007/s10530-015-1013-1`.

McKown, A.D., Guy, R.D., Azam, M.S., Drewes, E.C., Quamme, L.K., 2013. Seasonality and phenology alter functional leaf traits. Oecologia 172, 653–665. doi:`10.1007/s00442-012-2531-5`.

McLaughlan, C., Gallardo, B., Aldridge, D.C., 2014. How complete is our knowledge of the ecosystem services impacts of Europe's top 10 invasive species? Acta Oecologica 54, 119–130. doi:`10.1016/j.actao.2013.03.005`.

McNeil, B.E., Read, J.M., Sullivan, T.J., McDonnell, T.C., Fernandez, I.J., Driscoll, C.T., 2008. The spatial pattern of nitrogen cycling in the adirondack park, New York. Ecological Applications 18, 438–452. doi:`10.1890/07-0276.1`.

Melillo, J.M., Aber, J.D., Muratore, J.F., 1982. Nitrogen and lignin control of hardwood leaf litter decomposition dynamics. Ecology 63, 621–626. doi:`10.2307/1936780`.

Mellert, K.H., Göttlein, A., 2012. Comparison of new foliar nutrient thresholds derived from van den Burg's literature compilation with established central European references. European Journal of Forest Research 131, 1461–1472. doi:`10.1007/s10342-012-0615-8`.

Miao, X., Gong, P., Swope, S., Pu, R., Carruthers, R., Anderson, G.L., Heaton, J.S., Tracy, C.R., 2006. Estimation of yellow starthistle abundance through CASI-2 hyperspectral

imagery using linear spectral mixture models. Remote Sensing of Environment 101, 329–341. doi:`10.1016/j.rse.2006.01.006`.

Mirik, M., Norland, J.E., Crabtree, R.L., Biondini, M.E., 2005. Hyperspectral one-meter-resolution remote sensing in Yellowstone National Park, Wyoming: I. forage nutritional values. Rangeland Ecology & Management 58, 452–458. doi:`10.2111/04-17.1`.

Moroń, D., Lenda, M., Skórka, P., Szentgyörgyi, H., Settele, J., Woyciechowski, M., 2009. Wild pollinator communities are negatively affected by invasion of alien goldenrods in grassland landscapes. Biological Conservation 142, 1322–1332. doi:`10.1016/j.biocon.2008.12.036`.

Morsdorf, F., Mårell, A., Koetz, B., Cassagne, N., Pimont, F., Rigolot, E., Allgöwer, B., 2010. Discrimination of vegetation strata in a multi-layered Mediterranean forest ecosystem using height and intensity information derived from airborne laser scanning. Remote Sensing of Environment 114, 1403–1415. doi:`10.1016/j.rse.2010.01.023`.

Muggeo, V.M.R., 2003. Estimating regression models with unknown break-points. Statistics in Medicine 22, 3055–3071. doi:`10.1002/sim.154`.

Muggeo, V.M.R., 2008. segmented: an R package to fit regression models with broken-line relationships. R News 8, 20–25.

Müllerová, J., Brůna, J., Dvořák, P., Bartaloš, T., Vítková, M., 2016. Does the data resolution/origin matter? satellite, airborne and Uav imagery to tackle plant invasions. ISPRS - International Archives of the Photogrammetry, Remote Sensing and Spatial Information Sciences 41B7, 903–908. doi:`10.5194/isprs-archives-XLI-B7-903-2016`.

Nehring, S., Kowarik, I., Rabitsch, W., Essl, F., 2013. Naturschutzfachliche Invasivitäts-bewertungen für in Deutschland wild lebende gebietsfremde Gefäßpflanzen. BfN-Skripten 352, Bundesamt für Naturschutz, Bonn.

Niinemets, U., 2016. Leaf age dependent changes in within-canopy variation in leaf functional traits: a meta-analysis. Journal of Plant Research 129, 313–338. doi:`10.1007/s10265-016-0815-2`.

Næsset, E., Gobakken, T., 2008. Estimation of above- and below-ground biomass across regions of the boreal forest zone using airborne laser. Remote Sensing of Environment 112, 3079–3090. doi:`10.1016/j.rse.2008.03.004`.

Ollinger, S.V., 2011. Sources of variability in canopy reflectance and the convergent properties of plants. New Phytologist 189, 375–394. doi:`10.1111/j.1469-8137.2010.03536.x`.

Ollinger, S.V., Richardson, A.D., Martin, M.E., Hollinger, D.Y., Frolking, S.E., Reich, P.B., Plourde, L.C., Katul, G.G., Munger, J.W., Oren, R., Smith, M.L., U, K.T.P., Bolstad, P.V., Cook, B.D., Day, M.C., Martin, T.A., Monson, R.K., Schmid, H.P., 2008. Canopy nitrogen, carbon assimilation, and albedo in temperate and boreal forests: Functional relations and potential climate feedbacks. Proceedings of the National Academy of Sciences 105, 19336–19341. doi:`10.1073/pnas.0810021105`.

Ollinger, S.V., Smith, M.L., Martin, M.E., Hallett, R.A., Goodale, C.L., Aber, J.D., 2002. Regional variation in foliar chemistry and N cycling among forests of diverse

history and composition. Ecology 83, 339–355. doi:`10.1890/0012-9658(2002)083[0339:RVIFCA]2.0.CO;2`.

Ortenberg, F., 2011. Hyperspectral sensor characteristics: airborne, spaceborne, hand-held, and truck-mounted; integration of hyperspectral data with LIDAR, in: Thenkabail, P.S., Lyon, J.G., Huete, A. (Eds.), Hyperspectral remote sensing of vegetation. CRC Press, Boca Raton, pp. 39–68.

Panetta, F.D., Gooden, B., 2017. Managing for biodiversity: impact and action thresholds for invasive plants in natural ecosystems. NeoBiota 34, 53–66. doi:`10.3897/neobiota.34.11821`.

Parker, I.M., Simberloff, D., Lonsdale, W.M., Goodell, K., Wonham, M., Kareiva, P.M., Williamson, M.H., Holle, B.V., Moyle, P.B., Byers, J.E., Goldwasser, L., 1999. Impact: toward a framework for understanding the ecological effects of invaders. Biological Invasions 1, 3–19. doi:`10.1023/A:1010034312781`.

Pauchard, A., García, R.A., Peña, E., González, C., Cavieres, L.A., Bustamante, R.O., 2008. Positive feedbacks between plant invasions and fire regimes: *Teline monspessulana* (L.) K. Koch (Fabaceae) in central Chile. Biological Invasions 10, 547–553. doi:`10.1007/s10530-007-9151-8`.

Pauchard, A., Shea, K., 2006. Integrating the study of non-native plant invasions across spatial scales. Biological Invasions 8, 399–413. doi:`10.1007/s10530-005-6419-8`.

Peerbhay, K., Mutanga, O., Lottering, R., Bangamwabo, V., Ismail, R., 2016. Detecting bugweed (*Solanum mauritianum*) abundance in plantation forestry using multisource remote sensing. ISPRS Journal of Photogrammetry and Remote Sensing 121, 167–176. doi:`10.1016/j.isprsjprs.2016.09.014`.

Peterson, E.B., 2005. Estimating cover of an invasive grass (*Bromus tectorum*) using tobit regression and phenology derived from two dates of Landsat ETM+ data. International Journal of Remote Sensing 26, 2491–2507. doi:`10.1080/01431160500127815`.

Pinheiro, J., Bates, D., DebRoy, S., Sarkar, D., R Core Team, 2016. nlme: Linear and nonlinear mixed effects models, R package version 3.1-128. URL: `http://CRAN.R-project.org/package=nlme`.

Pinheiro, J., Bates, D., DebRoy, S., Sarkar, D., R Core Team, 2018. nlme: Linear and nonlinear mixed effects models, R package version 3.1-137. URL: `https://CRAN.R-project.org/package=nlme`.

Porder, S., Asner, G.P., Vitousek, P.M., 2005. Ground-based and remotely sensed nutrient availability across a tropical landscape. Proceedings of the National Academy of Sciences of the United States of America 102, 10909–10912. doi:`10.1073/pnas.0504929102`.

Powell, K.I., Chase, J.M., Knight, T.M., 2011. A synthesis of plant invasion effects on biodiversity across spatial scales. American Journal of Botany 98, 539–548. doi:`10.3732/ajb.1000402`.

Powell, K.I., Chase, J.M., Knight, T.M., 2013. Invasive plants have scale-dependent effects on diversity by altering species-area relationships. Science 339, 316–318. doi:`10.1126/science.1226817`.

Pullanagari, R.R., Kereszturi, G., Yule, I.J., 2016. Mapping of macro and micro nutrients of mixed pastures using airborne AisaFENIX hyperspectral imagery. ISPRS Journal of Photogrammetry and Remote Sensing 117, 1–10. doi:10.1016/j.isprsjprs.2016.03.010.

Pyšek, P., Hulme, P.E., 2010. Biological invasions in Europe 50 years after elton: time to sound the aLARM, in: Richardson, D.M. (Ed.), fifty years of invasion ecology. John Wiley & Sons, Chichester, pp. 71–88. doi:10.1002/9781444329988.ch7.

Pyšek, P., Jarošík, V., Hulme, P.E., Pergl, J., Hejda, M., Schaffner, U., Vilà, M., 2012. A global assessment of invasive plant impacts on resident species, communities and ecosystems: the interaction of impact measures, invading species' traits and environment. Global Change Biology 18, 1725–1737. doi:10.1111/j.1365-2486.2011.02636.x.

Pyšek, P., Lambdon, P.W., Arianoutsou, M., Kühn, I., Pino, J., Winter, M., 2009. Alien vascular plants of Europe, in: Handbook of alien species in Europe. Springer, Dordrecht, pp. 43–61. doi:10.1007/978-1-4020-8280-1_4.

Pyšek, P., Richardson, D.M., 2010. Invasive species, environmental change and management, and health. Annual Review of Environment and Resources 35, 25–55. doi:10.1146/annurev-environ-033009-095548.

Pyšek, P., Richardson, D.M., Rejmánek, M., Webster, G.L., Williamson, M., Kirschner, J., 2004. Alien plants in checklists and floras: towards better communication between taxonomists and ecologists. Taxon 53, 131–143. doi:10.2307/4135498.

R Core Team, 2016. R: A Language and Environment for Statistical Computing. R Foundation for Statistical Computing, Vienna, Austria. URL: https://www.R-project.org/.

R Core Team, 2018. R: A Language and Environment for Statistical Computing. R Foundation for Statistical Computing, Vienna, Austria. URL: https://www.R-project.org/.

Rautiainen, M., Stenberg, P., Nilson, T., Kuusk, A., 2004. The effect of crown shape on the reflectance of coniferous stands. Remote Sensing of Environment 89, 41–52. doi:10.1016/j.rse.2003.10.001.

Reich, P.B., 2012. Key canopy traits drive forest productivity. Proceedings of the Royal Society of London B: Biological Sciences 279, 2128–2134. doi:10.1098/rspb.2011.2270.

Reich, P.B., Walters, M.B., Ellsworth, D.S., 1991. Leaf age and season influence the relationships between leaf nitrogen, leaf mass per area and photosynthesis in maple and oak trees. Plant, Cell & Environment 14, 251–259. doi:10.1111/j.1365-3040.1991.tb01499.x.

Rejmanek, M., J. Pitcairn, M., 2002. When is eradication of exotic pest plants a realistic goal?, in: Veitch, C.R., Clout, M.N. (Eds.), Turning the Tide: The Eradication of Invasive Species. IUCN, Gland and Cambridge, pp. 249–253.

Ricciardi, A., Hoopes, M.F., Marchetti, M.P., Lockwood, J.L., 2013. Progress toward understanding the ecological impacts of nonnative species. Ecological Monographs 83, 263–282. doi:10.1890/13-0183.1.

Richardson, D.M., Pyšek, P., 2008. Fifty years of invasion ecology – the legacy of Charles Elton. Diversity and Distributions 14, 161–168. doi:`10.1111/j.1472-4642.2007.00464.x`.

Richardson, D.M., Pyšek, P., 2012. Naturalization of introduced plants: ecological drivers of biogeographical patterns. New Phytologist 196, 383–396. doi:`10.1111/j.1469-8137.2012.04292.x`.

Richardson, D.M., Pyšek, P., Carlton, J.T., 2011. A compendium of essential concepts and terminology in invasion ecology, in: Richardson, D.M. (Ed.), Fifty years of invasion ecology. John Wiley & Sons, Chichester, pp. 409–420. doi:`10.1002/9781444329988.ch30`.

Richardson, D.M., Pyšek, P., Rejmánek, M., Barbour, M.G., Panetta, F.D., West, C.J., 2000. Naturalization and invasion of alien plants: concepts and definitions. Diversity and Distributions 6, 93–107. doi:`10.1046/j.1472-4642.2000.00083.x`.

Richardson, S.J., Peltzer, D.A., Allen, R.B., McGlone, M.S., 2005. Resorption proficiency along a chronosequence: responses among communities and within species. Ecology 86, 20–25. doi:`10.1890/04-0524`.

Roberts, D.A., Ustin, S.L., Ogunjemiyo, S., Greenberg, J., Dobrowski, S.Z., Chen, J., Hinckley, T.M., 2004. Spectral and structural measures of northwest forest vegetation at leaf to landscape scales. Ecosystems 7, 545–562. doi:`10.1007/s10021-004-0144-5`.

Roberts, D.R., Bahn, V., Ciuti, S., Boyce, M.S., Elith, J., Guillera-Arroita, G., Hauenstein, S., Lahoz-Monfort, J.J., Schröder, B., Thuiller, W., Warton, D.I., Wintle, B.A., Hartig, F., Dormann, C., 2017. Cross-validation strategies for data with temporal, spatial, hierarchical, or phylogenetic structure. Ecography 40, 913–929. doi:`10.1111/ecog.02881`.

Rocchini, D., Andreo, V., Förster, M., Garzon-Lopez, C.X., Gutierrez, A.P., Gillespie, T.W., Hauffe, H.C., He, K.S., Kleinschmit, B., Mairota, P., Marcantonio, M., Metz, M., Nagendra, H., Pareeth, S., Ponti, L., Ricotta, C., Rizzoli, A., Schaab, G., Zebisch, M., Zorer, R., Neteler, M., 2015. Potential of remote sensing to predict species invasions: A modelling perspective. Progress in Physical Geography: Earth and Environment 39, 283–309. doi:`10.1177/0309133315574659`.

Roelofsen, H.D., van Bodegom, P.M., Kooistra, L., Witte, J.P.M., 2014. Predicting leaf traits of herbaceous species from their spectral characteristics. Ecology and Evolution 4, 706–719. doi:`10.1002/ece3.932`.

Ronk, A., Szava-Kovats, R., Zobel, M., Pärtel, M., 2017. Observed and dark diversity of alien plant species in Europe: estimating future invasion risk. Biodiversity and Conservation 26, 899–916. doi:`10.1007/s10531-016-1278-4`.

Sardans, J., Alonso, R., Janssens, I.A., Carnicer, J., Vereseglou, S., Rillig, M.C., Fernández-Martínez, M., Sanders, T.G.M., Peñuelas, J., 2016. Foliar and soil concentrations and stoichiometry of nitrogen and phosphorous across European *Pinus sylvestris* forests: relationships with climate, N deposition and tree growth. Functional Ecology 30, 676–689. doi:`10.1111/1365-2435.12541`.

Sardans, J., Janssens, I.A., Alonso, R., Veresoglou, S.D., Rillig, M.C., Sanders, T.G., Carnicer, J., Filella, I., Farré-Armengol, G., Peñuelas, J., 2015. Foliar elemental composition of European forest tree species associated with evolutionary traits and present environmental and competitive conditions. Global Ecology and Biogeography 24, 240–255. doi:`10.1111/geb.12253`.

Sardans, J., Peñuelas, J., 2015. Trees increase their P:N ratio with size. Global Ecology and Biogeography 24, 147–156. doi:`10.1111/geb.12231`.

Sasaki, T., Imanishi, J., Ioki, K., Morimoto, Y., Kitada, K., 2008. Estimation of leaf area index and canopy openness in broad-leaved forest using an airborne laser scanner in comparison with high-resolution near-infrared digital photography. Landscape and Ecological Engineering 4, 47–55. doi:`10.1007/s11355-008-0041-8`.

Schaepman, M.E., Jehle, M., Hueni, A., D'Odorico, P., Damm, A., Weyermann, J., Schneider, F.D., Laurent, V., Popp, C., Seidel, F.C., Lenhard, K., Gege, P., Küchler, C., Brazile, J., Kohler, P., De Vos, L., Meuleman, K., Meynart, R., Schläpfer, D., Kneubühler, M., Itten, K.I., 2015. Advanced radiometry measurements and Earth science applications with the Airborne Prism Experiment (APEX). Remote Sensing of Environment 158, 207–219. doi:`10.1016/j.rse.2014.11.014`.

Scharfy, D., Eggenschwiler, H., Venterink, H.O., Edwards, P.J., Güsewell, S., 2009. The invasive alien plant species *Solidago gigantea* alters ecosystem properties across habitats with differing fertility. Journal of Vegetation Science 20, 1072–1085. doi:`10.1111/j.1654-1103.2009.01105.x`.

Schlerf, M., Atzberger, C., Hill, J., Buddenbaum, H., Werner, W., Schüler, G., 2010. Retrieval of chlorophyll and nitrogen in Norway spruce (*Picea abies* L. Karst.) using imaging spectroscopy. International Journal of Applied Earth Observation and Geoinformation 12, 17–26. doi:`10.1016/j.jag.2009.08.006`.

Schmidt, J., Fassnacht, F.E., Lausch, A., Schmidtlein, S., 2017a. Assessing the functional signature of heathland landscapes via hyperspectral remote sensing. Ecological Indicators 73, 505–512. doi:`10.1016/j.ecolind.2016.10.017`.

Schmidt, J., Fassnacht, F.E., Neff, C., Lausch, A., Kleinschmit, B., Förster, M., Schmidtlein, S., 2017b. Adapting a Natura 2000 field guideline for a remote sensing-based assessment of heathland conservation status. International Journal of Applied Earth Observation and Geoinformation 60, 61–71. doi:`10.1016/j.jag.2017.04.005`.

Schmidtlein, S., Feilhauer, H., Bruelheide, H., 2012. Mapping plant strategy types using remote sensing. Journal of Vegetation Science 23, 395–405. doi:`10.1111/j.1654-1103.2011.01370.x`.

Seabloom, E.W., Kay, A., MacDougall, A.S., Hector, A., Risch, A.C., Simonsen, A., Mortensen, B., Melbourne, B.A., Dantonio, C.M., Stevens, C.J., Mitchell, C.E., Chu, C., Brown, C.S., Blumenthal, D.M., Gruner, D.S., Pyke, D.A., Borer, E.T., Wolkovich, E., Damschen, E.I., Cleland, E.E., Lind, E.M., Du, G., Hillebrand, H., Humphries, H.C., Firn, J., Knops, J.M.H., Lambrinos, J.G., Orrock, J.L., Morgan, J., Bakker, J.D., Moore, J.L., Klein, J.A., Wright, J., Cottingham, K.L., Davies, K.F., Kirkman, K.P., Pierre, K.J.L., Hofmockel, K.S., Brudvig, L.A., Ladwig, L., Sullivan, L., Biederman,

L.A., Yang, L., O'Halloran, L.R., Sankaran, M., Cadotte, M., Schuetz, M., Smith, M.D., Crawley, M.J., Hagenah, N., DeCrappeo, N.M., Frater, P., Adler, P.B., Wragg, P.D., Fay, P.A., Li, Q., McCulley, R.L., Marushia, R., Prober, S.M., Anderson, T.M., Jin, V.L., Harpole, W.S., Li, W., Hautier, Y., Buckley, Y.M., 2015. Plant species' origin predicts dominance and response to nutrient enrichment and herbivores in global grasslands. Nature Communications 6, 8710. doi:`10.1038/ncomms8710`.

Seebens, H., Blackburn, T.M., Dyer, E.E., Genovesi, P., Hulme, P.E., Jeschke, J.M., Pagad, S., Pyšek, P., Winter, M., Arianoutsou, M., Bacher, S., Blasius, B., Brundu, G., Capinha, C., Celesti-Grapow, L., Dawson, W., Dullinger, S., Fuentes, N., Jäger, H., Kartesz, J., Kenis, M., Kreft, H., Kühn, I., Lenzner, B., Liebhold, A., Mosena, A., Moser, D., Nishino, M., Pearman, D., Pergl, J., Rabitsch, W., Rojas-Sandoval, J., Roques, A., Rorke, S., Rossinelli, S., Roy, H.E., Scalera, R., Schindler, S., Štajerová, K., Tokarska-Guzik, B., van Kleunen, M., Walker, K., Weigelt, P., Yamanaka, T., Essl, F., 2017. No saturation in the accumulation of alien species worldwide. Nature Communications 8, 14435. doi:`10.1038/ncomms14435`.

Seebens, H., Essl, F., Dawson, W., Fuentes, N., Moser, D., Pergl, J., Pyšek, P., Kleunen, M.v., Weber, E., Winter, M., Blasius, B., 2015. Global trade will accelerate plant invasions in emerging economies under climate change. Global Change Biology 21, 4128–4140. doi:`10.1111/gcb.13021`.

Serbin, S.P., Singh, A., McNeil, B.E., Kingdon, C.C., Townsend, P.A., 2014. Spectroscopic determination of leaf morphological and biochemical traits for northern temperate and boreal tree species. Ecological Applications 24, 1651–1669. doi:`10.1890/13-2110.1`.

Serrano, L., Peñuelas, J., Ustin, S.L., 2002. Remote sensing of nitrogen and lignin in Mediterranean vegetation from AVIRIS data: Decomposing biochemical from structural signals. Remote Sensing of Environment 81, 355–364. doi:`10.1016/S0034-4257(02)00011-1`.

Shackleton, R.T., Shackleton, C.M., Kull, C.A., 2019. The role of invasive alien species in shaping local livelihoods and human well-being: A review. Journal of Environmental Management 229, 145–157. doi:`10.1016/j.jenvman.2018.05.007`.

Shipley, B., Lechowicz, M.J., Wright, I., Reich, P.B., 2006. Fundamental trade-offs generating the worldwide leaf economics spectrum. Ecology 87, 535–541. doi:`10.1890/05-1051`.

Simberloff, D., 2011. Charles elton: neither founder nor siren, but prophet, in: Richardson, D.M. (Ed.), Fifty years of invasion ecology. John Wiley & Sons, Chichester, pp. 11–24. doi:`10.1002/9781444329988.ch2`.

Simic, A., Chen, J.M., Noland, T.L., 2011. Retrieval of forest chlorophyll content using canopy structure parameters derived from multi-angle data: the measurement concept of combining nadir hyperspectral and off-nadir multispectral data. International Journal of Remote Sensing 32, 5621–5644. doi:`10.1080/01431161.2010.507257`.

Simpson, E.H., 1949. Measurement of diversity. Nature 163, 688. doi:`10.1038/163688a0`.

Singh, A., Serbin, S.P., McNeil, B.E., Kingdon, C.C., Townsend, P.A., 2015. Imaging spectroscopy algorithms for mapping canopy foliar chemical and morphological traits and their uncertainties. Ecological Applications 25, 2180–2197. doi:`10.1890/14-2098.1`.

Singh, N., Glenn, N.F., 2009. Multitemporal spectral analysis for cheatgrass (*Bromus tectorum*) classification. International Journal of Remote Sensing 30, 3441–3462. doi:`10.1080/01431160802562222`.

Skowronek, S., Asner, G.P., Feilhauer, H., 2017a. Performance of one-class classifiers for invasive species mapping using airborne imaging spectroscopy. Ecological Informatics 37, 66–76. doi:`10.1016/j.ecoinf.2016.11.005`.

Skowronek, S., Ewald, M., Isermann, M., Kerchove, R.V.D., Lenoir, J., Aerts, R., Warrie, J., Hattab, T., Honnay, O., Schmidtlein, S., Rocchini, D., Somers, B., Feilhauer, H., 2017b. Mapping an invasive bryophyte species using hyperspectral remote sensing data. Biological Invasions 19, 239–254. doi:`10.1007/s10530-016-1276-1`.

Skowronek, S., Van De Kerchove, R., Rombouts, B., Aerts, R., Ewald, M., Warrie, J., Schiefer, F., Garzón-López, C., Hattab, T., Honnay, O., Lenoir, J., Rocchini, D., Schmidtlein, S., Somers, B., Feilhauer, H., 2018. Transferability of species distribution models for the detection of an invasive alien bryophyte using imaging spectroscopy data. International Journal of Applied Earth Observation and Geoinformation 68, 61–72. doi:`10.1016/j.jag.2018.02.001`.

Smith, M.L., Martin, M.E., Plourde, L., Ollinger, S.V., 2003. Analysis of hyperspectral data for estimation of temperate forest canopy nitrogen concentration: comparison between an airborne (AVIRIS) and a spaceborne (Hyperion) sensor. IEEE Transactions of Geoscience and Remote Sensing 41, 1332–1337.

Somers, B., Asner, G.P., 2013. Invasive species mapping in Hawaiian rainforests using multi-temporal Hyperion spaceborne imaging spectroscopy. IEEE Journal of Selected Topics in Applied Earth Observations and Remote Sensing 6, 351–359. doi:`10.1109/JSTARS.2012.2203796`.

Somers, B., Asner, G.P., Tits, L., Coppin, P., 2011. Endmember variability in spectral mixture analysis: a review. Remote Sensing of Environment 115, 1603–1616. doi:`10.1016/j.rse.2011.03.003`.

Starfinger, U., Kowarik, I., Rode, M., Schepker, H., 2003. From desirable ornamental plant to pest to accepted addition to the flora? – the perception of an alien tree species through the centuries. Biological Invasions 5, 323–335. doi:`10.1023/B:BINV.0000005573.14800.07`.

Staska, B., Essl, F., Samimi, C., 2014. Density and age of invasive *Robinia pseudoacacia* modulate its impact on floodplain forests. Basic and Applied Ecology 15, 551–558. doi:`10.1016/j.baae.2014.07.010`.

Stenzel, S., Fassnacht, F.E., Mack, B., Schmidtlein, S., 2017. Identification of high nature value grassland with remote sensing and minimal field data. Ecological Indicators 74, 28–38. doi:`10.1016/j.ecolind.2016.11.005`.

Sterckx, S., Vreys, K., Biesemans, J., Iordache, M.D., Bertels, L., Meuleman, K., 2016. Atmospheric correction of APEX hyperspectral data. Miscellanea Geographica 20, 16–20. doi:`10.1515/mgrsd-2015-0022`.

Strayer, D.L., 2012. Eight questions about invasions and ecosystem functioning. Ecology Letters 15, 1199–1210. doi:`10.1111/j.1461-0248.2012.01817.x`.

Stricker, K.B., Hagan, D., Flory, S.L., 2015. Improving methods to evaluate the impacts of plant invasions: lessons from 40 years of research. AoB Plants 7, plv028. doi:`10.1093/aobpla/plv028`.

Suding, K.N., Lavorel, S., Chapin, F.S., Cornelissen, J.H.C., Díaz, S., Garnier, E., Goldberg, D., Hooper, D.U., Jackson, S.T., Navas, M.L., 2008. Scaling environmental change through the community-level: a trait-based response-and-effect framework for plants. Global Change Biology 14, 1125–1140. doi:`10.1111/j.1365-2486.2008.01557.x`.

Sun, X., Kang, H., Kattge, J., Gao, Y., Liu, C., 2015. Biogeographic patterns of multi-element stoichiometry of *Quercus variabilis* leaves across China. Canadian Journal of Forest Research 45, 1827–1834. doi:`10.1139/cjfr-2015-0110`.

Sundseth, K., 2014. Invasive alien species: a European response. Publication Office of the European Union, Luxembourg.

Sunny, A., Diwakar, S., Sharma, G.P., 2015. Native insects and invasive plants encounters. Arthropod-Plant Interactions 9, 323–331. doi:`10.1007/s11829-015-9384-x`.

Takahashi, M., Giambelluca, T.W., Mudd, R.G., DeLay, J.K., Nullet, M.A., Asner, G.P., 2011. Rainfall partitioning and cloud water interception in native forest and invaded forest in Hawai'i Volcanoes National Park. Hydrological Processes 25, 448–464. doi:`10.1002/hyp.7797`.

Talkner, U., Meiwes, K.J., Potočić, N., Seletković, I., Cools, N., Vos, B.D., Rautio, P., 2015. Phosphorus nutrition of beech (*Fagus sylvatica* L.) is decreasing in Europe. Annals of Forest Science 72, 919–928. doi:`10.1007/s13595-015-0459-8`.

Terwei, A., Zerbe, S., Zeileis, A., Annighöfer, P., Kawaletz, H., Mölder, I., Ammer, C., 2013. Which are the factors controlling tree seedling establishment in North Italian floodplain forests invaded by non-native tree species? Forest Ecology and Management 304, 192–203. doi:`10.1016/j.foreco.2013.05.003`.

Thiele, J., Kollmann, J., Markussen, B., Otte, A., 2009. Impact assessment revisited: improving the theoretical basis for management of invasive alien species. Biological Invasions 12, 2025–2035. doi:`10.1007/s10530-009-9605-2`.

Thorpe, A.S., Archer, V., DeLuca, T.H., 2006. The invasive forb, *Centaurea maculosa*, increases phosphorus availability in Montana grasslands. Applied Soil Ecology 32, 118–122. doi:`10.1016/j.apsoil.2005.02.018`.

Townsend, P.A., Foster, J.R., Chastain, R.A., Currie, W.S., 2003. Application of imaging spectroscopy to mapping canopy nitrogen in the forests of the central Appalachian Mountains using Hyperion and AVIRIS. IEEE Transactions on Geoscience and Remote Sensing 41, 1347–1354. doi:`10.1109/TGRS.2003.813205`.

Transon, J., D'Andrimont, R., Maugnard, A., Defourny, P., 2018. Survey of hyperspectral Earth observation applications from space in the Sentinel-2 context. Remote Sensing 10, 157. doi:`10.3390/rs10020157`.

Turbelin, A.J., Malamud, B.D., Francis, R.A., 2017. Mapping the global state of invasive alien species: patterns of invasion and policy responses. Global Ecology and Biogeography 26, 78–92. doi:`10.1111/geb.12517`.

Turner, W., Spector, S., Gardiner, N., Fladeland, M., Sterling, E., Steininger, M., 2003. Remote sensing for biodiversity science and conservation. Trends in Ecology and Evolution 18, 306–314. doi:10.1016/S0169-5347(03)00070-3.

USDA, 1999. Executive order 13112 - section 1. Definitions. URL: https://www.invasivespeciesinfo.gov/executive-order-13112-section-1-definitions.

Ustin, S.L., Gamon, J.A., 2010. Remote sensing of plant functional types. New Phytologist 186, 795–816. doi:10.1111/j.1469-8137.2010.03284.x.

Ustin, S.L., Gitelson, A.A., Jacquemoud, S., Schaepman, M., Asner, G.P., Gamon, J.A., Zarco-Tejada, P., 2009. Retrieval of foliar information about plant pigment systems from high resolution spectroscopy. Remote Sensing of Environment 113, S67–S77. doi:10.1016/j.rse.2008.10.019.

van Kleunen, M., Dawson, W., Essl, F., Pergl, J., Winter, M., Weber, E., Kreft, H., Weigelt, P., Kartesz, J., Nishino, M., Antonova, L.A., Barcelona, J.F., Cabezas, F.J., Cárdenas, D., Cárdenas-Toro, J., Castaño, N., Chacón, E., Chatelain, C., Ebel, A.L., Figueiredo, E., Fuentes, N., Groom, Q.J., Henderson, L., Inderjit, Kupriyanov, A., Masciadri, S., Meerman, J., Morozova, O., Moser, D., Nickrent, D.L., Patzelt, A., Pelser, P.B., Baptiste, M.P., Poopath, M., Schulze, M., Seebens, H., Shu, W.s., Thomas, J., Velayos, M., Wieringa, J.J., Pyšek, P., 2015. Global exchange and accumulation of non-native plants. Nature 525, 100–103. doi:10.1038/nature14910.

van Kleunen, M., Weber, E., Fischer, M., 2010. A meta-analysis of trait differences between invasive and non-invasive plant species. Ecology Letters 13, 235–245. doi:10.1111/j.1461-0248.2009.01418.x.

van Leeuwen, M., Nieuwenhuis, M., 2010. Retrieval of forest structural parameters using LiDAR remote sensing. European Journal of Forest Research 129, 749–770. doi:10.1007/s10342-010-0381-4.

Vanhellemont, M., Verheyen, K., Keersmaeker, L.D., Vandekerkhove, K., Hermy, M., 2008. Does Prunus serotina act as an aggressive invader in areas with a low propagule pressure? Biological Invasions 11, 1451–1462. doi:10.1007/s10530-008-9353-8.

Vaz, A.S., Alcaraz-Segura, D., Campos, J.C., Vicente, J.R., Honrado, J.P., 2018. Managing plant invasions through the lens of remote sensing: a review of progress and the way forward. Science of The Total Environment 642, 1328–1339. doi:10.1016/j.scitotenv.2018.06.134.

Verrelst, J., Camps-Valls, G., Muñoz-Marí, J., Rivera, J.P., Veroustraete, F., Clevers, J.G.P.W., Moreno, J., 2015. Optical remote sensing and the retrieval of terrestrial vegetation bio-geophysical properties – A review. ISPRS Journal of Photogrammetry and Remote Sensing 108, 273–290. doi:10.1016/j.isprsjprs.2015.05.005.

Vicente, J., Alves, P., Randin, C., Guisan, A., Honrado, J., 2010. What drives invasibility? A multi-model inference test and spatial modelling of alien plant species richness patterns in northern Portugal. Ecography 33, 1081–1092. doi:10.1111/j.1600-0587.2010.6380.x.

Vicente, J.R., Pinto, A.T., Araújo, M.B., Verburg, P.H., Lomba, A., Randin, C.F., Guisan, A., Honrado, J.P., 2013. Using life strategies to explore the vulnerability of ecosystem services to invasion by alien plants. Ecosystems 16, 678–693. doi:10.1007/s10021-013-9640-9.

Vilà, M., Basnou, C., Pyšek, P., Josefsson, M., Genovesi, P., Gollasch, S., Nentwig, W., Olenin, S., Roques, A., Roy, D., Hulme, P.E., DAISIE partners, 2010. How well do we understand the impacts of alien species on ecosystem services? A pan-European, cross-taxa assessment. Frontiers in Ecology and the Environment 8, 135–144. doi:`10.1890/080083`.

Vilà, M., Espinar, J.L., Hejda, M., Hulme, P.E., Jarošík, V., Maron, J.L., Pergl, J., Schaffner, U., Sun, Y., Pyšek, P., 2011. Ecological impacts of invasive alien plants: a meta-analysis of their effects on species, communities and ecosystems. Ecology Letters 14, 702–708. doi:`10.1111/j.1461-0248.2011.01628.x`.

Vilà, M., Tessier, M., Suehs, C.M., Brundu, G., Carta, L., Galanidis, A., Lambdon, P., Manca, M., Médail, F., Moragues, E., Traveset, A., Troumbis, A.Y., Hulme, P.E., 2006. Local and regional assessments of the impacts of plant invaders on vegetation structure and soil properties of Mediterranean islands. Journal of Biogeography 33, 853–861. doi:`10.1111/j.1365-2699.2005.01430.x`.

Vilà, M., Weiner, J., 2004. Are invasive plant psecies better competitors than native plant species?: evidence from pair-wise experiments. Oikos 105, 229–238. doi:`10.1111/j.0030-1299.2004.12682.x`.

Vilà-Cabrera, A., Martínez-Vilalta, J., Retana, J., 2015. Functional trait variation along environmental gradients in temperate and Mediterranean trees. Global Ecology and Biogeography 24, 1377–1389. doi:`10.1111/geb.12379`.

Vitousek, P.M., 1990. Biological invasions and ecosystem processes: towards an integration of population biology and ecosystem studies. Oikos 57, 7–13. doi:`10.2307/3565731`.

Vreys, K., Iordache, M.D., Biesemans, J., Meuleman, K., 2016. Geometric correction of APEX hyperspectral data. Miscellanea Geographica 20, 11–15. doi:`10.1515/mgrsd-2016-0006`.

Wagner, F.H., Sanchez, A., Tarabalka, Y., Lotte, R.G., Ferreira, M.P., Aidar, M.P.M., Gloor, E., Phillips, O.L., Aragão, L.E.O.C., 2019. Using the U-net convolutional network to map forest types and disturbance in the Atlantic rainforest with very high resolution images. Remote Sensing in Ecology and Conservation doi:`10.1002/rse2.111`.

Wang, K., Franklin, S.E., Guo, X., Cattet, M., 2010. Remote sensing of ecology, biodiversity and conservation: a review from the perspective of remote sensing specialists. Sensors 10, 9647–9667. doi:`10.3390/s101109647`.

Wang, Z., Wang, T., Darvishzadeh, R., Skidmore, A.K., Jones, S., Suarez, L., Woodgate, W., Heiden, U., Heurich, M., Hearne, J., 2016. Vegetation indices for mapping canopy foliar nitrogen in a mixed temperate forest. Remote Sensing 8, 491. doi:`10.3390/rs8060491`.

Wehr, A., Lohr, U., 1999. Airborne laser scanning—an introduction and overview. ISPRS Journal of Photogrammetry and Remote Sensing 54, 68–82. doi:`10.1016/S0924-2716(99)00011-8`.

Weidenhamer, J.D., Callaway, R.M., 2010. Direct and indirect effects of invasive plants on soil chemistry and ecosystem function. Journal of Chemical Ecology 36, 59–69. doi:`10.1007/s10886-009-9735-0`.

Wiens, J.A., 1989. Spatial scaling in ecology. Functional Ecology 3, 385–397. doi:`10.2307/2389612`.

Wilson, K.B., Baldocchi, D.D., Hanson, P.J., 2000. Spatial and seasonal variability of photosynthetic parameters and their relationship to leaf nitrogen in a deciduous forest. Tree Physiology 20, 565–578. doi:`10.1093/treephys/20.9.565`.

Windham, L., Ehrenfeld, J.G., 2003. Net impact of a plant invasion on nitrogen-cycling processes within a brackish tidal marsh. Ecological Applications 13, 883–896. doi:`10.1890/02-5005`.

Wright, I.J., Reich, P.B., Westoby, M., Ackerly, D.D., Baruch, Z., Bongers, F., Cavender-Bares, J., Chapin, T., Cornelissen, J.H.C., Diemer, M., Flexas, J., Garnier, E., Groom, P.K., Gulias, J., Hikosaka, K., Lamont, B.B., Lee, T., Lee, W., Lusk, C., Midgley, J.J., Navas, M.L., Niinemets, U., Oleksyn, J., Osada, N., Poorter, H., Poot, P., Prior, L., Pyankov, V.I., Roumet, C., Thomas, S.C., Tjoelker, M.G., Veneklaas, E.J., Villar, R., 2004. The worldwide leaf economics spectrum. Nature 428, 821–827. doi:`10.1038/nature02403`.

Wäldchen, J., Mäder, P., 2018. Plant species identification using computer vision techniques: a systematic literature review. Archives of Computational Methods in Engineering 25, 507–543. doi:`10.1007/s11831-016-9206-z`.

Xiao, Y., Zhao, W., Zhou, D., Gong, H., 2014. Sensitivity analysis of vegetation reflectance to biochemical and biophysical variables at leaf, canopy, and regional scales. IEEE Transactions on Geoscience and Remote Sensing 52, 4014–4024. doi:`10.1109/TGRS.2013.2278838`.

Yokomizo, H., Possingham, H.P., Thomas, M.B., Buckley, Y.M., 2009. Managing the impact of invasive species: the value of knowing the density-impact curve. Ecological Applications 19, 376–386. doi:`10.1890/08-0442.1`.

Zheng, G., Moskal, L.M., 2009. Retrieving elaf area index (LAI) using remote sensing: theories, methods and sensors. Sensors 9, 2719–2745. doi:`10.3390/s90402719`.

Zolkos, S.G., Goetz, S.J., Dubayah, R., 2013. A meta-analysis of terrestrial aboveground biomass estimation using lidar remote sensing. Remote Sensing of Environment 128, 289–298. doi:`10.1016/j.rse.2012.10.017`.

Acknowledgements

Abbreviations and acronyms

AIC	Akaike information criterion
APEX	Airborne prism experiment
gPLS	Generalized partial least squares
LAI	Leaf area index
LiDAR	Light detection and ranging
LMA	Leaf mass per area
LMM	Linear mixed model
N:P	Leaf nitrogen to phosphorus ratio
NDVI	Normalized difference vegetation index
NIR	Near-infrared (700 nm - 1 μm)
N$_{mass}$	Mass based leaf nitrogen content
PLSR	Partial least squares regression
P$_{mass}$	Mass based leaf phosphorus content
r	Person or Spearman correlation coefficient
R	Coefficient of determination
RMSE	Root mean squared error
RTM	Radiative transfer model
SAC	Spatial autocorrelation
SLA	Specific leaf area
SWIR	Shortwave-infrared (1 μm - 3 μm)
TIR	Termal-infrared (1 μm - 3 μm)
UAV	Unmanned areal vehicle
VIS	Visible region of the electromagnetic spectrum (400 nm - 700 nm)

Additional abbreviations used for LiDAR-derived variables are listed in table 2.1.

Eidesstattliche Versicherung

gemäß §6 Abs. 1 Ziff. 4 der Promotionsordnung des Karlsruher Instituts für Technologie für die Fakultät für für Bauingenieur-, Geo- und Umweltwissenschaften.

1. Bei der eingereichten Dissertation zu dem Thema **„Analyzing the ecosystem impact of invasive alien plant species using remote sensing"** handelt es sich um meine eigenständig erbrachte Leistung.

2. Ich habe nur die angegebenen Quellen und Hilfsmittel benutzt und mich keiner unzulässigen Hilfe Dritter bedient. Insbesondere habe ich wörtlich oder sinngemäß aus anderen Werken über-nommene Inhalte als solche kenntlich gemacht.

3. Die Arbeit oder Teile davon habe ich bislang nicht an einer Hochschule des In- oder Auslands als Bestandteil einer Prüfungs- oder Qualifikationsleistung vorgelegt.

4. Die Richtigkeit der vorstehenden Erklärungen bestätige ich.

5. Die Bedeutung der eidesstattlichen Versicherung und die strafrechtlichen Folgen einer unrichtigen oder unvollständigen eidesstattlichen Versicherung sind mir bekannt.

Ich versichere an Eides statt, dass ich nach bestem Wissen die reine Wahrheit erklärt und nichts verschwiegen habe.

Ort und Datum   Unterschrift